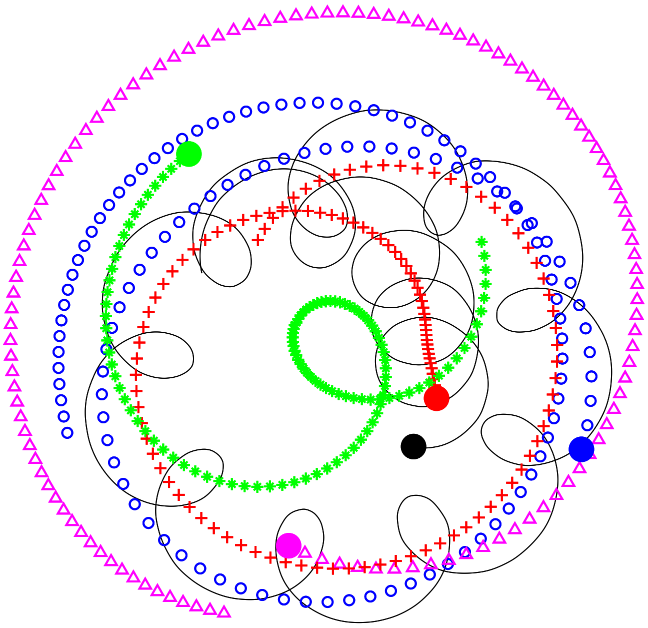

Geometry and Control of Two-Dimensional Vortex-Driven Transport

Gil Miguel Marques

Thesis carried out as part of the Doctoral Program in Applied Mathematics

Department of Mathematics

2026

Supervisor

Sílvio M. A. Gama, Associate Professor, Centre of Mathematics of the University of Porto, Faculty of Sciences of the University of Porto

Co-supervisor

Marco Martins Afonso, Research Fellow, SIT Technologies & Università di Genova, Italy

To my grandparents.

Acknowledgements

First and foremost, I would like to express my sincere gratitude to my supervisors Dr. Sílvio Gama and Dr. Marco Martins Afonso, as well as my initial co-supervisor Dr. Fernando Lobo Pereira, who unfortunately left us in June 2022, for all the support, help and availability throughout my Ph.D. Thank you for believing and trusting in me even when I wouldn't trust myself. A special thank you to Dra. Maria João Rodrigues for her continued support, friendship and trust.

Thank you to all the people who crossed my path during my studies in the University of Porto, contributing to my academic and personal growth. In particular, a special word of appreciation to Joana Lima, Ana Afonso, Catarina Leite, João Maurício and Raquel Albuquerque.

An enormous word of gratitude to music, for helping me in every way possible and for keeping me sane everyday. Thank you to all the great friends it brought me, more notably to my Bons Sons family: Teresa Colaço, Raquel Segadães, Filipa Almeida, João Neves and our most recent adoptee Leonor Segadães. A special thank you to Björk Guðmundsdóttir for everything she has done for me and for this world.

Thank you to Dra. Cidalina Reis Ferreira and Dr. José Vale for your tireless support, care and help throughout all the health issues I had during the past few years. I don't know if I would be here today without your help.

I am grateful to all my friends that have supported me throughout life and never stopped believing in me, even if sometimes we don't communicate or spend time together as much as I would have liked. Thank you to every one of you.

A special shoutout to everyone in my crew スライムーガルズ, both past and present members, for all the friendship and tech support help.

Last but not least, I am deeply grateful to my family: to my mom for all the support and sacrifices she made for me; to my grandparents, wherever you are, you are the reason for me to be the person I am, and you'll always be with me.

The research in this thesis had financial support from Fundação para a Ciência e a Tecnologia (FCT) through grant PD/BD/150537/2019, and CMUP – Centro de Matemática da Universidade do Porto, member of LASI, which is financed by national funds through FCT – Fundação para a Ciência e a Tecnologia, I.P., under the project with reference:

UID/00144/2025, doi: https://doi.org/10.54499/UID/00144/2025. This work also benefited from the research activities associated with the project "REFARMING: Renewable Energy Solutions for Sustainable Tech-Enabled Greenhouses and Vertical Farming Systems"(NORTE2030-FEDER 02719900), co-funded by the European Union through the NORTE 2030 Regional Programme, under Portugal 2030.

“ Nature hasn’t gone anywhere. It is all around us, all the planets, galaxies and so on. We are nothing in comparison. ”

Björk, 2011

UNIVERSIDADE DO PORTO

Resumo

Faculdade de Ciências da Universidade do Porto
Departamento de Matemática

Programa Doutoral em Matemática Aplicada

Geometria e Controlo de Transporte Impulsionado por Vórtices Bidimensionais

por Gil Miguel Marques

Esta tese desenvolve uma formulação matemática para a modelação e controlo do movimento de partículas passivas em fluidos impulsionados por vórtices. O problema é tratado em $\mathbb{R}^2$ e são considerados modelos de vórtices viscosos e não viscosos.

O Capítulo 2 introduz uma formulação para a modelação, controlo e otimização do movimento de uma partícula passiva advectada por um vórtice pontual. Num tal fluido, o problema de controlo de mover uma partícula passiva entre dois pontos pré-definidos num intervalo de tempo fixo minimizando a energia gasta é resolvido utilizando o Princípio do Máximo de Pontryagin. Tirando partido do movimento circular induzido por um vórtice pontual, a análise foca-se no conjunto de controlos que actua apenas na coordenada radial do movimento. O controlo ótimo resultante depende explicitamente do tempo e admite uma expressão analítica.

O mesmo problema é considerado num ambiente viscoso no Capítulo 3. A viscosidade é modelada através de um vórtice de Lamb-Oseen e é encontrada uma extremal com dependência explícita do tempo. Contrariamente ao caso não viscoso, não é possível encontrar uma expressão analítica para o controlo ótimo, sendo o problema convertido num problema de procura de parâmetros, envolvendo dois parâmetros que estão relacionados com as coordenadas radial e angular do ponto inicial. O custo energético do processo aumenta com a viscosidade desde que a partícula mantenha o número de voltas em torno do vórtice. Se um aumento na viscosidade reduzir o número de voltas necessárias para uma solução do problema, o custo de energia cresce ainda mais.

No Capítulo 4 é proposto um método para estimar as circulações e posições de vórtices pontuais em $\mathbb{R}^2$ utilizando dados de trajectórias de partículas passivas na presença de

ruído Gaussiano. A abordagem divide-se em duas etapas: primeiramente, as circulações dos vórtices são estimadas a partir da velocidade das partículas passivas; seguidamente, as trajectórias dos vórtices são reconstruídas através de uma hierarquia de problemas de otimização. Cada um destes problemas requer a integração de um sistema de equações diferenciais durante um sub-intervalo de tempo específico. Estes sub-intervalos têm todos a mesma amplitude, determinada pela autocorrelação das trajectórias das partículas passivas.

O Capítulo 5 explora mais a fundo o problema proposto no Capítulo 3, apresentando alguns pontos que foram deixados por explorar no artigo original: é possível ter candidatos à trajectória ótima com diferentes números de voltas completas em torno do vórtice e, para minimizar a energia gasta, as soluções preferenciais são as que apresentam menor número de voltas. Além disso, observa-se que existem intervalos de viscosidade para os quais não é possível encontrar uma solução.

Finalmente, o Capítulo 6 apresenta um estudo analítico que caracteriza as ilhas atmosféricas em sistemas de dois vórtices pontuais. Tal é feito através do estudo da dinâmica de partículas passivas em $\mathbb{R}^2$: as trajectórias destas partículas de teste são utilizadas para encontrar os pontos de estagnação do sistema e as trajectórias especiais que particionam o plano bi-dimensional em regiões de comportamento dinâmico distinto. São encontradas as expressões que definem a fronteira das ilhas atmosféricas e utilizadas para calcular o perímetro e área destas regiões.

Esta tese contribui para uma melhor compreensão da dinâmica de vórtices e do controlo em fluidos impulsionados por vórtices, estabelecendo uma ponte entre estas duas áreas.

UNIVERSIDADE DO PORTO

Abstract

Faculdade de Ciências da Universidade do Porto

Departamento de Matemática

PhD in Applied Mathematics

Geometry and Control of Two-Dimensional Vortex-Driven Transport

by Gil Miguel Marques

This thesis develops a mathematical framework for the modelling and control of the motion of passive particles in vortex-driven flows. This is treated in $\mathbb{R}^2$, considering both inviscid and viscous vortex models.

Chapter 2 introduces a formulation for the modelling, control and optimisation of the motion of a passive particle advected by a point vortex. In such a flow, the control problem of moving a passive particle between two prescribed points within a fixed time, while minimising the energy expended, is solved by using Pontryagin's Maximum Principle. By taking advantage of the rotational motion induced by the point vortex, the analysis focuses on the set of controls that act only on the radial component of motion. The resulting optimal control is explicitly time-dependent and admits an analytical expression.

The same problem is considered in a viscous environment in Chapter 3. Viscosity is modelled via a Lamb–Oseen vortex, and an explicit time-dependent extremal is found. Unlike the inviscid scenario, it is not possible to derive an analytical expression for the optimal control, and the problem is transformed into a parameter search problem involving two parameters related to the radial and angular coordinates of the initial point. The energy cost of the process increases with viscosity as long as the passive particle maintains the number of full turns around the vortex. If increased viscosity reduces the number of full turns needed for a solution of the problem, the energy cost rises further.

Chapter 4 proposes a method for estimating the circulations and positions of point vortices in $\mathbb{R}^2$ by using data of trajectories of passive particles in the presence of Gaussian noise. The approach is divided into two steps: first, vortex circulations are estimated by using the velocities of the passive particles; second, the vortex trajectories are reconstructed through a hierarchy of optimisation problems. Each of these problems requires

the integration of a system of differential equations over a specific time sub-interval. The sub-intervals all have the same amplitude, determined by the autocorrelation of the passive particles'trajectories.

Chapter 5 explores further the problem posed in Chapter 3, presenting some points that were left unexplored in the original article: it is possible to have optimal trajectory candidates with different numbers of full turns around the vortex and the solutions with fewer full turns are preferred for minimising the energy spent in the process. Furthermore, it is observed that there exist ranges of viscosity for which no solution can be found.

Finally, Chapter 6 presents an analytical study that characterises atmospheric islands in systems of two point vortices. This is achieved by studying the dynamics of passive particles in $\mathbb{R}^2$: the trajectories of these test particles are used to find the stagnation points of the system and the special trajectories that partition the two-dimensional plane into regions of distinct dynamical behaviour. Analytical expressions that define the boundary of the atmospheric islands are derived and used to compute their perimeter and area.

This thesis contributes to a better understanding of the dynamics of vortices and control on vortex flows, providing a bridge between these two areas.

Contents

List of Figures

List of Tables

Errata

The articles included in this thesis are reproduced in their published form. After publication, a small number of typographical errors were identified. These corrections do not affect the scientific content, results, or conclusions of the work.

Chapter 2

Page 21, Figure 2.3: In the third line of the caption, “above” should read “below”.

Page 24, Equation (2.25): t^* should read $\tilde{t}$. The A in the denominator of the expression for $\theta(t)$ should be removed.

Chapter 3

Page 40, line 21: $\tilde{\theta}$ should read $\tilde{t}$.

Page 49, line 12: “that that” should read “that”.

Chapter 5

Page 78, line 13: “three or more full turns” should read “three full turns”.

Chapter 6

Page 92, line 12: $e^{i\theta t}$ should read $e^{-i\theta t}$.

Page 95, line 11: “the the” should read “the”.

Chapter 1

Introduction

Transport phenomena in fluids play a pivotal role in a wide variety of physical systems, many of which are essential to human life. These systems encompass a broad spectrum of applications and range from small to very large scale systems. For instance, in a geophysical context, the advection of air parcels and tracers can impact weather patterns and climate dynamics [1], [2]. In oceanography, particle transport controls mixing and the evolution of coherent structures such as eddies and gyres [3]. At small scales, fluid-driven transport emerges in microfluidic devices and biological flows [4]. At large scales, these processes are responsible for shaping the dynamics of atmospheres and oceans, and can even influence astrophysical systems [5] such as galactic interactions and galaxy mergers.

A common feature across these diverse settings is the presence of coherent, vortex-like structures. Vortices shape their surroundings, impose a local velocity field, and strongly influence particle transport. Consequently, understanding the dynamics of passive particles in vortex-dominated flows allows for a deeper understanding of predicting transport, designing effective control strategies, and extracting information about the underlying fluid motion.

From a modelling perspective, a vortex-based description of a flow provides a powerful balance between physical relevance and mathematical tractability. Idealised vortex models capture crucial features present in real flows—such as rotation, trapping, and long-range interactions—while significantly reducing the mathematical complexity of the classical Navier–Stokes equations. By reducing the infinite-dimensional fluid system to a finite-dimensional dynamical system, vortex-based models enable the use of analytical tools from Hamiltonian mechanics, optimal control, and geometric analysis, which are generally intractable in the full Navier–Stokes framework.

There is also a growing interest in how one can influence, or even exploit, transport processes. Advances in various fields have motivated a panoply of questions, such as: how can a particle be steered efficiently in a complex flow [6] ? How much control effort is required to overcome natural advection [7] ? How can observations of particle trajectories be used to infer hidden flow structures [8], [9] ? Questions like these naturally lead to problems in optimal control and estimation, formulated directly in a Lagrangian framework.

Concurrently, the geometry of particle transport plays a fundamental role in determining long-term behaviour. In incompressible flows, the domain is partitioned into dynamically distinct regions by separatrices and transport barriers. Vortex-dominated flows are a particularly rich environment for this, giving rise to coherent structures like vortex cores and bounded regions of motion that strongly constrain particle trajectories. Understanding the formation and persistence of these structures is crucial for explaining certain observed phenomena, such as particle trapping and mixing.

This thesis is motivated by the intricacies between the themes mentioned above: the physics of vortex-driven flows, the geometry of Lagrangian transport, and the analysis of control and estimation problems for passive particles.

1.1 Fluid Dynamics and Lagrangian Transport

Understanding fluid dynamics is essential for the study of the transport of particles, tracers, and other advected quantities. The dynamics of a Newtonian fluid are described by conservation laws for the mass, momentum, and energy, which are mathematically written as differential equations:

$$\frac{\partial \rho}{\partial t} + \nabla \cdot (\rho \mathbf{u}) = 0\,, \tag{1.1}$$

$$\rho\left(\frac{\partial \mathbf{u}}{\partial t} + (\mathbf{u}\cdot\nabla)\mathbf{u}\right) = -\nabla p + \nabla\cdot\boldsymbol{\tau} + \rho\mathbf{f}\,, \tag{1.2}$$

$$\frac{\partial E}{\partial t} + \nabla\cdot\Big((E+p)\mathbf{u}\Big) = \nabla\cdot(\boldsymbol{\tau}\cdot\mathbf{u}) + \nabla\cdot(\kappa\nabla T) + \rho\mathbf{f}\cdot\mathbf{u}\,, \tag{1.3}$$

where $\mathbf{u}(\mathbf{x}, t)$ is the velocity field, $\rho(\mathbf{x}, t)$ is the density of the fluid, $p(\mathbf{x}, t)$ is the pressure, $\boldsymbol{\tau}$ is the viscous stress tensor, $\mathbf{f}$ is the sum of all the external body forces, E is the total energy per unit volume, T is the temperature, and κ is the thermal conductivity. $\mathbf{x}$ and t represent, respectively, the space and time coordinates. Equations (1.2) are here presented in their most general, compressible form, and are called the *Navier–Stokes equations.*

For a Newtonian fluid, the viscous stress tensor can be written as

$$\boldsymbol{\tau} = \mu(\nabla \mathbf{u} + (\nabla \mathbf{u})^{\mathsf{T}}) + \lambda(\nabla \cdot \mathbf{u})\mathbf{I},$$

where μ and λ are the dynamic and bulk viscosities, respectively, and are also known as the *Lamé parameters*.

1.1.1 The Incompressible Navier–Stokes Equations

In the majority of flows (e.g., most liquids, oceans, the lower atmosphere), density variations are small compared to some reference value ρ_0. Likewise, pressure fluctuations are also moderate relative to the mean. In such a regime, fluid parcels experience very small volumetric changes and the flow can be treated as *incompressible* (i.e., a fluid parcel preserves its volume as it evolves). By rewriting the mass conservation equation (1.1) in terms of the material derivative*,

$$\frac{D\rho}{Dt} + \rho\,\nabla \cdot \mathbf{u} = 0, \tag{1.4}$$

it is clear that, if density variations are negligible, i.e. $\rho \approx \rho_0$ and $\frac{D\rho}{Dt} \approx 0$, equation (1.4) is equivalent to

$$\nabla \cdot \mathbf{u} = 0. \tag{1.5}$$

Thus, incompressibility produces a divergence-free velocity field. Under this assumption, the mass conservation equation reduces to (1.5), and the momentum equation simplifies to the incompressible *Navier–Stokes equations*,

$$\frac{\partial \mathbf{u}}{\partial t} + (\mathbf{u} \cdot \nabla)\mathbf{u} = -\frac{1}{\rho_0}\nabla p + \nu \nabla^2 \mathbf{u} + \mathbf{f}, \tag{1.6}$$

where $\nu = \mu/\rho_0$ is the kinematic viscosity. The energy equation is decoupled from the momentum dynamics and is usually treated separately.

Equations (1.5) and (1.6) together constitute the standard form used in the study of incompressible flows and serve as the starting point for Lagrangian particle transport analysis.

*The material derivative of a scalar or vector field $\phi(\mathbf{x}, t)$ is defined as $\frac{D\phi}{Dt} := \partial_t \phi + \mathbf{u} \cdot \nabla \phi$, and represents the rate of change of ϕ following a fluid parcel.

It is important to note that any sufficiently smooth vector field that decays to zero rapidly enough at infinity can be decomposed in a solenoidal (divergence-free) and an irrotational (curl-free) component. This decomposition is due to Helmholtz [10], and is usually called Helmholtz decomposition. An attempt to gather the most common techniques for the computation of the decomposition, as well as a proof of Helmholtz's Theorem, can be found in [11].

Thus, a solution of the Navier–Stokes equations that satisfies the conditions of Helmholtz's Theorem can be written as

$$\mathbf{u} = \underbrace{\nabla \times \boldsymbol{\psi}}_{\text{divergence-less component}} + \underbrace{\nabla \varphi}_{\text{curl-less component}}, \tag{1.7}$$

where $\boldsymbol{\psi}$ is a vector field (which can be chosen as solenoidal by fixing the gauge) and φ is a scalar field, usually called the velocity potential.

Taking the divergence and curl of $\mathbf{u}$ in this form yields

$$\nabla \cdot \mathbf{u} = \underbrace{\nabla \cdot (\nabla \times \boldsymbol{\psi})}_{0} + \nabla \cdot \left(\nabla \varphi\right) = 0 \quad \Leftrightarrow \quad \nabla^2 \varphi = 0, \tag{1.8}$$

$$\nabla \times \mathbf{u} = \nabla \times (\nabla \times \boldsymbol{\psi}) + \underbrace{\nabla \times \left(\nabla \varphi\right)}_{0} = \nabla \underbrace{(\nabla \cdot \boldsymbol{\psi})}_{0} - \nabla^2 \boldsymbol{\psi} \quad \Leftrightarrow \quad \nabla^2 \boldsymbol{\psi} = -\nabla \times \mathbf{u}, \tag{1.9}$$

highlighting that the evolution of each component is governed by distinct principles. In fact, the curl-less component corresponds to a potential flow, which can involve sources or sinks. However, these sources and sinks would violate the incompressible condition, and thus, this component does not contribute to the velocity field of incompressible flows.

1.1.2 Eulerian and Lagrangian Perspectives

Equation (1.6) holds in an *Eulerian* framework, where the velocity and pressure are observed at fixed points in space. This is the natural frame of reference when analysing global flow structures such as vortices, jets, and shear layers.

In contrast, in order to track individual fluid parcels or passive particles along their trajectories, using a *Lagrangian* framework is more natural. The idea of the Lagrangian viewpoint is that a particle located at $\mathbf{x}(t)$ evolves according to

$$\frac{d\mathbf{x}}{dt} = \mathbf{u}(\mathbf{x}(t), t)\,. \tag{1.10}$$

Since $\mathbf{x}(t)$ represents the actual trajectories of particles, this approach is particularly useful when studying particle transport and mixing. It also highlights how coherent structures, such as vortices, influence particle trajectories over time.

These frameworks complement each other: while the Eulerian approach provides insight into the global structure of the flow, the Lagrangian description captures the dynamics of particle movement and how they interact with coherent features. In vortex-dominated flows, the Lagrangian perspective is notably valuable, as it facilitates the analysis of transport barriers, trapping regions, and the design of control strategies for advected particles.

1.2 Vorticity Formulation and Two-Dimensional Flows

In many observed phenomena, the dynamics are clearly influenced by rotational effects, with vortex or vortex-like structures playing a fundamental role in the dynamics of a system. This motivates the introduction of a quantity that measures the local rotation of a flow: the *vorticity* is defined as the curl of the velocity field,

$$\boldsymbol{\omega} = \nabla \times \mathbf{u} \,. \tag{1.11}$$

In order to obtain an equation for the evolution of vorticity, it suffices to take the curl of the (incompressible) Navier–Stokes equations (1.6). This yields the *vorticity equation*,

$$\frac{\partial \boldsymbol{\omega}}{\partial t} + (\mathbf{u} \cdot \nabla)\boldsymbol{\omega} = (\boldsymbol{\omega} \cdot \nabla)\mathbf{u} + \nu \nabla^2 \boldsymbol{\omega} + \nabla \times \mathbf{f} \,, \tag{1.12}$$

where the pressure term vanishes due to the identity $\nabla \times \nabla p = \mathbf{0}$. The term $(\boldsymbol{\omega} \cdot \nabla)\mathbf{u}$ vanishes in a two-dimensional environment and represents vortex stretching and tilting [12], a unique feature of three-dimensional flows that plays a fundamental role in the development of turbulence.

Some useful identities can be obtained by taking the divergence and curl of $\boldsymbol{\omega}$:

$$\nabla \cdot \boldsymbol{\omega} = \nabla \cdot (\nabla \times \mathbf{u}) = 0 \,, \tag{1.13}$$

$$\nabla \times \boldsymbol{\omega} = \nabla \times (\nabla \times \mathbf{u}) = \nabla (\nabla \cdot \mathbf{u}) - \nabla^2 \mathbf{u} \,. \tag{1.14}$$

The first identity follows from the fact that the curl of any sufficiently smooth vector field is divergence-free and therefore holds independently of any assumptions on the flow.

The second identity follows from vector calculus and, under the incompressibility condition, $\nabla \cdot \mathbf{u} = 0$, reduces to

$$\nabla \times \boldsymbol{\omega} = -\nabla^2 \mathbf{u}\,. \tag{1.15}$$

This relation shows that, in incompressible flows, the velocity field can be recovered from the vorticity by solving a Poisson problem, subject to appropriate boundary conditions.

Furthermore, if an incompressible flow satisfies Helmholtz's Theorem, equation (1.9) directly relates the solenoidal vector field $\boldsymbol{\psi}$ to the vorticity: $\nabla^2 \boldsymbol{\psi} = -\boldsymbol{\omega}$. This yields a Poisson equation for each component of $\boldsymbol{\psi}$. Formally, the solution to this can be written as

$$\boldsymbol{\psi}(\mathbf{x}) = \int G(\mathbf{x} - \mathbf{x_0})\, \boldsymbol{\omega}(\mathbf{x_0})\, d\mathbf{x_0}\,, \tag{1.16}$$

where the integral is over the whole space and Green's function $G(\mathbf{x})$ depends on the geometry of the space where the problem is posed. In particular, for the unbound spaces $\mathbb{R}^2$ and $\mathbb{R}^3$,

$$G(\mathbf{x}) = \begin{cases} -\dfrac{1}{2\pi} \log \|\mathbf{x}\|\,, & \text{in } \mathbb{R}^2 \\ \dfrac{1}{4\pi\|\mathbf{x}\|}\,, & \text{in } \mathbb{R}^3 \end{cases}. \tag{1.17}$$

Hence, for an incompressible flow, the velocity field can be computed easily from the vorticity field:

$$\mathbf{u}(\mathbf{x}) = \nabla \times \boldsymbol{\psi}(\mathbf{x}) = \nabla \times \int G(\mathbf{x} - \mathbf{x_0})\, \boldsymbol{\omega}(\mathbf{x_0})\, d\mathbf{x_0} = \int \nabla G(\mathbf{x} - \mathbf{x_0}) \times \boldsymbol{\omega}(\mathbf{x_0})\, d\mathbf{x_0}\,. \tag{1.18}$$

Alternatively, in matrix form, the velocity field can be expressed as

$$\mathbf{u}(\mathbf{x}) = \int \mathbf{K}(\mathbf{x} - \mathbf{x_0})\, \boldsymbol{\omega}(\mathbf{x_0})\, d\mathbf{x_0}\,, \tag{1.19}$$

where $K(\mathbf{x})$ is the Biot-Savart Kernel:

$$\mathbf{K}(\mathbf{x}) = \begin{cases} \dfrac{1}{2\pi\|\mathbf{x}\|^2}(-y, x)\,, & \text{in } \mathbb{R}^2 \\ \dfrac{1}{4\pi\|\mathbf{x}\|^3} \begin{pmatrix} 0 & z & -y \\ -z & 0 & x \\ y & -x & 0 \end{pmatrix}, & \text{in } \mathbb{R}^3 \end{cases}. \tag{1.20}$$

In a two-dimensional incompressible flow, the vorticity formulation of fluid dynamics is especially beneficial. The velocity field takes the form

$$\mathbf{u}(x, y, t) = (u(x, y, t),\, v(x, y, t),\, 0)\,, \tag{1.21}$$

which originates a vorticity vector with only one non-zero component:

$$\boldsymbol{\omega} = (0,\, 0,\, \omega)\,, \qquad \omega = \frac{\partial v}{\partial x} - \frac{\partial u}{\partial y}\,. \tag{1.22}$$

Thus, vorticity gets effectively reduced to a scalar quantity, and the two-dimensional vorticity equation for a system where no external forces are applied can be written in scalar form as

$$\frac{\partial \omega}{\partial t} + (\mathbf{u} \cdot \nabla)\omega = \nu \nabla^2 \omega\,. \tag{1.23}$$

Notice that the vortex-stretching term vanishes because $\boldsymbol{\omega} \cdot \nabla = \omega \dfrac{\partial}{\partial z}$, simplifying the dynamics greatly.

Two-dimensional flows are particularly interesting since numerous flows show some degree of stratification where the dynamics happen in layers that behave approximately as two-dimensional systems. The absence of vortex stretching also enriches the geometric structure of the flow, making it even possible to formulate the problem in a Hamiltonian framework under certain conditions.

1.3 Point Vortex Dynamics

The main motivation for point vortex models comes from what is seen in real flows: vortex-like structures. In a three-dimensional vorticity field, any curve that is everywhere tangent to the local vorticity vector is called a *vortex line*. A collection of vortex lines passing through a closed curve in the fluid form a surface that is referred to as *vortex tube*, and are thus defined by the equation $\boldsymbol{\omega} \cdot \mathbf{n} = 0$ ($\mathbf{n}$ represents the normal vector to the surface). Examples of vortex tubes in nature include structures like tornadoes and waterspouts, while man-made vortex tubes can be observed, for instance, at the tips of aircraft wings.

The strength of a vortex tube (i.e., how much it affects rotational motion around it) can be quantified by the *circulation*, which is defined as

$$\Gamma = \oint_C \mathbf{u} \cdot d\mathbf{s} = \int_S \boldsymbol{\omega} \cdot \mathbf{n} dS\,, \tag{1.24}$$

where C is any simple closed curve that encircles the vortex tube (e.g., a curve lying in a cross-section of the tube) and S is any surface bounded by C, with orientation given by the normal vector $\mathbf{n}$. Notice that, since $\nabla \cdot \boldsymbol{\omega} = 0$, the flux of vorticity through S is invariant under continuous deformations of the surface S within the vortex tube. Consequently, the circulation is independent of the chosen curve C. Vortex tubes must thus be closed, extend into infinity or terminate at solid boundaries or fluid-fluid interfaces.

Another important characteristic of circulation is that it stays constant in time for any inviscid flow (i.e., a flow with zero viscosity). This result is a consequence of Kelvin's circulation theorem. In the presence of viscosity, the dissipation of vorticity introduces frictional losses and time dependence, which also cause changes in the geometric configuration of the tube [13]. Further discussion on the geometry of vortex tubes can be found in [14], [15].

Finally, if a vortex tube has a cross-section with infinitesimal dimension, it is called a *vortex filament.*

1.3.1 The Point Vortex Model

The vorticity distribution in a plane that is locally orthogonal to a vortex filament is highly concentrated in the vicinity of the centreline of the filament, located at $\mathbf{x_0}$. Thus, in this plane, the vorticity distribution can be approximated by

$$\omega\left(\mathbf{x}\right) = \frac{\Gamma}{2\pi}\phi_{\epsilon}\left(\mathbf{x} - \mathbf{x_0}\right), \tag{1.25}$$

where $\phi_{\epsilon}\left(\mathbf{x}\right) = \phi\left(\mathbf{x}/\epsilon\right)/\epsilon$ and ϕ is a suitable radially symmetric function whose integral over all space equals 1.

In the limit case $\epsilon \to 0$, this object is called a *point vortex*, concentrating the vorticity in a single point in space. Mathematically this corresponds to choosing $\phi_{\epsilon} = \delta\left(\mathbf{x}\right)$, the usual Dirac-delta function.

This motivates the study of a simplified two-dimensional problem that reduces the study of vortex filaments in a three-dimensional space to a set of local problems in two-dimensional spaces.

The *point vortex model* is in fact a singular solution of the two-dimensional vorticity equation in an incompressible flow with zero viscosity (i.e., $\nu = 0$). The vorticity is concentrated at discrete points in space, each of which corresponds to a point vortex. A set of n point vortices with circulations $\Gamma_k \in \mathbb{R}$, located at $\mathbf{x}_k\left(t\right)$ $(k = 1, \ldots, n)$ is represented by the vorticity distribution

$$\omega(\mathbf{x},t) = \sum_{k=1}^{n} \Gamma_k \, \delta\left(\mathbf{x} - \mathbf{x}_k(t)\right) . \tag{1.26}$$

In two dimensions, equation (1.9) reduces to the one-dimensional equation $\nabla^2\psi = -\omega$. When solved for the vorticity distribution in (1.26), this yields

$$\psi(\mathbf{x},t) = -\frac{1}{2\pi} \sum_{k=1}^{n} \Gamma_k \log \|\mathbf{x} - \mathbf{x}_k(t)\| . \tag{1.27}$$

In the context of two-dimensional flows, ψ is usually called the *stream function* of the system. Since the flow is incompressible, velocity can easily be retrieved from the stream function as

$$\mathbf{u}(\mathbf{x},t) = \left(u(\mathbf{x},t), v(\mathbf{x},t)\right) = \left(\frac{\partial\psi}{\partial y}, -\frac{\partial\psi}{\partial x}\right) , \tag{1.28}$$

generating a velocity field that is induced by the point vortices,

$$u(\mathbf{x},t) = -\frac{1}{2\pi} \sum_{k=1}^{n} \Gamma_k \frac{y - y_k(t)}{\|\mathbf{x} - \mathbf{x}_k(t)\|^2} , \qquad v(\mathbf{x},t) = \frac{1}{2\pi} \sum_{k=1}^{n} \Gamma_k \frac{x - x_k(t)}{\|\mathbf{x} - \mathbf{x}_k(t)\|^2} , \tag{1.29}$$

which enables a study of the point vortex model in a Lagrangian framework. A more compact form of the Lagrangian equations of motion is obtained by using complex variables $z = x + iy$ $(i^2 = -1)$. In this formulation, the trajectory of a particle located at a position $z(t)$ in a system of n point vortices evolves according to

$$\dot{z}^*(t) = \frac{1}{2\pi i} \sum_{k=1}^{n} \frac{\Gamma_k}{z(t) - z_k(t)} , \tag{1.30}$$

where * represents the complex conjugate.

Since point vortices are elements of the flow, their trajectories must also evolve according to these equations of motion. In fact, a point vortex located at $z_j(t)$ is advected by the other $n-1$ vortices, satisfying the equation

$$\dot{z}_j^*(t) = \frac{1}{2\pi i} \sum_{\substack{k=1 \\ k\neq j}}^{n} \frac{\Gamma_k}{z_j(t) - z_k(t)} . \tag{1.31}$$

Furthermore, the dynamical equations for the movement of point vortices can be rewritten in a Hamiltonian formalism as

$$\Gamma_k \dot{x}_k(t) = \frac{\partial H}{\partial y_k} , \qquad \Gamma_k \dot{y}_k(t) = -\frac{\partial H}{\partial x_k} , \qquad k = 1\ldots,n , \tag{1.32}$$

where H represents the Hamiltonian and is given by

$$H(\mathbf{x}_1, \dots, \mathbf{x}_n, t) = -\frac{1}{4\pi} \sum_{k=1}^{n} \sum_{\substack{j=1 \\ j \neq k}}^{n} \Gamma_k \Gamma_j \log \|\mathbf{x}_k(t) - \mathbf{x}_j(t)\| \,. \tag{1.33}$$

Likewise, the motion of a passive particle in the flow can be written in a Hamiltonian framework by identifying the particle Hamiltonian with the stream function, ψ, of the system.

The fact that this model admits a natural Hamiltonian formulation provides a powerful and alternative framework for the understanding of conserved quantities and phase-space geometry of these systems. In particular, the Hamiltonian of the point vortex model is conserved in time, simplifying the analysis of the dynamics further. A comprehensive analysis of the Hamiltonian formalism in point vortex models can be found in [16].

1.3.2 Viscosity and the Breakdown of Hamiltonian Structure

While the point vortex model captures essential inviscid features, neglecting viscous effects is not appropriate in every system. The *Lamb–Oseen vortex* is the solution of the two-dimensional incompressible vorticity equation (1.23) in a viscous flow for an initial vorticity distribution of the form $\omega(z, t = 0) = \Gamma\delta(z - z_0)$, i.e., a point vortex with circulation Γ, located at z_0. This originates a vorticity distribution that is diffused radially outward with a Gaussian profile:

$$\omega(z, t) = \frac{\Gamma}{4\pi\nu t} \exp\left(-\frac{|z - z_0|^2}{4\nu t}\right). \tag{1.34}$$

An important result on the Lamb–Oseen vortex is that it is an asymptotically stable attracting solution of the vorticity equation for any integrable initial vorticity configuration, as was proven by Gallay & Wayne [17]. For instance, the superposition of n point vortices $\omega(z, t = 0) = \sum_{k=1}^{n} \Gamma_k \delta(z - z_k)$ is indeed such a configuration.

This idea originates the *multi-Gaussian model* of point vortices, which assumes that the vorticity field is a superposition of n Lamb–Oseen vortices at all times: the vorticity generated by each vortex spreads axisymmetrically as if the vortex was isolated, modelling the diffusive term in the vorticity equation ($\nu\nabla^2\omega$); the trajectory of the centre of each vortex is advected by the remaining $n - 1$ vortices, originating a trajectory directed by the velocity field, as expected due to the convective term $(\mathbf{u} \cdot \nabla)\,\omega$ in the vorticity equation.

Gallay also showed that under certain conditions, the solution of the Navier–Stokes equation in the inviscid limit $\nu \to 0$ for δ-Dirac initial conditions converges to a superposition of Lamb–Oseen vortices [18]. This provides yet another reason for the viability of the multi-Gaussian model in the description of fluids.

Thus, for the multi-Gaussian model with n Lamb–Oseen vortices, with circulations Γ_k and located at z_k ($k = 1, \ldots, n$), the vorticity distribution can be written

$$\omega(z,t) = \frac{1}{4\pi\nu t} \sum_{k=1}^{n} \Gamma_k \exp\left(-\frac{|z - z_k|^2}{4\nu t}\right), \tag{1.35}$$

originating a velocity field

$$\dot{z}^*(z,t) = \frac{1}{2\pi i} \sum_{k=1}^{n} \frac{\Gamma_k}{z - z_k} \left[1 - \exp\left(-\frac{|z - z_k|^2}{4\nu t}\right)\right]. \tag{1.36}$$

Similar to the inviscid scenario, the equations of motion for a Lamb–Oseen vortex identified by the index j are

$$\dot{z}_j^*(z,t) = \frac{1}{2\pi i} \sum_{\substack{k=1 \\ k \neq j}}^{n} \frac{\Gamma_k}{z_j - z_k} \left[1 - \exp\left(-\frac{|z_j - z_k|^2}{4\nu t}\right)\right]. \tag{1.37}$$

The inclusion of viscosity breaks the simplified Hamiltonian structure present in the point vortex model, as vorticity is dissipated through viscous forces. As a consequence, the velocity field also decays in time and cannot be represented by a time-independent Hamiltonian. However, it is possible to write a generalized Hamiltonian such that Hamilton's equations still hold [19]:

$$H(z_1, \ldots, z_n, t) = \frac{1}{2\pi} \sum_{k=1}^{n} \sum_{j>k} \Gamma_k \Gamma_j \int_0^{\ell_{kj}} \frac{1}{s} \left[1 - \exp\left(-\frac{s^2}{4\nu t}\right)\right] ds\,, \tag{1.38}$$

where $\ell_{kj} = |z_k - z_j|$.

While the explicit time-dependence of the Hamiltonian breaks the integrability of the system, the dynamics of particles remain Hamiltonian for each fixed time.

1.4 Scope and Outline of the Thesis

This thesis investigates the dynamics of two-dimensional vortex flows, focusing on aspects related to the geometrical characterisation of coherent structures in the flow, optimal control of passive particles and tracking of point vortices. The results are presented in the form of five published articles in Chapters 2–6 addressing, respectively

- the optimal control of a passive particle in an inviscid two-dimensional flow,
- the optimal control of a passive particle in a viscous two-dimensional flow,
- the estimation of vortex parameters from Lagrangian particle observations,
- a further analysis on the optimal control of a passive particle in a viscous two-dimensional flow
- the geometric characterisation of regularity regions in a system of two point vortices.

Chapter 7 closes the thesis with a discussion and summary of the findings in this work. The references at the end of this Chapter are solely the ones cited in this Introduction. A General Bibliography with all references listed throughout this thesis can be found at the end.

References

[1] G. K. Vallis, *Atmospheric and Oceanic Fluid Dynamics*. Cambridge, U.K.: Cambridge University Press, 2006, p. 745. DOI: 10.1017/9781107588417.

[2] J. Weiss and A. Provenzale, *Transport and Mixing in Geophysical Flows* (Lecture Notes in Physics). Springer Berlin Heidelberg, 2008, ISBN: 9783540752141. DOI: 10.1007/978-3-540-75215-8.

[3] M. C. Denes, G. Froyland, and S. R. Keating, "Persistence and material coherence of a mesoscale ocean eddy," *Phys. Rev. Fluids*, vol. 7, p. 034 501, 3 Mar. 2022. DOI: 10.1103/PhysRevFluids.7.034501.

[4] M. Ferreira, V. Carvalho, J. Ribeiro, R. A. Lima, S. Teixeira, and D. Pinho, "Advances in microfluidic systems and numerical modeling in biomedical applications: A review," *Micromachines*, vol. 15, no. 7, 2024, ISSN: 2072-666X. DOI: 10.3390/mi15070873.

[5] C. J. Clarke and R. F. Carswell, *Principles of Astrophysical Fluid Dynamics*. 2003. DOI: 10.2277/0521853311.

[6] J. Buzhardt and P. Tallapragada, "Controlled transport of fluid particles by micro-rotors in a stokes flow using linear transfer operators," *Physics of Fluids*, vol. 36, no. 3, p. 032 021, Mar. 2024, ISSN: 1070-6631. DOI: 10.1063/5.0195528.

[7] C. Calascibetta, L. Biferale, F. Borra, A. Celani, and M. Cencini, "Optimal tracking strategies in a turbulent flow," *Communications Physics*, vol. 6, no. 1, p. 256, 2023. DOI: 10.1038/s42005-023-01366-y.

[8] D. Chang, C. R. Edwards, F. Zhang, and J. Sun, "A data assimilation framework for data-driven flow models enabled by motion tomography," *International Journal of Intelligent Robotics and Applications*, vol. 3, no. 2, pp. 158–177, 2019. DOI: 10.1007/s41315-019-00092-5.

[9] K. Zhou and S. J. Grauer, *On the joint observability of flow fields and particle properties from lagrangian trajectories: Evidence from neural data assimilation*, 2025. DOI: 10.48550/arXiv.2510.00479.

[10] H. Helmholtz, "Über integrale der hydrodynamischen gleichungen, welche den wirbelbewegungen entsprechen.," ger, *Journal für die reine und angewandte Mathematik*, vol. 55, pp. 25–55, 1858.

[11] H. Bhatia, G. Norgard, V. Pascucci, and P.-T. Bremer, "The helmholtz-hodge decomposition—a survey," *IEEE Transactions on Visualization and Computer Graphics*, vol. 19, no. 8, pp. 1386–1404, 2013. DOI: 10.1109/TVCG.2012.316.

[12] H. Tennekes and J. L. Lumley, *A First Course in Turbulence*. Cambridge, Massachusetts: MIT Press, 1972.

[13] G. K. Batchelor, *An Introduction to Fluid Dynamics* (Cambridge Mathematical Library). Cambridge University Press, 2000. DOI: 10.1017/CBO9780511800955.

[14] C. Truesdell, *The Kinematics of Vorticity* (Indiana University Publications Science Series 19). Bloomington, Indiana: Indiana University Press, 1954.

[15] H. K. Moffatt, "The degree of knottedness of tangled vortex lines," *Journal of Fluid Mechanics*, vol. 35, pp. 117–129, Jan. 1969. DOI: 10.1017/S0022112069000991.

[16] P. Newton, *The N-Vortex Problem: Analytical Techniques* (Applied Mathematical Sciences). Springer New York, 2010, ISBN: 9781441929167. DOI: 10.1007/978-1-4684-9290-3.

[17] T. Gallay and C. E. Wayne, "Global stability of vortex solutions of the two-dimensional navier-stokes equation," *Communications in Mathematical Physics*, vol. 255, no. 1, pp. 97–129, 2005. DOI: 10.1007/s00220-004-1254-9.

[18] T. Gallay, "Interaction of vortices in weakly viscous planar flows," *Archive for Rational Mechanics and Analysis*, vol. 200, no. 2, pp. 445–490, 2011. DOI: 10.1007/s00205-010-0362-2.

[19] S.-C. Kim and S.-I. Sohn, "Interactions of three viscous point vortices," *Journal of Physics A: Mathematical and Theoretical*, vol. 45, no. 45, p. 455 501, Oct. 2012. DOI: 10.1088/1751-8113/45/45/455501.

Chapter 2

Optimal Control of a Passive Particle Advected by a Point Vortex

Published in Advanced Research in Technologies, Information, Innovation and Sustainability, 2021

Gil Marques, Teresa Grilo, Sílvio Gama and Fernando L. Pereira

Abstract: The objective of this work is to develop a mathematical framework for modeling, control and optimization of the movement of a passive particle advected by a point vortex. Dynamic equations are rewritten in polar coordinates, where the control acts only on the radial coordinate. The optimal control found is explicitly time dependent. This framework should provide a sound basis for the design and control of new advanced engineering systems arising in many important classes of applications, some of which encompass underwater gliders and mechanical fishes.

The research effort has been focused in applying necessary conditions of optimality for some class of flow driven dynamic control systems, by using the vortex methods. The control problem of moving a passive particle between two given points driven by this class of flow in a prescribed time and minimizing the energy of the process has been solved by using the maximum principle.

2.1 Introduction

In this paper, we present a research work being developed in the framework of optimal control of dynamic systems, whose state evolves through the interaction of ordinary differential equations [1], [2], [3], which will provide a sound basis for the design and control of new advanced engineering systems. In Figure 2.1, two representative examples of the class of applications are considered: (i) underwater gliders, i.e., winged autonomous underwater vehicles (AUVs), which locomote by modulating their buoyancy and their attitude in its environment; and (ii) robotic fishes. Motion modeling of these two types of systems can be found in [4], [5], [6], [7], [8].

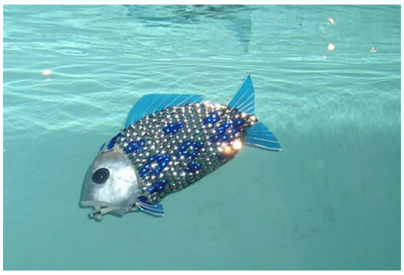

Figure 2.1: Underwater glider (left), robotic fish (right).

A vortex [9], [10] is a point with circulation that generates a rotational flow field. Let us consider a 2D flow specified in the complex plane by N point vortices each one located in $z_i, i = 1, \dots, N$ [11], [12], [13], [14]. In this context, the motion of any passive particle advected by this flow is given by the following dynamic equation

$$\dot{z}^* (t) = \frac{1}{2\pi i} \sum_{i=1}^{N} \frac{k_i}{z(t) - z_i(t)} \,. \tag{2.1}$$

However, in this article, we consider the case for which the dynamic system is driven by one vortex and we solve a control problem that consists in moving a particle between two given points, by applying necessary conditions of optimality in the form of a maximum principle [15], [16].

2.2 Velocity field driven by a vortex

Consider a flow with a point vortex at the origin $(0,0)$, with vorticity k, and let $z(t) = x(t) + y(t)i$ be the position of the particle placed in this flow, at time t. In the complex form, the dynamic equations of the particle positioned in z subject to the velocity field given by the vortex is

$$\dot{z}^{*}(t) = \frac{1}{2\pi i}\frac{k}{z(t)} \ . \tag{2.2}$$

In polar coordinates, the position of the particle is given by

$$z(t) = \rho(t)\, e^{i\theta(t)} \,, \tag{2.3}$$

and the derivative, with respect to t, is

$$\dot{z}(t) = \dot{\rho}(t) e^{i\theta(t)} + i\rho(t)\,\dot{\theta}(t)\, e^{i\theta(t)} \ . \tag{2.4}$$

Therefore, the complex conjugate of the derivative is

$$\dot{z}^{*}(t) = \dot{\rho}(t)\, e^{-i\theta(t)} - i\rho(t)\,\dot{\theta}(t)\, e^{-i\theta(t)} \,, \tag{2.5}$$

and, from (2.2) and (2.5), we obtain

$$\dot{\rho}(t) - i\rho(t)\,\dot{\theta}(t) = -i\frac{k}{2\pi}\frac{1}{\rho(t)} \ . \tag{2.6}$$

By separating the equalities of the real and imaginary parts of both sides of this equation, we have the following dynamic equations of the particle in polar form

$$\begin{cases} \dot{\rho}(t) = 0 \\ \dot{\theta}(t) = \frac{k}{2\pi}\frac{1}{\rho^{2}(t)} \end{cases} \tag{2.7}$$

So, the position of the particle, in each time t, is given by

$$z(t) = \rho(0)\, e^{i\left(\dfrac{kt}{2\pi\rho^{2}(0)} + \theta(0)\right)} \ . \tag{2.8}$$

In figure 2.2, we have the trajectory of the particle with the initial position in (x_0, y_0), where the circulation of the vortex is $k > 0$. For the case $k < 0$, the trajectory would be the same, but with clockwise motion.

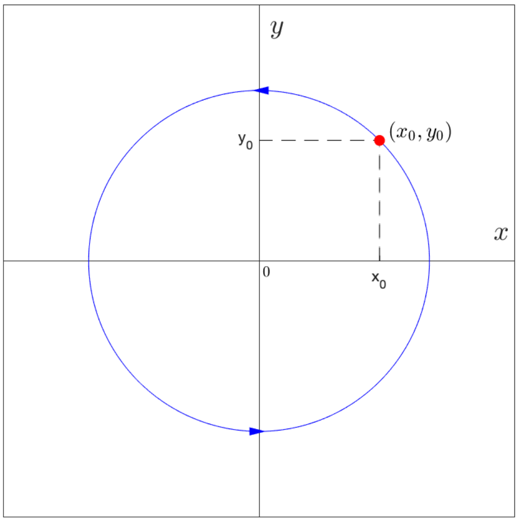

FIGURE 2.2: Trajectory of a free particle, initially located at (x_0, y_0), advected by a point vortex located at the origin ($k > 0$).

2.3 Control problem

Consider a flow like the one presented in Section 2.2 and a passive particle placed in the flow with initial position (x_0, y_0). The objective of this work is to determine the control function $u(\cdot)$ to be applied to the particle, so that it will move in the flow from the given initial position to the end point (x_f, y_f), minimizing the cost function $g(X(T))$, while subject to the flow field. Let $X(t) = (x(t), y(t))$ be the position of the particle at time t.

The control problem can be then formulated as follows:

$$\begin{cases} \text{Minimize} \quad g(X(T)) \\ \text{subject to} \\ \dot{X}(t) = F(X(t), u(t)) \\ X(0) = (x_0, y_0) \\ X(T) = (x_f, y_f) \\ \dot{X}(T) = 0 \\ \|u(t)\|_\infty \leq 1 \end{cases} , \qquad \forall t \in [0, T] . \tag{2.9}$$

The maximum principle [15], allows us to determine the optimal control $u^*(\cdot)$ by using the maximization of the Pontryagin's function $H(X, P, u)$ (here, P is the adjoint variable satisfying $-\dot{P} = \nabla_X H(X, P, u)$, being ∇_X the gradient of H with respect to X) almost everywhere with respect to the Lebesgue measure (from here onwards, functions are specified in this sense), together with the satisfaction of the appropriate boundary conditions.

2.3.1 Minimum energy problem

Here, our cost function is the total control power consumption

$$\int_0^T u^2 \, dt \, .$$

We want to minimize the power spent to move the particle between the initial and final points so that, at the final prescribed time T, the particle is at (ρ_T, θ_T).

To obtain the Mayer's problem [17], we consider a new time dependent variable $w(\cdot)$ that satisfies $\dot{w} = u^2$. Thus, our control problem is formulated as follows:

$$\begin{cases} \text{Minimize} \quad w(T) \\ \text{subject to} \\ \dot{\rho}(t) = u(t) \\ \dot{\theta}(t) = \frac{k}{2\pi} \frac{1}{\rho^2(t)} \\ \dot{w}(t) = u^2(t) \\ \rho(0) = \rho_0 \\ \rho(T) = \rho_T \\ \dot{\rho}(T) = 0 \\ \theta(0) = \theta_0 \\ \theta(T) = \theta_T \\ w(0) = 0 \\ \|u(t)\|_\infty \leq 1 \end{cases} , \qquad \forall t \in [0, T]. \tag{2.10}$$

We impose the radial velocity $\dot{\rho}$ to go to zero at $t = T$, so that the control is smooth and differentiable during the arrival at the circular trajectory of radius ρ_T. For simplicity, we will consider only the case where $\rho_T < \rho_0$. The case $\rho_T > \rho_0$ follows analogously.

For this problem, the Pontryagin's function is

$$H(t, \rho, \theta, w, p_\rho, p_\theta, p_w) = p_\rho u + p_\theta \frac{k}{2\pi\rho^2} + p_w u^2 \, , \tag{2.11}$$

and the dynamic equations for the adjoint variables are

$$\begin{cases} -\dot{p}_\rho &= -p_\theta \frac{k}{\pi\rho^3} \\ -\dot{p}_\theta &= 0 \\ -\dot{p}_w &= 0 \end{cases}, \tag{2.12}$$

and, thus,

$$\begin{cases} p_\rho &= C_\rho - C_\theta \frac{k}{\pi} \int_t^T \rho^{-3}(\tau)\, d\tau \\ p_\theta &= C_\theta \\ p_w &= -1 \end{cases}. \tag{2.13}$$

where C_ρ and C_θ are integration constants. Furthermore, we know that the optimal solution should maximize the Hamiltonian H. From $\dfrac{dH}{dt} = 0$, it is possible to conclude that the optimal control u^* satisfies

$$u^*(t) = \begin{cases} \min\left\{\dfrac{p_\rho}{2}, 1\right\}, & \text{if} \quad p_\rho \geq 0 \\ \max\left\{\dfrac{p_\rho}{2}, -1\right\}, & \text{if} \quad p_\rho < 0 \end{cases}, \tag{2.14}$$

and, thus, it is possible to distinguish between two different behaviors on the radial motion of the passive particle:

1. If $u^*(t) = \pm 1$, we have

$$\dot{\rho} = \pm 1 \Rightarrow \rho(t) = \rho(t_0) \pm (t - t_0). \tag{2.15}$$

2. If $u^*(t) = \dfrac{p_\rho}{2}$, we have

$$\dot{\rho} = \frac{p_\rho}{2} \quad \Rightarrow \quad \ddot{\rho} = \frac{\dot{p}_\rho}{2} = \frac{C_\theta k}{2\pi\rho^3}. \tag{2.16}$$

The second order ordinary differencial equation (2.16) can easily be integrated once to obtain ($\dot{\rho}$ is an integrating factor)

$$\dot{\rho}^2 = A^2 - \frac{C_\theta k}{2\pi\rho^2},$$

for some $A^2 \in \mathbb{R}^+$.

Since we impose $\dot{\rho}\left(\rho = \rho_T\right) = 0$, we conclude that

$$\dot{\rho}^2 = A^2 \left[1 - \left(\frac{\rho_T}{\rho} \right)^2 \right], \quad A^2 = \frac{C_\theta k}{2\pi \rho_T^2}, \tag{2.17}$$

and, thus,

$$-\dot{\rho} = |A| \sqrt{1 - \left(\frac{\rho_T}{\rho} \right)^2}, \tag{2.18}$$

where we take the negative square root, for the reason of $\rho_T < \rho_0$.

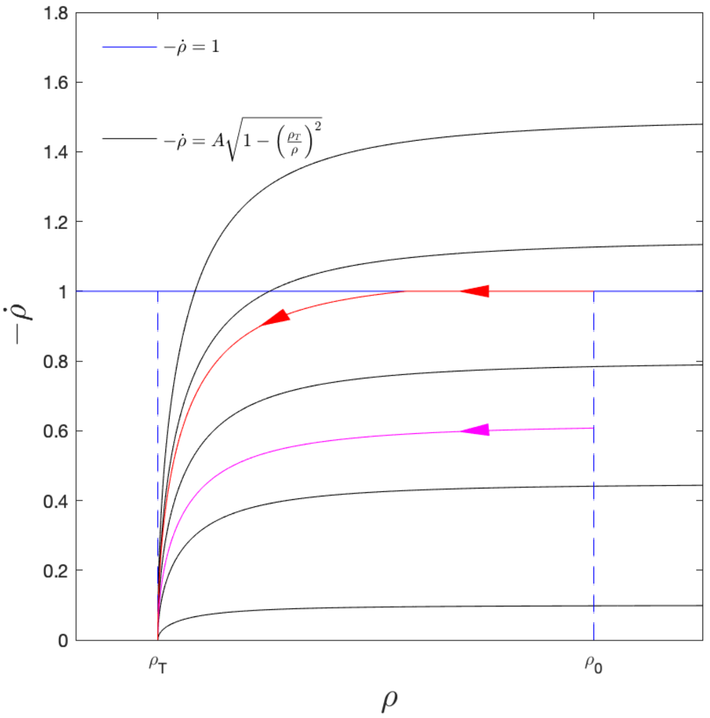

Figure 2.3: Illustration of the possible dynamics for the solution of the problem. The different black lines correspond to different values of $A = \sqrt{\frac{C_\theta k}{2\pi \rho_T^2}}$. The horizontal blue line corresponds to the control $u = -1$, and so the dynamics can happen above this line. There are two qualitatively different types of trajectories: (i) the particle follows a variable (that is, time-varying) control, until it reaches a trajectory with radius ρ_T (pink curve); (ii) the particle is first pulled by a control $u = -1$, which then switches into a variable control that is active until the particle reaches a trajectory with radius ρ_T (red curve).

The possible radial trajectories of the particle are clearly seen, if we analyze the behavior of $\dot{\rho}$. In Figure 2.3, we plot we plot $-\dot{\rho}$ against ρ. The different black lines correspond to different values of $A = \sqrt{\frac{C_\theta k}{2\pi \rho_T^2}}$ and, thus, possible trajectories for the passive particle.

The horizontal blue line corresponds to a control $u = -1$, and the movement of the particle has to happen on this line or below it. Therefore, there are two possible types of trajectory for a particle starting at ρ_0.

If $A^2\left[1-\left(\frac{\rho_T}{\rho_0}\right)^2\right] \leq 1$, then the particle is never driven by the control $u=-1$, but by the variable (that is, time-varying) control, describing a curve like the pink one until it reaches ρ_T.

On the other hand, assuming $A^2\left[1-\left(\frac{\rho_T}{\rho_0}\right)^2\right] > 1$, then the particle is driven by the control $u=-1$, for some time, before switching to the variable control law (2.16) until it reaches ρ_T, as depicted by the red curve in the figure.

We will identify these types of trajectory by type I and type II, respectively. Notice that the trajectory depends solely on the value of A^2, which we have yet to determine.

We now analyze these two different types of trajectory in more detail in order to determine A.

2.3.1.1 Trajectory of type I

In a trajectory of type I, the particle starts its motion under the variable control that diminishes its radius until it arrives at ρ_T, at some time t^*. From this point onwards, the particle will describe a circular motion with constant radius around the vortex until it arrives at the prescribed angle θ_T, at time T.

In the time interval $[0,t^*]$, the movement of the particle is given by the solution of the IVP

$$\begin{cases} \dot{\rho} = -A\sqrt{1-\left(\dfrac{\rho_T}{\rho}\right)^2} \\ \dot{\theta} = \dfrac{k}{2\pi}\dfrac{1}{\rho^2} \\ \rho(0)=\rho_0, \quad \theta(0)=\theta_0 \end{cases}, \tag{2.19}$$

which is

$$\begin{cases} \rho^2(t) = \rho_0^2 + A^2t^2 - 2A\sqrt{\rho_0^2-\rho_T^2}\,t \\ \theta(t) = \theta_0 + \dfrac{k}{2\pi A\rho_T}\left[\tan^{-1}\left(\sqrt{\left(\dfrac{\rho_0}{\rho_T}\right)^2-1}\right) - \right. \\ \qquad \left. -\tan^{-1}\left(\sqrt{\left(\dfrac{\rho_0}{\rho_T}\right)^2-1}-\dfrac{At}{\rho_T}\right)\right] \end{cases}, \quad t\in[0,t^*]. \tag{2.20}$$

The time t^* can be easily calculated from the condition $\rho(t^*) = \rho_T$, and we get $t^* = \frac{1}{A}\sqrt{\rho_0^2 - \rho_T^2}$.

In the time interval $]t^*, T]$, the radius remains constant $\rho(t) = \rho_T$, while the angular position obeys the equation

$$\dot{\theta} = \frac{k}{2\pi\rho_T^2},$$

and, thus, we get

$$\begin{cases} \rho(t) = \rho_T \\ \theta(t) = \theta(t^*) + \dfrac{k}{2\pi\rho_T^2}(t - t^*) \end{cases}, \quad t \in]t^*, T]. \tag{2.21}$$

Notice that we can have $t^* = T$ and, in this scenario, the particle arrives at the final point at the same time, as the variable control goes to zero.

Since we are dealing with a circular motion, one can actually still arrive at the final position with an angle of $\theta_T + 2N\pi$, $N \in \mathbb{N} \cup \{0\}$. Thus, from $\theta(T) = \theta_T + 2N\pi$, we can write

$$\begin{aligned} \theta_T + 2N\pi = \theta_0 + \frac{k}{2\pi A\rho_T}\tan^{-1}\left(\sqrt{\left(\frac{\rho_0}{\rho_T}\right)^2 - 1}\right) \\ + \frac{k}{2\pi A\rho_T^2}\left[T - \frac{1}{A}\sqrt{\rho_0^2 - \rho_T^2}\right], \end{aligned} \tag{2.22}$$

from where we can determine A as

$$A = \frac{k\rho_T\left[\tan^{-1}\left(\sqrt{\left(\frac{\rho_0}{\rho_T}\right)^2 - 1}\right) - \sqrt{\left(\frac{\rho_0}{\rho_T}\right)^2 - 1}\right]}{2\pi\rho_T^2(\theta_T - \theta_0 + 2N\pi) - kT}, \tag{2.23}$$

and, thus, the optimal trajectory and optimal control, as long as this value is compatible with $A^2\left[1 - \left(\frac{\rho_T}{\rho_0}\right)^2\right] \leq 1$.

2.3.1.2 Trajectory of type II

In a trajectory of type II, the particle starts its motion under the constant control $u = -1$, until some time $\tilde{t}$, reducing the trajectory to one with a radius $\tilde{\rho}$.

At this point, the control switches into the variable control law that further diminishes the trajectory radius to ρ_T, at some time t^*.

In the remainder of the trajectory, the particle will describe a circular motion with constant radius around the vortex, until it arrives at the prescribed angle θ_T, at time T.

In the time interval $\left[0, \tilde{t}\right]$, the trajectory of the particle satisfies the IVP

$$\begin{cases} \dot{\rho} = -1 \\ \dot{\theta} = \dfrac{k}{2\pi}\dfrac{1}{\rho^2} \\ \rho\left(0\right) = \rho_0, \quad \theta\left(0\right) = \theta_0 \end{cases}, \tag{2.24}$$

which has the solution

$$\begin{cases} \rho\left(t\right) = \rho_0 - t \\ \theta\left(t\right) = \theta_0 + \dfrac{k}{2\pi A\rho_0}\,\dfrac{t}{\rho_0 - t} \end{cases}, \quad t \in \left[0, t^*\right]. \tag{2.25}$$

The time $\tilde{t}$ is such that $\rho\left(\tilde{t}\right) = \rho_0 - \tilde{t} = \tilde{\rho}$, and $A\sqrt{1 - \left(\frac{\rho_T}{\tilde{\rho}}\right)^2} = 1$. Thus, we arrive at

$$\begin{cases} \tilde{\rho}^2 = \dfrac{A^2}{A^2 - 1}\rho_T^2 \\ \tilde{t} = \rho_0 - \sqrt{\dfrac{A^2}{A^2 - 1}}\rho_T \end{cases}. \tag{2.26}$$

Remark: $\theta\left(\tilde{t}\right) = \theta_0 + \frac{k}{2\pi\rho_T}\left[\sqrt{\frac{A^2 - 1}{A^2}} - \frac{\rho_T}{\rho_0}\right] = \tilde{\theta}$.

In the time interval $\left]\tilde{t}, t^*\right]$, the motion of the particle is ruled by the variable control and it satisfies the same differential equations of the IVP (2.19), although with initial conditions $\rho\left(\tilde{t}\right) = \tilde{\rho}$, and $\theta\left(\tilde{t}\right) = \tilde{\theta}$. The solution is thus

$$\begin{cases} \rho^2\left(t\right) = \tilde{\rho}^2 + A^2\left(t - \tilde{t}\right)^2 - 2A\sqrt{\tilde{\rho}^2 - \rho_T^2}\left(t - \tilde{t}\right) \\ \theta\left(t\right) = \tilde{\theta} + \dfrac{k}{2\pi A\rho_T}\left[\tan^{-1}\left(\sqrt{\left(\dfrac{\tilde{\rho}}{\rho_T}\right)^2 - 1}\right) - \right. \\ \qquad \left. - \tan^{-1}\left(\sqrt{\left(\dfrac{\tilde{\rho}}{\rho_T}\right)^2 - 1} - \dfrac{A\left(t - \tilde{t}\right)}{\rho_T}\right)\right] \end{cases}, \quad t \in \left]\tilde{t}, t^*\right]. \tag{2.27}$$

Finally, on the time interval $\left]t^*, T\right]$, the movement is the same as in the correspondent time interval of a trajectory of type I: the radius remains constant $\rho\left(t\right) = \rho_T$, while the angular position obeys the equation $\dot{\theta} = \frac{k}{2\pi\rho_T^2}$. Thus,

$$\begin{cases} \rho\left(t\right)=\rho_{T} \\ \theta\left(t\right)=\theta\left(t^{*}\right)+\dfrac{k}{2\pi\rho_{T}^{2}}\left(t-t^{*}\right) \end{cases}, \quad t\in\left]t^{*},T\right]. \tag{2.28}$$

Opposite to what happened in a trajectory of type I, it is not possible to write an explicit expression of A. From $\theta(T)=\theta_T+2N\pi, N\in\mathbb{N}\cup\{0\}$, after some calculation, we can write an implicit equation for A :

$$\begin{aligned} \frac{2\pi\rho_{T}}{k}\left[\theta_{T}-\theta_{0}+2N\pi\right]+\frac{\rho_{T}^{2}+\rho_{0}^{2}}{\rho_{T}\rho_{0}}-\frac{T}{\rho_{T}} &= \\ =\frac{1}{A}\left[2\sqrt{A^{2}-1}+\tan^{-1}\left(\frac{1}{\sqrt{A^{2}-1}}\right)\right]. \end{aligned} \tag{2.29}$$

This equation is consistent with the expression (2.22), since in the limit $\tilde{t}\rightarrow 0$, we recover that expression. By taking this limit would correspond to the scenario without constraints on the control.

It is also important to notice that the family of curves

$$\dot{\rho}^{2}=A^{2}\left[1-\left(\frac{\rho_{T}}{\rho}\right)^{2}\right],$$

with $A>0$, constitutes the family of curves with minimal energy for this problem. Thus, if there is any trajectory of type I that is a solution to the problem, it is also the minimal energy solution. In this scenario, any trajectory of type II, that takes the particle from the initial point to the final point, will have higher energy cost.

In Figure 2.4, we show the optimal trajectory for the problem of moving a particle from the initial position $\left(x_0,y_0\right)=(2,2)$ to the final position $\left(x_f,y_f\right)=(1,1)$, in $T=100$ units of time, in an environment controlled by a point vortex, located at the origin, with circulation $k=1$. In the red-depicted part of the trajectory, the particle is under the influence of the variable control, while in the black-depicted part, it is only under the influence of the velocity field generated by the vortex. We found $A\approx 0.0460$ and the energy spent in moving the particle was, approximately, 0.9685.

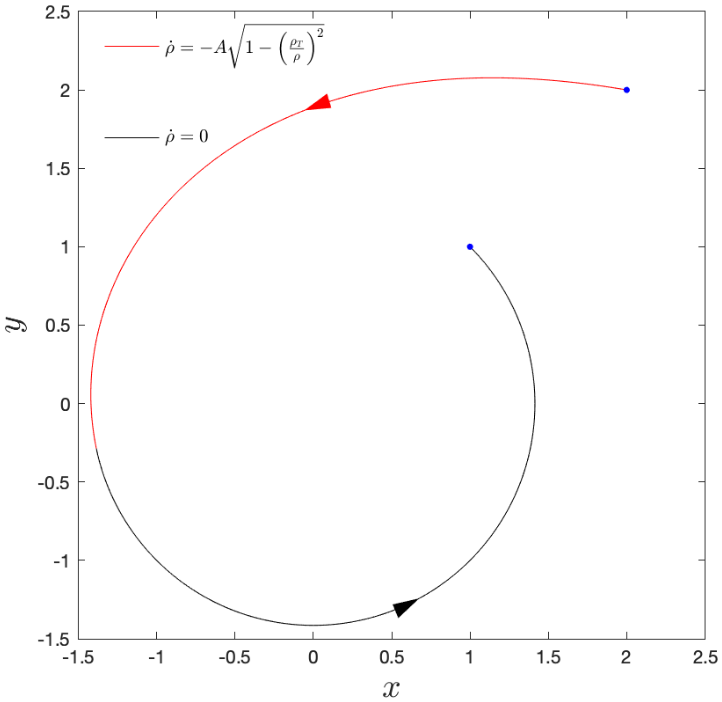

FIGURE 2.4: Optimal trajectory of a particle that moves from $(2,2)$ to $(1,1)$, in $T = 100$ units of time, on an environment controlled by a point vortex of circulation $k = 1$, located at the origin. The other parameters are $\rho_0^2 = 8$, $\rho_T^2 = 2$, $\theta_0 = \theta_T = \frac{\pi}{2}$, $N = 1$. The optimal trajectory corresponds to $A \approx 0.0460$, and the energy spent was, approximately, 0.9685 .

2.4 Conclusions and future work

The problem discussed in this work is simple, since the dynamics of the control system are defined by a set of autonomous ODE's. Also, the conditions resulting from the application of the maximum principle can be solved in an explicit way.

In this problem, only the radius is directly affected by the control, since we just need to either pull the particle closer to the vortex or push it farther away in a way that minimizes the cost function and reaches the desired final position at the instant T. We plan to investigate further in this problem, studying and comparing different scenarios by changing the constants in the problem and eventually tackle it in an environment constituted by a viscous vortex or a set of N vortices.

2.5 Acknowledgements

This work was partially supported by CMUP (UID/MAT/00144/2019), which is funded by FCT with national (MCTES) and European structural funds through the programs

FEDER, under the partnership agreement PT2020; by SYSTEC - POCI-01-0145-FEDER-006933/SYSTEC funded by ERDF - COMPETE2020 - FCT/MEC - PT2020; by project MAGIC - POCI-01-0145- FEDER-032485, funded by ERDF NORTE 2020; and by project SNAP - reference NORTE-01-0145-FEDER-000085, co-financed by the European Regional Development Fund (ERDF), through the North Portugal Regional Operational Programme (NORTE2020), under the PORTUGAL 2020 Partnership Agreement.

References

[1] F. Clarke, Y. Ledyaev, R. Stern, and P. Wolenski, *Nonsmooth Analysis and Control Theory* (Graduate Texts in Mathematics). Springer New York, 2008, ISBN: 9780387226255. DOI: `10.1007/b97650`.

[2] S. Mitter and J. Lions, *Optimal Control of Systems Governed by Partial Differential Equations* (Grundlehren der mathematischen Wissenschaften). Springer Berlin Heidelberg, 1971, ISBN: 9783540051152.

[3] B. Protas, "Vortex dynamics models in flow control problems," *Nonlinearity*, vol. 21, no. 9, R203, Jul. 2008. DOI: `10.1088/0951-7715/21/9/R01`.

[4] N. Mahmoudian, J. Geisbert, and C. Woolsey, "Dynamics and control of underwater gliders i: Steady motions," Virginia Center for Autonomous Systems, Technical Report VaCAS-2007-01, 2009.

[5] N. Mahmoudian and C. Woolsey, "Dynamics and control of underwater gliders ii: Motion planning and control," Virginia Center for Autonomous Systems, Technical Report VaCAS-2010-02, 2010.

[6] J. Liu and H. Hu, "Biological inspiration: From carangiform fish to multi-joint robotic fish," *Journal of Bionic Engineering*, vol. 7, no. 1, pp. 35–48, 2010, ISSN: 1672-6529. DOI: `10.1016/S1672-6529(09)60184-0`.

[7] F. L. Pereira, T. Grilo, and S. Gama, "Optimal multi-process control of a two vortex driven particle in the plane," *IFAC-PapersOnLine*, vol. 50, no. 1, pp. 2193–2198, 2017, 20th IFAC World Congress, ISSN: 2405-8963. DOI: `10.1016/j.ifacol.2017.08.280`.

[8] F. L. Pereira, T. Grilo, and S. Gama, "Optimal power consumption motion control of a fish-like vehicle in a vortices vector fiele," in *OCEANS 2017 - Aberdeen*, 2017, pp. 1–4. DOI: `10.1109/OCEANSE.2017.8085026`.

[9] H. Aref, “Integrable, chaotic, and turbulent vortex motion in two-dimensional flows,” *Annual Review of Fluid Mechanics*, vol. 15, no. Volume 15, 1983, pp. 345–389, 1983, ISSN: 1545-4479. DOI: 10.1146/annurev.fl.15.010183.002021.

[10] A. Babiano, G. Boffetta, A. Provenzale, and A. Vulpiani, “Chaotic advection in point vortex models and two-dimensional turbulence,” *Physics of Fluids*, vol. 6, no. 7, pp. 2465–2474, Jul. 1994, ISSN: 1070-6631. DOI: 10.1063/1.868194.

[11] G. K. Batchelor, *An Introduction to Fluid Dynamics* (Cambridge Mathematical Library). Cambridge University Press, 2000. DOI: 10.1017/CBO9780511800955.

[12] P. Newton, *The N-Vortex Problem: Analytical Techniques* (Applied Mathematical Sciences). Springer New York, 2010, ISBN: 9781441929167. DOI: 10.1007/978-1-4684-9290-3.

[13] A. Chorin, *Vorticity and Turbulence* (Applied Mathematical Sciences). Springer, 1994, ISBN: 9780387941974. DOI: 10.1007/978-1-4419-8728-0.

[14] S. Gama and P. Milheiro-Oliveira, “Statistical properties of passive tracers in a positive four-point vortex model,” *Phys. Rev. E*, vol. 62, pp. 1424–1426, 1 Jul. 2000. DOI: 10.1103/PhysRevE.62.1424.

[15] L. S. Pontryagin, V. G. Boltyanskii, R. V. Gamkrelidze, and E. F. Mishchenko, *The Mathematical Theory of Optimal Processes*. New York, NY: Interscience Publishers, 1961, translated by K. N. Triruguf, edited by T. W. Neustadt.

[16] A. V. Arutyunov, D. Y. Karamzin, and F. L. Pereira, “The maximum principle for optimal control problems with state constraints by r.v. gamkrelidze: Revisited,” *Journal of Optimization Theory and Applications*, vol. 149, no. 3, pp. 474–493, 2011. DOI: 10.1007/s10957-011-9807-5.

[17] M. Levi, *Classical Mechanics with Calculus of Variations and Optimal Control: An Intuitive Introduction* (Student Mathematical Library). American Mathematical Society, 2014, ISBN: 9780821891384.

Chapter 3

Optimal Control of a Passive Particle Advected by a Lamb–Oseen (Viscous) Vortex

Published in Computation, 2022

Gil Marques, Sílvio Gama and Fernando L. Pereira

Abstract: This work concerns the optimal control of a passive particle in viscous flows. This is relevant since, while there are many studies on optimal control in inviscid flows, there is little to no work in this context for viscous flows, and viscosity cannot always be neglected. Furthermore, in many tasks, there is a need to reduce the energy spent; thus, energy-optimal solutions to problems are important. The aim of this work is to investigate how to optimally move a passive particle advected by a Lamb–Oseen (viscous) vortex between two given points in space in a given time interval while minimising the energy spent on this process. We take a control acting only on the radial component of the motion, and, by using the Pontryagin's Maximum Principle, we find an explicit time-dependent extremal. We also analyse how the energy cost changes with the viscosity of the flow. The problem is transformed into a parameter search problem with two parameters related to the radial and angular coordinates of the initial point. The energy cost of the process increases with viscosity as long as the passive particle maintains the number of full

turns it makes around the vortex. However, the energy cost increases if the increase in viscosity forces the particle to make fewer full revolutions around the vortex.

3.1 Introduction

In this article, we present a research work developed in the framework of the optimal control of dynamical systems whose state is driven by ordinary differential equations [1], [2]. This work provides a solid foundation for the design and control of new, advanced engineering systems, such as (i) underwater gliders, i.e., winged autonomous underwater vehicles (AUVs), moving by modulating their buoyancy, and their attitude in the environment, or (ii) robotic fish. Motion modelling of these two types of systems can be found in [3], [4], [5], respectively. These systems are useful because they can be used for a variety of automated tasks in a real fluid, such as (i) transporting materials in a flow or (ii) measuring physical quantities of the flow itself, if equipped with the right sensors/tools. Controlling the movement of these robots in a real flow is therefore crucial to be sure that they work as we expect them to.

Vorticity is a useful description of a flow. A vortex is a point with circulation that generates a rotational flow field. Consider a 2D flow specified in the complex plane by N point vortices, each located in z_i [6], [7]. In this context, the motion of any passive particle advected by this flow is given by the following dynamical equation

$$\dot{z}^* (t) = \frac{1}{2\pi i} \sum_{j=1}^{N} \frac{k_j}{z (t) - z_j (t)} , \tag{3.1}$$

where k_j is the circulation—or strength—of the j-th vortex, and the Cartesian coordinates are specified in a complex formulation as $z = x + yi$. Table 3.1 summarises the nomenclature used throughout this article.

Table 3.1: Nomenclature table.

Symbol	Meaning	SI Units
t	Time	s
$z = x + y\,i$	Position in polar coordinates	m
ρ	Radial coordinate	m
θ	Angular coordinate	rad
k	Circulation	$\mathrm{m^2s^{-1}}$
ν	Kinematic viscosity	$\mathrm{m^2s^{-1}}$
u	Control	$\mathrm{ms^{-1}}$

However, no flow is completely free of viscosity, and it is important to consider this fact. A simple way to model vortices in a viscous flow is the Lamb–Oseen formulation [8], [9], which is the solution of the Navier–Stokes equations for an initial condition in which the full vorticity of the flow is concentrated in a single point in the plane. This originates a vorticity field that decays and is diffused radially outwards with a Gaussian profile (see [6], [10]).

An important result about the Lamb–Oseen vortex is that it is an asymptotically stable attracting solution of the vorticity equation for any integrable initial vorticity configuration, as proven by Gallay and Wayne [11]. The superposition of N point vortices is such a configuration, which gave rise to the idea of the multi-Gaussian model. This model assumes that the vorticity field is a superposition of Lamb–Oseen vortices at all times, modelling the behaviour of both the diffusive term and convective term of the vorticity equations through the interaction of the vortices with each other.

More recently, Gallay [12] has shown that under certain conditions, the solution of the Navier–Stokes equations in the inviscid limit for δ-Dirac initial conditions converges to a superposition of Lamb–Oseen vortices. This provides yet another reason for the suitability of the multi-Gaussian model in the description of fluids.

The motion of a passive particle in such a model should follow the velocity field generated by the system of N vortices, which is given by [13]

$$\dot{z}^*(t) = \frac{1}{2\pi i}\sum_{j=1}^{N}\frac{k_j}{z(t)-z_j(t)}\left[1-\exp\left(-\frac{|z-z_j|^2}{4\nu t}\right)\right], \tag{3.2}$$

where ν is the kinematic viscosity of the flow. This is consistent with Model (3.1) as we recover the inviscid equation in the limit $\nu \to 0$.

This work is a continuation of the study made by Marques et al. (2021) [14], where the advection of passive particles is made by an (inviscid) point vortex. In [14], it is shown that the control is explicitly time-dependent, being possible to determine it exclusively by analytical methods. Unfortunately, the same is not possible in the work we are addressing here because of the presence of the viscous terms in Equation (3.2); therefore, using numerical computation is necessary. In this article, we consider the case for which the dynamic system is driven by one Lamb–Oseen vortex, and we solve a control problem that consists of moving a particle between two given points by applying the necessary conditions of optimality in the form of a maximum principle [15]. We focus on the case where the flow is characterised by a single vortex, and we want to move a single passive particle between two points in the 2D plane by acting only on the radial component of the velocity. The inviscid case ($\nu = 0$) has been studied by Marques et al. (2021) [14]: it is shown that this radial control is explicitly time-dependent and that it can be determined exclusively by analytical methods. Unfortunately, this is not possible in a viscous environment where the dynamical system is driven by a Lamb–Oseen vortex. The viscous terms in the equations of motion (3.2) hinder the possibility of finding an analytical solution to the problem, so one must resort to numerical computation to find approximate solutions. This article presents a first study of this problem in a viscous environment: we consider the case where the dynamical system is driven by a single Lamb–Oseen vortex, and we solve a control problem consisting of moving a particle between two given points by applying necessary optimality conditions in the form of a maximum principle [15]. This problem follows the idea of the more general Problem 2 proposed in Protas [16]. Sections 3.2 and 3.3 are devoted to the mathematical formulation of the problem. In Section 3.4, we derive the optimal control and study the optimal trajectories for the passive particle for different kinematic viscosities. The conclusions and future work constitute the last section.

3.2 Velocity Field Driven by a Lamb–Oseen Vortex

Consider a viscous flow with some kinematic viscosity ν and a Lamb–Oseen vortex at the origin $(0, 0)$, with vorticity k. Let $z(t) = x(t) + y(t)i$ be the position of a passive particle placed in this flow at time t. In the complex formulation, the dynamic equation for the particle positioned in z subject to the velocity field generated by the vortex is

$$\dot{z}^*(t) = \frac{1}{2\pi i}\frac{k}{z(t)}\left[1 - \exp\left(-\frac{|z(t)|^2}{4\nu t}\right)\right] . \tag{3.3}$$

In polar coordinates, the position of the particle is given by

$$z(t) = \rho(t)\, e^{i\theta(t)} \tag{3.4}$$

and the derivative with respect to t is

$$\dot{z}(t) = \dot{\rho}(t)e^{i\theta(t)} + i\rho(t)\,\dot{\theta}(t)\, e^{i\theta(t)} . \tag{3.5}$$

Therefore, the complex conjugate of the derivative is

$$\dot{z}^*(t) = \dot{\rho}(t)\, e^{-i\theta(t)} - i\rho(t)\,\dot{\theta}(t)\, e^{-i\theta(t)} \tag{3.6}$$

and from Equations (3.3) and (3.6), we obtain

$$\dot{\rho}(t) - i\rho(t)\,\dot{\theta}(t) = -i\frac{k}{2\pi}\frac{1}{\rho(t)}\left[1 - \exp\left(-\frac{\rho^2(t)}{4\nu t}\right)\right] . \tag{3.7}$$

By separating the equalities of the real and imaginary parts of both sides of the equation, we have the following dynamic equations for the particle in polar form

$$\begin{cases} \dot{\rho}(t) = 0 \\ \dot{\theta}(t) = \frac{k}{2\pi}\frac{1}{\rho^2(t)}\left[1 - \exp\left(-\frac{\rho^2(t)}{4\nu t}\right)\right] \end{cases} , \tag{3.8}$$

which are not solvable analytically. However, it is easy to qualitatively characterise the motion of the particle: it is a circular motion with a constant radius and a variable angular velocity that decreases to 0 as time approaches ∞.

3.3 Control Problem

Consider a flow like the one presented in Section 3.2 and a passive particle placed in the flow with initial position (x_0, y_0). The objective of this problem is to determine the control function $u(\cdot)$ to be applied to the particle so that it moves in the flow from the given initial position to the endpoint (x_f, y_f) while minimising the cost function $g(X(T))$ while subject to the flow field. Let $X(t) = (x(t), y(t))$ be the position of the particle at time t. The control problem can be formulated as follows:

$$\begin{cases} \text{Minimize} \quad g(X(T)) \\ \text{subject to} \\ \dot{X}(t) = F(X(t), u(t)) \\ X(0) = (x_0, y_0) \\ X(T) = (x_f, y_f) \\ \|u(t)\|_\infty \leq 1 \end{cases}, \forall t \in [0, T]. \tag{3.9}$$

The maximum principle [15] allows us to determine the set of optimal control candidates u^* by using the maximisation of the Pontryagin–Hamiltonian function $H(X, P, u)$ (here, P is the adjoint variable satisfying $-\dot{P}^T = \nabla_X H(X^*, P, u^*)$ along the optimal reference control process, where ∇_X is the gradient of H with respect to X) almost everywhere with respect to the Lebesgue measure (from here on, functions are specified in this sense), together with the satisfaction of the appropriate boundary conditions.

3.4 Minimum Energy Problem

Our cost function here is the total control power consumption, i.e., the energy used to move the particle,

$$\int_0^T u^2 \, dt \ .$$

We want to minimise the power spent to move the particle between some specified initial (ρ_0, θ_0) and final points so that the particle is at (ρ_T, θ_T) at the final time T.

To obtain the Mayer's problem, we consider a new variable $w(t)$ satisfying the condition $\dot{w} = u^2$. Our control problem can thus be formulated as follows:

$$\left\{\begin{array}{l} \text{Minimize} \quad w(T) \\ \text{subject to} \\ \dot{\rho} = u \\ \dot{\theta} = \frac{k}{2\pi}\frac{1}{\rho^2}\left[1 - \exp\left(-\frac{\rho^2}{4\nu t}\right)\right] \\ \dot{w} = u^2 \\ \rho(0) = \rho_0 \\ \rho(T) = \rho_T \\ \theta(0) = \theta_0 \\ \theta(T) = \theta_T \\ w(0) = 0 \\ \|u(t)\|_\infty \leq 1 \end{array}\right. , \forall t \in [0, T]. \tag{3.10}$$

In addition, we impose the radial velocity $\dot{\rho}$ approaches zero at ρ_T so that the control is smooth and differentiable during the arrival at the circular trajectory of radius ρ_T. For simplicity, we will only consider the case where $\rho_T < \rho_0$. The case $\rho_T > \rho_0$ follows analogously.

For this problem, the Pontryagin–Hamiltonian function is

$$H(t, \rho, \theta, w, p_\rho, p_\theta, p_w, u) = p_\rho u + p_\theta \frac{k}{2\pi\rho^2}\left[1 - \exp\left(-\frac{\rho^2}{4\nu t}\right)\right] + p_w u^2 \tag{3.11}$$

and the dynamic equations for the adjoint variable are

$$\left\{\begin{array}{rcl} -\dot{p}_\rho & = & -p_\theta \frac{k}{\pi\rho^3}\left[1 - \frac{\rho^2 + 4\nu t}{4\nu t}\exp\left(-\frac{\rho^2}{4\nu t}\right)\right] \\ -\dot{p}_\theta & = & 0 \\ -\dot{p}_w & = & 0 \end{array}\right. . \tag{3.12}$$

While the differential equation for p_ρ is impossible to solve analytically, from the transversality conditions, it is possible to further conclude that $p_w(t) = -1$ and that p_θ is constant ($p_\theta = C_\theta$).

Thus, the Pontryagin–Hamiltonian function can be rewritten as

$$H(t,\rho,\theta,w,p_\rho,p_\theta,p_w,u) = p_\rho u + C_\theta \frac{k}{2\pi\rho^2}\left[1-\exp\left(-\frac{\rho^2}{4\nu t}\right)\right] - u^2. \tag{3.13}$$

Furthermore, we know that the optimal control u^* should maximise the Hamiltonian at any time; thus,

$$\begin{aligned} u^* &= \arg\max_{|u|\le 1} H(t,\rho^*,\theta^*,p_\rho,u) \\ &= \arg\max_{|u|\le 1}\left\{p_\rho u + C_\theta \frac{k}{2\pi\left(\rho^*\right)^2}\left[1-\exp\left(-\frac{\left(\rho^*\right)^2}{4\nu t}\right)\right] - u^2\right\} \\ &= \arg\max_{|u|\le 1}\left\{p_\rho u - u^2\right\} \end{aligned} \tag{3.14}$$

and the optimal control should satisfy

$$u^*(t) = \begin{cases} \min\left\{\frac{p_\rho}{2},1\right\}, & \text{if} \quad p_\rho \ge 0 \\ \max\left\{\frac{p_\rho}{2},-1\right\}, & \text{if} \quad p_\rho < 0 \end{cases}. \tag{3.15}$$

While the angular motion of the particle follows the same dynamic equation independently of the control, it is possible to distinguish between two different behaviours for the radial motion of the passive particle:

(a) If $u^*(t) = \pm 1$,

$$\dot{\rho}^* = \pm 1 \Rightarrow \rho^*(t) = \rho_0 \pm (t-t_0). \tag{3.16}$$

(b) If $u^*(t) = \frac{p_\rho}{2}$, then we have

$$\dot{\rho}^* = \frac{p_\rho}{2} \Rightarrow \ddot{\rho}^* = \frac{\dot{p}_\rho}{2} = \frac{C_\theta k}{2\pi\left(\rho^*\right)^3}\left[1-\frac{\left(\rho^*\right)^2+4\nu t}{4\nu t}\exp\left(-\frac{\left(\rho^*\right)^2}{4\nu t}\right)\right]. \tag{3.17}$$

If $|\frac{p_\rho}{2}| \ge 1$ at a certain point of the process, it means that the time T is not sufficient to complete the transport of the particle without applying the control $u = \pm 1$. This constant control is more energy-consuming than a variable control implicitly defined by the nonlinear Equation (3.17). In this scenario, we start by applying the $u = \pm 1$ control for the time period $[t_0, \xi]$ until the particle is in a state where it can be brought to the final position by applying the variable control in the remaining time $T - \xi$.

Unfortunately, there is no way to explicitly calculate $\frac{p_\rho}{2}$ to determine the switching points for the control. Therefore, to solve the problem, we have to take a different approach. We now analyse the case where $|\frac{p_\rho}{2}| < 1$ throughout the whole process.

If the trajectory never uses the control $u = \pm 1$, then we can divide the motion of the passive particle into two regimes. During the first regime of motion, the particle is pulled radially inwards by a variable control from ρ_0 until its radial coordinate reaches ρ_T at an unspecified time $\tilde{t}$. The angular motion is influenced by two different factors: the fact that the particle approaches the vortex contributes to the acceleration of the motion, while the fact that the vortex loses strength over time due to the viscosity of the fluid contributes to the deceleration of the motion.

The movement of the particle during this regime is determined by the solution of the following differential equations, valid for the time interval $\left[0, \tilde{t}\right]$:

$$\begin{cases} \ddot{\rho}^* = \dfrac{C_\theta k}{2\pi \left(\rho^*\right)^3} \left[1 - \dfrac{\left(\rho^*\right)^2 + 4\nu t}{4\nu t} \exp\left(-\dfrac{\left(\rho^*\right)^2}{4\nu t}\right)\right] \\ \dot{\theta}^* = \dfrac{k}{2\pi} \dfrac{1}{\left(\rho^*\right)^2} \left[1 - \exp\left(-\dfrac{\left(\rho^*\right)^2}{4\nu t}\right)\right] \\ \rho^*(0) = \rho_0, \quad \theta^*(0) = \theta_0, \quad \dot{\rho}^*\left(\tilde{t}\right) = 0, \quad \rho^*\left(\tilde{t}\right) = \rho_T \end{cases}. \tag{3.18}$$

Notice that $\dot{\rho}^*(t) \neq 0$ for $t \in \left[0, \tilde{t}\right]$ and that we cannot solve this problem because we do not know a priori the value of $\tilde{t}$. However, assuming we could, the particle would end at the point $\left(\rho_T, \tilde{\theta}\right)$ in polar coordinates.

The second regime of the motion happens when the particle is describing a circular motion of constant radius ρ_T in the time interval $\left[\tilde{t}, T\right]$ and follows the differential equations

$$\begin{cases} \dot{\rho}^* = 0 \\ \dot{\theta}^* = \dfrac{k}{2\pi} \dfrac{1}{\left(\rho^*\right)^2} \left[1 - \exp\left(-\dfrac{\left(\rho^*\right)^2}{4\nu t}\right)\right] \\ \rho^*\left(\tilde{t}\right) = \rho_T, \quad \theta^*\left(\tilde{t}\right) = \tilde{\theta}, \quad \rho^*(T) = \rho_T, \quad \theta^*(T) = \theta_T \end{cases}. \tag{3.19}$$

In order to solve this problem, we have to work backwards from the final point since this second regime of motion has an actual (numerically) solvable system of differential equations. Note, however, that solving this control problem is now reduced to finding for the parameters $\tilde{t}$ and C_θ that give us a solution of Systems (3.18) and (3.19) with minimal energy. We first investigate how the solutions of these systems behave when we change these parameters.

In each of the following studies, the approximate solutions of the differential equations were obtained through the Runge–Kutta–Fehlberg method [17] with a step size of $\Delta t = 10^{-4}$ s. All results presented below use SI units. Viscosity values depend on the physical conditions of the fluid such as temperature and are typically in the range of 10^{-2}–10^{-7} m^{2}s^{-1}. For example, typical seawater at 20 °C has a low kinematic viscosity of about 1.15×10^{-6} m^{2}s^{-1}, while typical printer inks at about 38 °C can have viscosities of up to 2.2×10^{-3} m^{2}s^{-1}.

In order to check how the parameters affect the solutions of this problem, we set $\nu = 10^{-2}$ m^{2}s^{-1}, $\rho_0 = 2\sqrt{2}$ m, $\rho_T = \sqrt{2}$ m, $\theta_0 = \theta_T = \pi/4$, $k = 1$ m^{2}s^{-1} and $T = 200$ s. In Figure 3.1, we set $\tilde{t} = 70$ s and varied C_θ. The large dashed circumferences correspond to circular trajectories of radius $\sqrt{2}$ m and $2\sqrt{2}$ m, the open circles identify the specified initial and final points for the problem, and the red curve represents the trajectory of the particle corresponding to the second regime of motion. The blue and pink lines represent two possible trajectories for the particle in the first regime of motion, corresponding to different values for C_θ. The black dots correspond to a variety of possible initial positions for the simulation, each for a different C_θ. We note that the radial coordinate of the initial position increases with C_θ and that changing this parameter alone is not sufficient to retrieve the desired initial position. Therefore, $\tilde{\theta}$ must play a role in this.

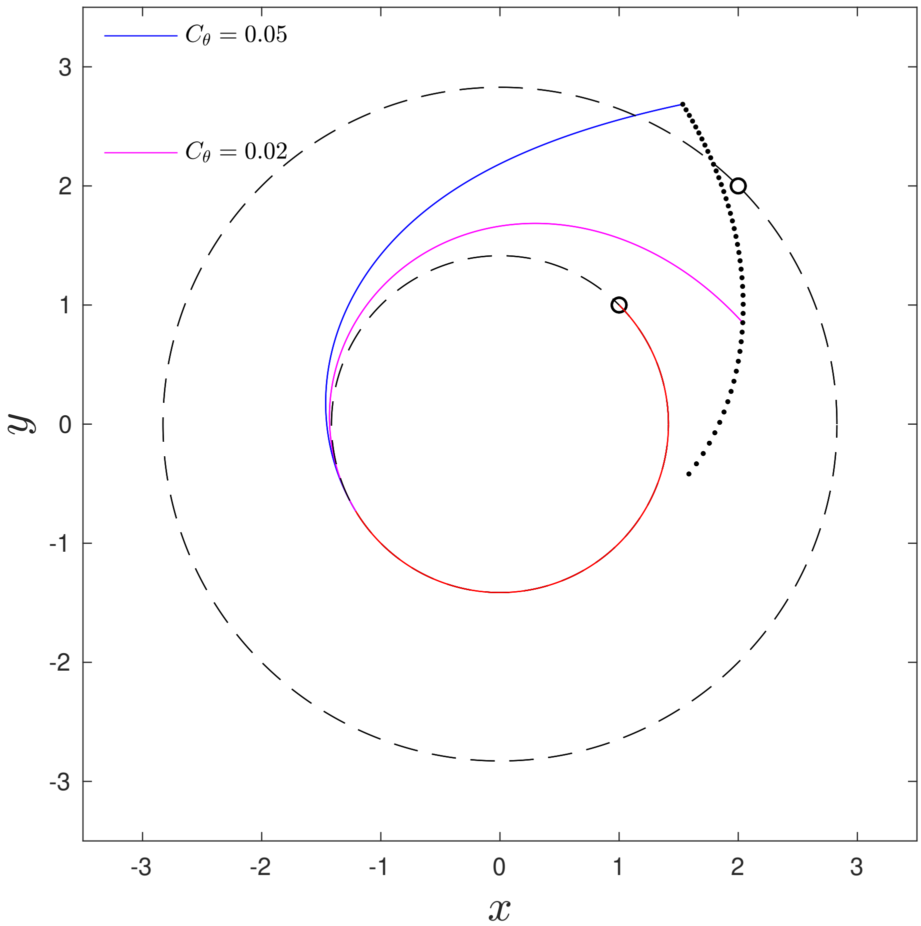

Figure 3.1: We want to move the particle from $(2, 2)$ to $(1, 1)$. The red line represents the motion of the particle during the second regime, while the blue and pink lines represent two possible trajectories on the first regime for different C_θ. The black dots represent possible initial positions for the particle for different values of C_θ. We see that even if we change C_θ, we cannot reach the desired initial position (represented by the open circle), so we have to change $\tilde{t}$.

Figure 3.2 is similar to Figure 3.1 but now illustrates how the initial position for the simulations is affected by the parameter $\tilde{t}$. We see that for a radial coordinate equal to that of the initial position of the particle, larger values of $\tilde{t}$ will result in simulated initial points with a larger angular coordinate. Thus, we can think of C_θ as the parameter that controls the radial coordinate and $\tilde{t}$ as the parameter that controls the angular coordinate for the simulated initial position.

From this behaviour, we develop a simple algorithm to solve the proposed control problem. The idea is as follows:

(1) Arbitrate a $\tilde{t} \in [0, T]$. Find two distinct values $a_t, b_t \in [0, T]$, $b_t > a_t$, which give rise to two curves of simulated initial positions that go under and over the initial position (like the dotted curves in Figure 3.2);

(2) Solve Equation (3.19) backwards in time from T to $\tilde{t}=\frac{a_t+b_t}{2}$ in order to obtain $\tilde{\theta}$;

(3) Arbitrate a C_θ. Find an interval $[a_c, b_c]$ of values for C_θ such that $\rho(0) < \rho_0$ if $C_\theta = a_c$ and $\rho(0) > \rho_0$ if $C_\theta = b_c$;

(4) Solve Equation (3.18) backwards in time. If $\rho(0) > \rho_0$, adjust C_θ to a lower value; if $\rho(0) < \rho_0$, adjust C_θ to a higher value. Re-solve the system until $\rho(0) = \rho_0$. Solve Equation (3.18) backwards in time with $C_\theta = \frac{c_a+c_b}{2}$. If $\rho(0) < \rho_0$, adjust $a_c = C_\theta$; if $\rho(0) > \rho_0$, adjust $b_c = C_\theta$. Iterate the system until $\rho(0) = \rho_0$.

(5) After attaining $\rho(0) = \rho_0$, check for $\theta(0)$: if $\theta(0) > \theta_0$, adjust $\tilde{t}$ to a lower value; if $\theta(0) < \theta_0$, adjust $\tilde{t}$ to a higher value; if $\theta(0) < \theta_0$, adjust $a_t = \tilde{t}$; if $\theta(0) > \theta_0$, adjust $b_t = \tilde{t}$. Repeat the process from (2) until $\theta(0) = \theta_0$.

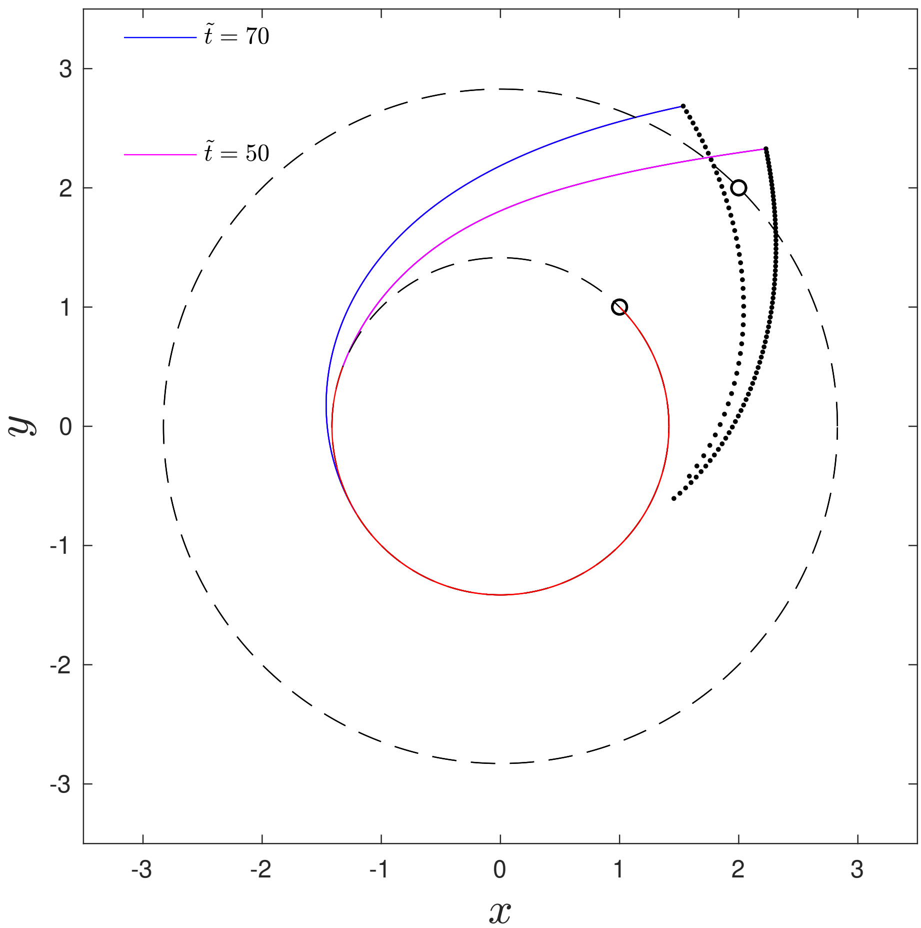

FIGURE 3.2: We want to move the particle from $(2,2)$ to $(1,1)$. The red line represents the motion of the particle in the second regime, while the blue and pink lines represent two possible trajectories in the first regime for different C_θ and $\tilde{t}$. The black dots represent possible initial positions for the particle for different values of these parameters. We see that a change in C_θ affects the radial coordinate, while a change in $\tilde{t}$ affects the angular coordinate of the simulated initial point.

Using this technique, we can analyse the possible candidates for the optimal solutions to the problem and identify the one that minimises the energy spent on moving the particle. For example, Figure 3.3 shows two possible solutions to the problem with $\nu = 10^{-4}$ m^{2}s^{-1}, $\rho_0 = 2\sqrt{2}$ m, $\rho_T = \sqrt{2}$ m, $\theta_0 = \theta_T = \pi/4$, $k = 1$ m^{2}s^{-1} and $T = 250$ s. These two solutions are candidates that arose from the maximum principle, yet the solution shown in red has a higher energy cost than the one depicted in blue. The existence of multiple candidates arises in the case where T is large enough to allow the particle to circle around the vortex multiple times. The optimal solution is the one in which the particle makes the fewest revolutions on the trajectory of a smaller radius, i.e., the solution in which the control is active for the most time. This is due to the quadratic cost function: it is better to pull the particle slowly inwards over a longer period of time than to pull it quickly over a shorter period of time.

Finally, we investigate the behaviour of solutions when we change the viscosity of the environment. We worked once again on the problem with $\rho_0 = 2\sqrt{2}$ m, $\rho_T = \sqrt{2}$ m, $\theta_0 = \theta_T = \pi/4$, $k = 1$ m^{2}s^{-1} and $T = 250$ s. In Table 3.2, we summarise the parameters $\tilde{t}$ and C_θ that we found for the optimal solution for different kinematic viscosities ranging from 10^{-5} m^{2}s^{-1} to 10^{-2} m^{2}s^{-1}, as well as the energy costs in each of these scenarios. For completeness, the analytical values for $\nu = 0$ m^{2}s^{-1} are also given (from Marques et al. [14]). Note that for low viscosity, the rounded values might be the same, but they actually differ in decimal places, which are not shown and can be computed to any desired accuracy as long as it is within the machine's reach.

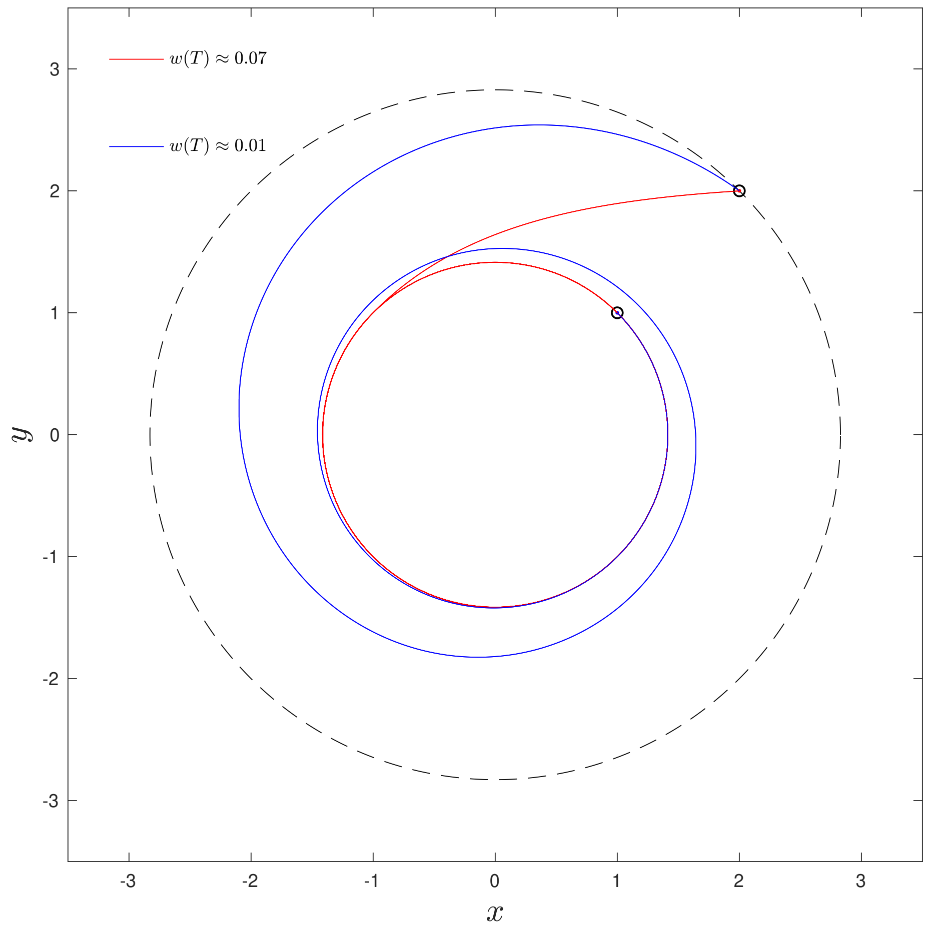

FIGURE 3.3: Depiction of two possible solutions for the problem with parameters $\nu = 10^{-4}$ m^{2}s^{-1}, $\rho_0 = 2\sqrt{2}$ m, $\rho_T = \sqrt{2}$ m, $\theta_0 = \theta_T = \pi/4$, $k = 1$ m^{2}s^{-1} and $T = 250$ s. The solution depicted by the blue line is optimal since it has a lower energy cost $(w\,(T)) \approx 0.01$) than the one depicted in red $(w\,(T)) \approx 0.07$). Both of these candidates arose from applying the maximum principle to the problem.

TABLE 3.2: Values of the parameters and energy costs for the optimal solutions of the problem with $\rho_0 = 2\sqrt{2}$ m, $\rho_T = \sqrt{2}$ m, $\theta_0 = \theta_T = \pi/4$, $k = 1$ m^{2}s^{-1} and $T = 250$ s for various kinematic viscosities. The $\nu = 0$ scenario is presented for comparison, and the values of the parameters were calculated analytically from Marques et al. [14].

$\boldsymbol{\nu}$ $(\mathbf{m^2 s^{-1}})$	**0**	$\mathbf{10^{-5}}$	$\mathbf{10^{-4}}$	$\mathbf{10^{-3}}$	$\mathbf{2 \times 10^{-3}}$	$\mathbf{4 \times 10^{-3}}$	$\mathbf{10^{-2}}$
$\tilde{t}$ (s)	232.89	232.87	232.87	220.97	156.20	26.49	163.32
C_θ (m^{2}s^{-1})	0.0014	0.0014	0.0014	0.0018	0.0043	0.11	0.019
w (T)	0.010	0.010	0.010	0.011	0.016	0.090	0.021

As expected, the energy cost seems to increase with viscosity, as we have to put more force into the system to move the particle through a more viscous flow. However, there are jumps in this behaviour as we can see when comparing the scenarios of $\nu = 2 \times 10^{-3}$ m^{2}s^{-1}, $\nu = 4 \times 10^{-3}$ m^{2}s^{-1} and $\nu = 10^{-2}$ m^{2}s^{-1} (for a visual representation of these optimal trajectories, see Figures 3.4 and 3.5). The increase in viscosity changes the possible trajectories for the particle in their nature. In the case where $\nu = 2 \times 10^{-3}$ m^{2}s^{-1}, the parameters allow for two types of solutions: one where the particle makes less than one complete turn around the vortex under the control (and then more than one full revolution around the vortex under no control) and a second where the particle makes more than one complete turn around the vortex under the control (and then less than a complete revolution around the vortex under no control). This is the same scenario as in Figure 3.3, and the optimal trajectory that minimises the energy cost is the one where the control is active for the longest time. Increasing the viscosity to $\nu = 4 \times 10^{-3}$ m^{2}s^{-1} is sufficient to exclude this second type of trajectory from the possible optimal trajectories, and we are left with the sole possibility of a trajectory where the particle is pushed harder and faster into a circular trajectory with the same radius as the final point and then makes more than one full revolution around the vortex while subject only to the velocity field of the flow. This increases the energy cost considerably. If we increase the viscosity further—to 10^{-2} m^{2}s^{-1}—we are now in a scenario where the particle cannot reach the target point in two complete turns around the vortex, and the optimal trajectory requires only one complete revolution around the vortex. The fact that we now need one less revolution around the vortex to move the particle significantly reduces the energy cost of the process.

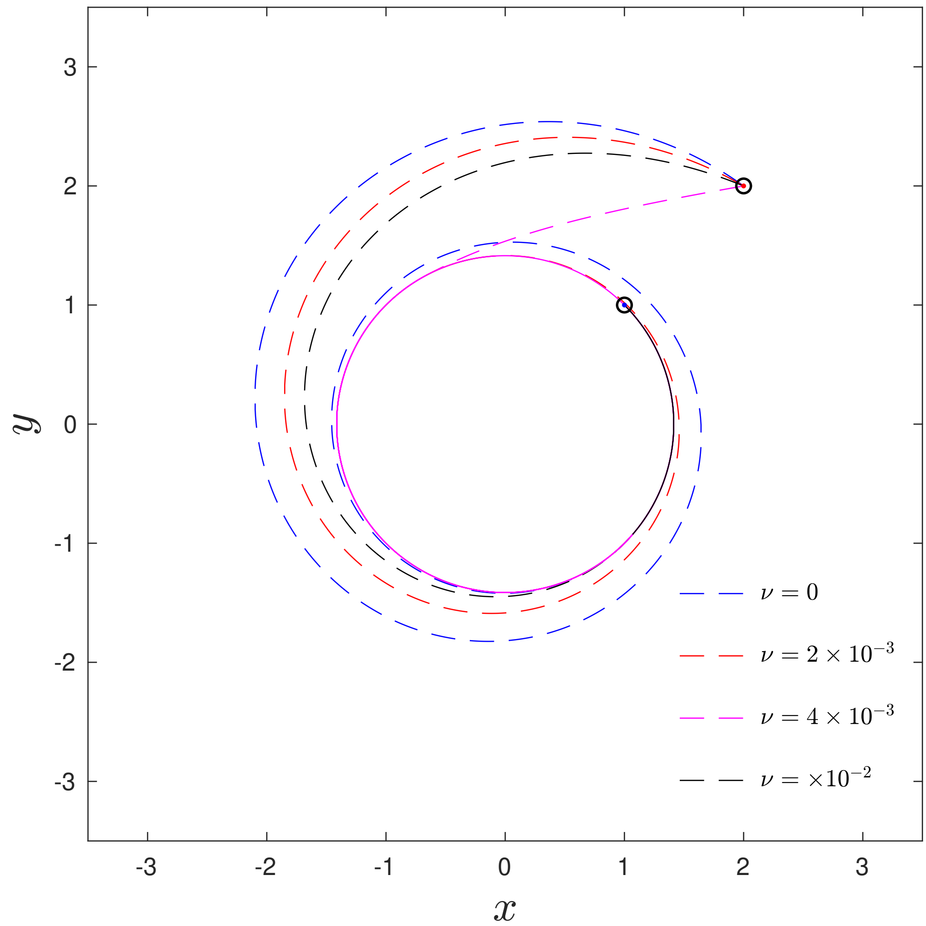

FIGURE 3.4: Optimal trajectories for the particle in the problem with parameters $\rho_0 = 2\sqrt{2}$ m, $\rho_T = \sqrt{2}$ m, $\theta_0 = \theta_T = \pi/4$, $k = 1$ m^{2}s^{-1} and different kinematic viscosities for the flow. The dashed lines correspond to the part of the trajectory where the control is active, and the solid lines indicate the part of the trajectory where the control is off. For comparison, the scenario $\nu = 0$ m^{2}s^{-1} is shown, and the trajectory is drawn with the parameters obtained analytically from the expressions given by Marques et al. [14].

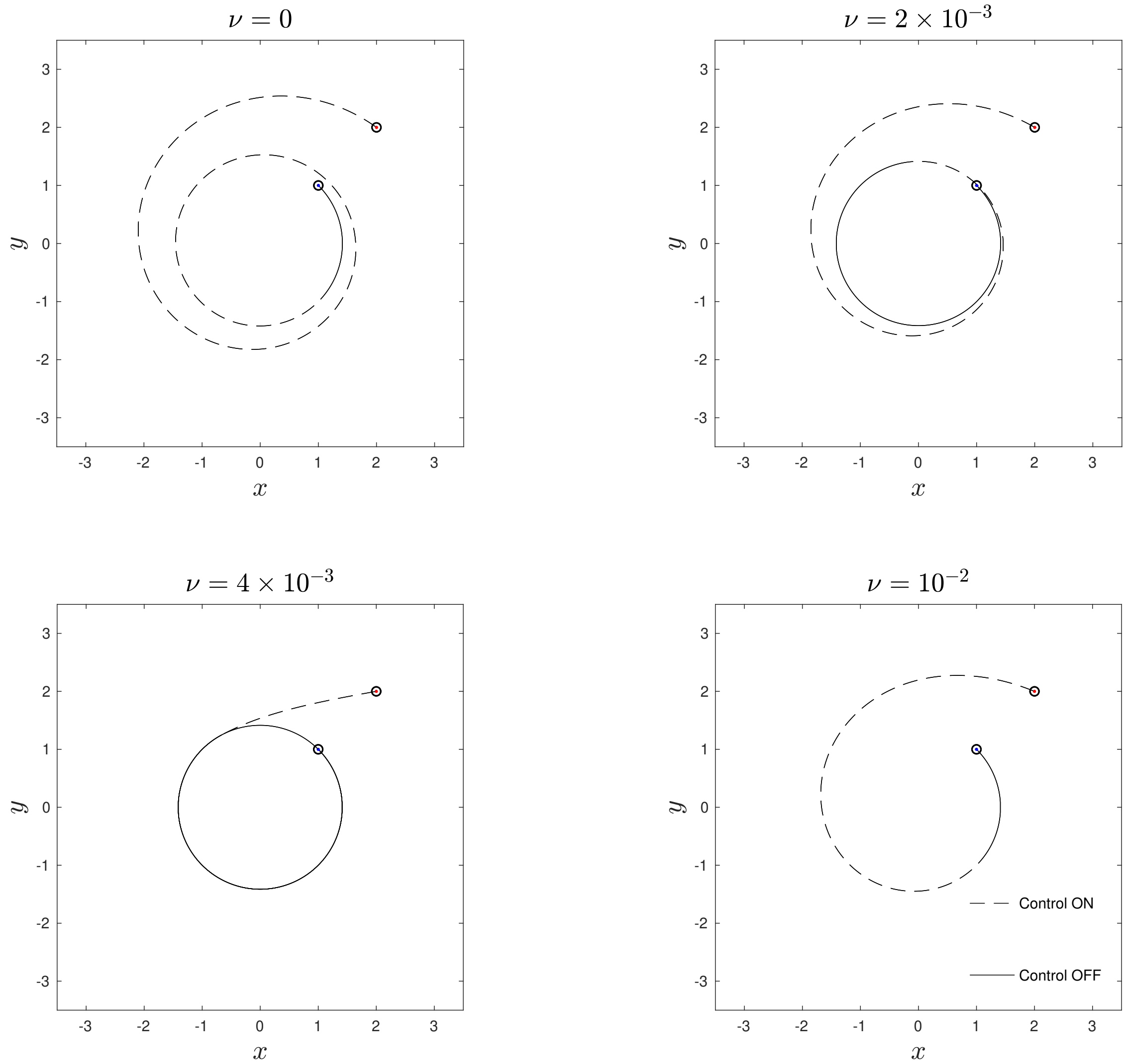

Figure 3.5: Optimal trajectories for the particle in the problem with parameters $\rho_0 = 2\sqrt{2}$ m, $\rho_T = \sqrt{2}$ m, $\theta_0 = \theta_T = \pi/4$, $k = 1$ m^{2}s^{-1} and different kinematic viscosities for the flow. The dashed lines correspond to the part of the trajectory where the control is active, and the solid lines indicate the part of the trajectory where the control is off. For comparison, the scenario $\nu = 0$ m^{2}s^{-1} is shown, and the trajectory is drawn with the parameters obtained analytically from the expressions given by Marques et al. [14].

Thus, in fact, the energy cost of displacing a particle in this scenario increases with viscosity as long as the number of revolutions required to reach the final remains the same. If the number of turns needed to complete the process decreases, the energy cost of the displacement decreases. This is illustrated in Figure 3.6, where we plot the viscosity of the flow against the energy cost for the optimal solution.

The region where the number of revolutions of optimal solutions changes is difficult to analyse, as we have no way of finding the optimal solution in the scenario where there is a time frame where the control $u = \pm 1$ is active. These types of solutions lie in this region. It is also not known whether it is possible to find a solution for any value of kinematic viscosity for a given problem. This is particularly difficult to analyse around the switching point of the number of revolutions of optimal solutions.

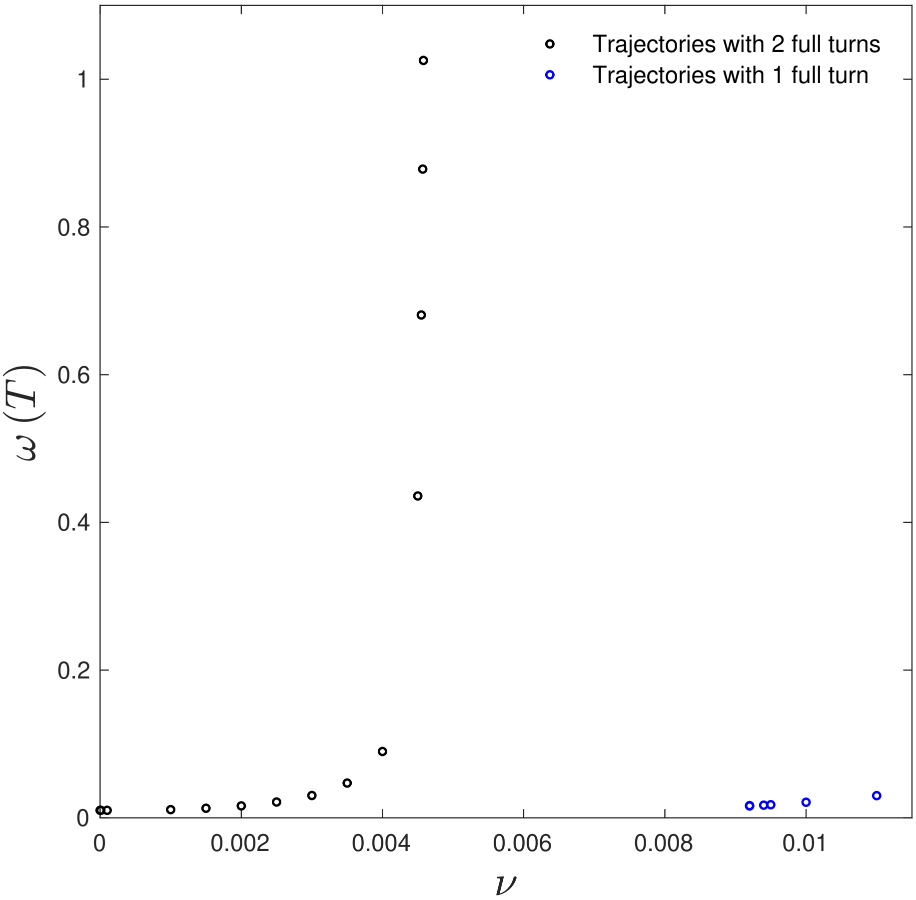

FIGURE 3.6: Energy cost for the problem with parameters $\rho_0 = 2\sqrt{2}$ m, $\rho_T = \sqrt{2}$ m, $\theta_0 = \theta_T = \pi/4$, $k = 1$ m^{2}s^{-1} and different kinematic viscosities for the flow. The cost increases with viscosity for solutions of the same nature (i.e., the number of full turns of the particle around the vortex), but there is a sharp decrease in energy when the nature of the solution changes to a smaller number of complete revolutions.

3.5 Conclusions and Future Work

The full Navier–Stokes equations are difficult to analyse and integrate. The task becomes even more hazardous if we want to combine the full description of flows with optimal control. The point vortex description of flows preserves the more important nonlinear features of the full flow description and, being a low-dimensional description, allows us to deal with more complex problems, such as the optimal control of flows. Although there has been some work on optimal control of inviscid vortices, the literature on the optimal control in viscous vortex flows is still scarce. We study how to optimally move a passive particle between two points in space in a given time in a viscous flow where the dynamics are driven by a Lamb–Oseen vortex. Even though the case study presented here is simple, it cannot be solved explicitly due to the nature of the differential equations arising from the maximum principle. However, it is possible to understand how the solutions behave and transform the problem into a parameter-search problem. We analyse how these parameters affect the optimal trajectories of a passive particle in a viscous environment ruled by a Lamb–Oseen vortex and how the energy cost is affected by the viscosity of the flow. In order to solve it, we turn the problem around and look for a way to move the particle from the final position to the initial position. Two parameters appear in the equations: C_θ, which affects the radial coordinate of the initial position, and $\tilde{t}$, which affects the angular coordinate of the initial position. Furthermore, we find that the energy cost of displacing a particle in such a scenario (i) increases with viscosity as long as the number of complete revolutions around the vortex remains the same; (ii) decreases when the viscosity increases such that that the number of complete turns required for the process decreases. We plan to conduct further research in this area, in particular analysing the behaviour of solutions where the control $u = \pm 1$ is active during a certain period of time and eventually tackling an environment with multiple vortices or using different types of admissible controls.

Author Contributions: Conceptualization, G.M., S.G. and F.L.P.; methodology, G.M., S.G. and F.L.P.; software, G.M.; validation, G.M.; formal analysis, G.M., S.G. and F.L.P.; investigation, G.M., S.G. and F.L.P.; writing—original draft preparation, G.M.; writing—review and editing, G.M.; supervision, S.G. and F.L.P.; funding acquisition, G.M., S.G. and F.L.P. All authors have read and agreed to the published version of the manuscript.

Funding: This work was partially supported by (i) grant ref. PD/BD/150537/2019 through Fundação para a Ciência e a Tecnologia (FCT); (ii) CMUP, ref. UIDB/00144/2020 funded through FCT; (iii) SYSTEC, ref. POCI-01-0145-FEDER-006933 funded by ERDF | COMPETE2020 | FCT/MEC | PT2020; (iv) project MAGIC POCI-01-0145-FEDER-032485, funded by FEDER via COMPETE 2020—POCI and by FCT/MCTES via PIDDAC; and (v) project SNAP NORTE-01-0145-FEDER-000085, funded by the European Regional Development Fund (ERDF), through the North Portugal Regional Operational Programme (NORTE2020), under the PORTUGAL 2020 Partnership Agreement.

Conflicts of Interest: The authors declare no conflict of interest.

References

[1] F. Clarke, Y. Ledyaev, R. Stern, and P. Wolenski, *Nonsmooth Analysis and Control Theory* (Graduate Texts in Mathematics). Springer New York, 2008, ISBN: 9780387226255. DOI: 10.1007/b97650.

[2] S. Mitter and J. Lions, *Optimal Control of Systems Governed by Partial Differential Equations* (Grundlehren der mathematischen Wissenschaften). Springer Berlin Heidelberg, 1971, ISBN: 9783540051152.

[3] N. Mahmoudian, J. Geisbert, and C. Woolsey, "Dynamics and control of underwater gliders i: Steady motions," Virginia Center for Autonomous Systems, Technical Report VaCAS-2007-01, 2009.

[4] N. Mahmoudian and C. Woolsey, "Dynamics and control of underwater gliders ii: Motion planning and control," Virginia Center for Autonomous Systems, Technical Report VaCAS-2010-02, 2010.

[5] J. Liu and H. Hu, "Biological inspiration: From carangiform fish to multi-joint robotic fish," *Journal of Bionic Engineering*, vol. 7, no. 1, pp. 35–48, 2010, ISSN: 1672-6529. DOI: 10.1016/S1672-6529(09)60184-0.

[6] G. K. Batchelor, *An Introduction to Fluid Dynamics* (Cambridge Mathematical Library). Cambridge University Press, 2000. DOI: 10.1017/CBO9780511800955.

[7] P. Newton, *The N-Vortex Problem: Analytical Techniques* (Applied Mathematical Sciences). Springer New York, 2010, ISBN: 9781441929167. DOI: 10.1007/978-1-4684-9290-3.

[8] C. Oseen, *Über Wirbelbewegung in einer reibenden Flüssigkeit* (Arkiv för matematik, astronomi och fysik). Almqvist & Wiksell, 1911.

[9] P. G. Saffman, *Vortex Dynamics* (Cambridge Monographs on Mechanics). Cambridge University Press, 1993. DOI: 10.1017/CBO9780511624063.

[10] S. B. Pope, *Turbulent Flows.* Cambridge University Press, 2000. DOI: `10.1017/CBO9781316179475`.

[11] T. Gallay and C. E. Wayne, "Global stability of vortex solutions of the two-dimensional navier-stokes equation," *Communications in Mathematical Physics*, vol. 255, no. 1, pp. 97–129, 2005. DOI: `10.1007/s00220-004-1254-9`.

[12] T. Gallay, "Interaction of vortices in weakly viscous planar flows," *Archive for Rational Mechanics and Analysis*, vol. 200, no. 2, pp. 445–490, 2011. DOI: `10.1007/s00205-010-0362-2`.

[13] S.-C. Kim and S.-I. Sohn, "Interactions of three viscous point vortices," *Journal of Physics A: Mathematical and Theoretical*, vol. 45, no. 45, p. 455 501, Oct. 2012. DOI: `10.1088/1751-8113/45/45/455501`.

[14] G. Marques, T. Grilo, S. Gama, and F. L. Pereira, "Optimal control of a passive particle advected by a point vortex," in *Advanced Research in Technologies, Information, Innovation and Sustainability*, T. Guarda, F. Portela, and M. F. Santos, Eds., Cham: Springer International Publishing, 2021, pp. 512–523, ISBN: 978-3-030-90241-4. DOI: `10.1007/978-3-030-90241-4_39`.

[15] L. S. Pontryagin, V. G. Boltyanskii, R. V. Gamkrelidze, and E. F. Mishchenko, *The Mathematical Theory of Optimal Processes.* New York, NY: Interscience Publishers, 1961, translated by K. N. Triruguf, edited by T. W. Neustadt.

[16] B. Protas, "Vortex dynamics models in flow control problems," *Nonlinearity*, vol. 21, no. 9, R203, Jul. 2008. DOI: `10.1088/0951-7715/21/9/R01`.

[17] E. Fehlberg, *Low-order Classical Runge-Kutta Formulas with Stepsize Control and Their Application to Some Heat Transfer Problems* (NASA technical report). National Aeronautics and Space Administration, 1969.

Chapter 4

Tracking Point Vortices and Circulations via Advected Passive Particles: an Estimation Approach

Published in IEEE Control Systems Letters, Vol. 7, 2023

Gil Marques, Marco Martins Afonso and Sílvio Gama

Abstract: We present a novel method for estimating the circulations and positions of point vortices in a two-dimensional (2D) environment using trajectory data of passive particles in the presence of Gaussian noise. The method comprises two algorithms: the first one calculates the vortex circulations, while the second one reconstructs the vortex trajectories. This reconstruction is done thanks to a hierarchy of optimization problems, involving the integration of systems of differential equations, over time sub-intervals all with the same amplitude defined by the autocorrelation function for the advected passive particles'trajectories. Our findings indicate that accurately tracking the position of vortices and determining their circulations is achievable, even when passive particle trajectories are affected by noise.

4.1 Introduction

The objective of this work is to showcase a way to find the strength (or circulation) and trajectory of a system of point vortices by using the data of trajectories of passive particles.

This is within the scope of the problems proposed by Protas [1], more specifically his Problem 4, in which he considers the scenario of reconstructing some state of a vortex dynamical system by using incomplete or noisy data.

The inverse problem of this, i.e. tracking passive particles advected by point vortices with known circulations is well documented in the literature. For example, the work [2] uses Poincaré sections and canonical transformations to investigate the Hamiltonian dynamics of passive markers in the flow created by two point vortices. In [3], the authors use data from coherent Lagrangian structures to determine when and where vortex formation occurs in flows around a 2D panel, and in [4] the authors employ vortices to approximate the dynamics of an incompressible flow.

The study of point vortices and passive particles is interesting for understanding the global evolution of atmospheric and oceanic vortices [5], [6], [7].

Section 4.2 serves as an introduction to the formalism of point vortex dynamics. In Section 4.3 we detail the problem we are tackling, presenting a method to solve it in Section 4.4. We present the results obtained from testing the method on simulated corrupted data in Section 4.5, and finally in Section 4.6 we sum up some conclusions and ideas for future work.

4.2 Point Vortices

In the vorticity formulation, the two-dimensional incompressible Navier–Stokes equations can be written as

$$\frac{\partial \omega}{\partial t} + (\mathbf{u} \cdot \nabla)\, \omega = \nu \nabla^2 \omega, \tag{4.1}$$

where ω is the vorticity, $\mathbf{u}$ is the velocity field and ν is the kinematic viscosity. In an inviscid flow ($\nu = 0$), equation (4.1), also known as Euler's equation, possesses the singular solutions

$$\omega\left(x, y, t\right) = \sum_{v} \Gamma_v\, \delta\left(\left(x, y\right) - \left(x_v\left(t\right), y_v\left(t\right)\right)\right). \tag{4.2}$$

The scalar Γ_v denotes the circulation of the point vortex located in $\left(x_v\left(t\right), y_v\left(t\right)\right)$ and can be thought of as a measure of the rotation strength of the flow around the point vortex.

These singular solutions of the 2D incompressible Navier–Stokes equations [8], [9], [10], [11] were first studied by Helmholtz [12], and further explored by Kelvin[13] and Kirchhoff[14]. They correspond to a scenario where the vorticity of a flow is concentrated in some well-defined points in space and enable a simpler description of the dynamics of such a system. Knowing the position and strength of each vortex in the system suffices to obtain the full velocity field at that instant, and thus knowing the dynamics of the vortices themselves in some time interval is enough to characterize the velocity field during that same time interval.

While a single point vortex, if left alone, will stay in the position $\left(x_0, y_0\right)$ forever and its circulation Γ will induce a time-independent velocity field in the plane, in a system of multiple point vortices the dynamics become more complex.

Consider a 2D inviscid flow in the complex plane that is described by N_v point vortices located in the positions $z_v = x_v + iy_v$ $(v = 1, \ldots, N_v\,; i^2 = -1)$. The velocity field generated by each of these vortices will affect the remaining $N_v - 1$ point vortices, making them move in the 2D plane, which causes the velocity field to change in time. Assuming there is no other object or force interfering in the flow, the motion of point vortices follows the differential equations

$$\dot{z}_v^* = \frac{1}{2\pi i} \sum_{\substack{s=1 \\ s \neq v}}^{N_v} \frac{\Gamma_s}{z_v - z_s}, \quad v = 1, \ldots, N_v\,, \tag{4.3}$$

where Γ_s is the circulation of vortex s and * denotes the complex conjugate.

However, when looking at real phenomena, it can be difficult to state precisely where the vortices are located and what is their circulation. A test particle, or a passive particle, is a particle that does not affect the flow and thus does not act on the vortices. Thus, they can be considered as point vortices with zero circulation. These passive particles, whose number we assume to be N_p, can be easier to trace and the trajectory $z_p\left(\cdot\right)$ of any of them follows the equations of motion

$$\dot{z}_p^* = \frac{1}{2\pi i} \sum_{v=1}^{N_v} \frac{\Gamma_v}{z_p - z_v}, \quad p = 1, \ldots, N_p\,. \tag{4.4}$$

4.3 Problem

Assuming we have a way to track individual passive particles in a flow (for example, using drones, meteorological sensors, particle image/tracking velocimetry techniques), consider the problem of finding the circulations and positions of a system of N_v point vortices, while only knowing the number of vortices in the system and the trajectory of N_p passive particles advected by that system of vortices.

In fact, since the trajectories of passive particles are sampled, what we have access to are discrete measurements of the particle trajectories. For simplicity, let us assume that these measurements are taken on N_t equally spaced time instants $t_k = t_0 + hk$ in the time interval $\left[t_0, t_f\right]$, where h is the time increment.

Thus, one way to approach the problem of reconstituting the vortices trajectories is to use the information on the particle trajectories to trace back the vortices that originated them, by trying to reconstitute the measured particle trajectories using the knowledge of the equations of motion for both the particles and the vortices. This can be summed up in the following problem:

$$\begin{cases} \underset{\substack{z_v(t_0)\in\mathbb{C} \\ \Gamma_v\in\mathbb{R}\setminus\{0\} \\ 1\leq v\leq N_v}}{\text{Minimize}} \quad \sum_{k=0}^{N_t-1}\sum_{p=1}^{N_p} ||\widetilde{z}_p\left(t_k\right) - z_p\left(t_k\right)||^2 \\ \text{subject to} \\ \qquad \dot{\widetilde{z}}_p^* = \dfrac{1}{2\pi i}\displaystyle\sum_{v=1}^{N_v}\dfrac{\Gamma_v}{\widetilde{z}_p - z_v}, \quad p = 1,\ldots,N_p\,, \\ \qquad \dot{z}_v^* = \dfrac{1}{2\pi i}\displaystyle\sum_{\substack{s=1\\ s\neq v}}^{N_v}\dfrac{\Gamma_s}{z_v - z_s}, \quad v = 1,\ldots,N_v \\ \qquad \widetilde{z}_p\left(t_0\right) = z_p\left(t_0\right) \end{cases} \tag{4.5}$$

where $||\cdot||$ is the usual Euclidean norm and $\widetilde{z}_p\left(t\right)$ is an estimate of the position of particle p at time t as obtained from solving the corresponding differential equations. This is an estimate because we do not know the true values for Γ_v or the initial conditions $z_v\left(t_0\right)$.

As a consequence to solving this problem, we will obtain the information about the vortices circulations and trajectories.

4.4 Method

Notice that first and foremost, since the particle trajectory data is prone to unknown measurement errors, we actually do not measure the real $z_p\left(t_k\right)$, but a quantity $z_p\left(t_k\right) + \Delta z_p\left(t_k\right)$, where $\Delta z_p\left(t\right)$ is the error associated with that measurement. By using a smoothing algorithm to diminish the impact of measurement errors in the data, we can then obtain estimations for the particle trajectories. From here onward, z_p will be used to denote the filtered data in order to not overload the notation.

From the filtered trajectories one can use a finite-differences method to estimate the velocity of the passive particles $\dot{z}_p(t)$. However, if velocity data are available, one can smooth such data directly instead of estimating them from the filtered trajectory data, which is something that would introduce further errors in the velocity estimates.

We can take advantage of the fact that Γ_v is constant in time to divide the problem into two sub-problems. First, we will find the circulations of the vortices, and afterwards use them to find better estimates for the vortices trajectories.

4.4.1 Estimating the circulations

For any given time t for which we have data for, the unknowns in (4.4) are Γ_v and $z_v(t)$. These amount, in reality, to $3N_v$ unknowns and thus we need to know the trajectories of at least $3N_v/2$ particles (each brings two pieces of information) in order to build a system of equations that is not underdetermined. After building such a system, one can use a nonlinear solver method to find a solution of the system. This will require an initial guess for both the circulations and positions of the vortices that should be provided based on analysis of the data: either the movement of the particles in the flow or actual visual imagery of the environment should hint towards what range of values one can expect for these quantities.

Doing so for time t_k will return estimates for the circulations Γ_v and for $z_v(t_k)$ — the positions of the vortices at time t_k. We will identify these estimates as $\widetilde{\Gamma}_{v_k}$ and $\widetilde{z}_{v_k}$. The index k on the circulations is used just to identify that such a value was estimated using the data at time t_k, as the circulation is in fact independent of time.

One can then use $\widetilde{z}_{v_k}$ as an initial condition for (4.3) in order to find an initial guess for $z_v(t_{k+1})$ and build the same nonlinear system of equations as before for time t_{k+1}, solve it and obtain estimates for $z_v(t_{k+1})$ and a new estimate for Γ_v: $\widetilde{\Gamma}_{v_{k+1}}$. In order to explore the parameter space further, one can update the initial guess for the circulations as $\widetilde{\Gamma}_{v_k}(1+\delta_v)$, where δ_v is a uniform random variable that ranges from $-\epsilon$ to ϵ (ϵ is some small positive number).

Repeating this procedure from t_0 to t_f will result in a set of values $\left\{\widetilde{\Gamma}_{v_k} : k = 1, \ldots, N_t\right\}$, all of which are estimates for the vortex circulations. By doing an outlier analysis one can remove any abnormal value and find estimates for the vortex circulations using the average or median of the leftover values in order to obtain $\widetilde{\Gamma}_v$, a more robust estimate for these quantities. One can even repeat this whole procedure using these more robust estimates as the initial guess in order to refine the results. Algorithm 1 sums up this procedure.

4.4.2 Estimating the vortex trajectories

Having obtained the circulations, we have now simplified the problem (4.5) as Γ_v is now fixed at $\widetilde{\Gamma}_v$.

It is known that, in general, vortex systems exhibit chaotic dynamics for $N_v \geq 4$ [8], [15]. A practical consequence of this fact is that, when solving equations such as (4.5) or (4.4), even a small error in the initial condition can be highly amplified given enough time and the computed trajectories can be completely different from the real ones. Our approach to deal with this problem is to partition the trajectory and work on the reconstitution of each part separately and sequentially. However, one needs to first find a criteria for building such a partition which should take into account what is known about the chaoticity of the system.

One way to measure the degree of chaos in such a system are Lyapunov exponents[16], [17]. In particular, the largest Lyapunov exponent measures the (exponential) rate at which two nearby trajectories separate from each other, and thus its inverse gives us the time needed for two nearby trajectories to separate for a factor of e. This also tells us that the system has some degree of memory but, after a certain time, the evolution is mostly uncorrelated with the states past a certain point in time. Lyapunov exponents

Algorithm 1 Finding the circulations

Set a value for ϵ
Estimate the velocities of passive particles
Provide an initial guess for the circulations and positions of the vortices at $t = t_0$
$k \leftarrow 1$
while $k \leq N_t$ **do**
    Use a nonlinear solver to find $\widetilde{\Gamma}_{v_k}$ and $\widetilde{z}_{v_k}$, estimates for Γ_v and $z_v\left(t_k\right)$ with the appropriate initial conditions
    Use $\widetilde{z}_{v_k}$ and (4.3) to find an estimate for $z_v\left(t_{k+1}\right)$
    Generate random numbers δ_v uniformly in the interval $[-\epsilon, \epsilon]$
    Use $\widetilde{\Gamma}_{v_k}\left(1+\delta_v\right)$ as an updated initial guess for the circulations
    $k \leftarrow k+1$
end while
Run an outlier analysis over the values $\widetilde{\Gamma}_{v_k}$
Obtain a more robust estimate of the circulations using the average or median of the leftover $\widetilde{\Gamma}_{v_k}$ values

for the system of vortices and for passive particles with a chaotic movement are different. Nevertheless, in a chaotic system, they seem to be within the same order of magnitude [18]. Thus, since we have no information about the vortices themselves, we need to use the passive particles to get an estimate of such quantities. However, Lyapunov exponents computation is slow and heavy and, in a scenario where one wants to follow vortices in real time, it is not a quantity suitable to use. Autocorrelation functions, nonetheless, are fast to compute and can be used to find the time after which the state of the system has little to no memory of its initial state.

By computing autocorrelation functions for the passive particles' trajectories, we can find the time τ it takes for the system to lose most of its memory from the initial state. We do this by setting an arbitrary cutoff $0 < \alpha < 1$ and computing $\tau : \forall p \in \left\{1, \ldots, N_p\right\}, \, |\, \rho_p \left(t > \tau\right) | \leq \alpha$, where ρ_p denotes the autocorrelation function for the trajectory of the particle p.

Thus, in order to reconstitute the full vortex trajectories we must reconstitute $n = \left\lceil \frac{t_f - t_0}{\tau} \right\rceil$ partitions of the form $P_j = \left[t_0 + j\tau, t_0 + \left(j+1\right)\tau\right], \, j = 0, 1, \ldots, n-2$, and $P_{n-1} = \left[t_0 + \left(n-1\right)\tau, t_f\right]$. Each of these sub-problems constitutes an optimization problem akin to (4.5) that can be written as

$$\begin{cases} \underset{\substack{z_v\left(t_0+j\tau\right)\in\mathbb{C}\\ 1\leq v\leq N_v}}{\text{Minimize}} \quad \displaystyle\sum_{k=j\tau/h}^{\left(j+1\right)\tau/h} \sum_{p=1}^{N_p} ||\widetilde{z}_p\left(t_k\right) - z_p\left(t_k\right)||^2 \\ \text{subject to} \\ \dot{\widetilde{z}}_p^* = \dfrac{1}{2\pi i} \displaystyle\sum_{v=1}^{N_v} \dfrac{\widetilde{\Gamma}_v}{\widetilde{z}_p - z_v}, \quad p = 1, \ldots, N_p \\ \dot{z}_v^* = \dfrac{1}{2\pi i} \displaystyle\sum_{\substack{s=1\\ s\neq v}}^{N_v} \dfrac{\widetilde{\Gamma}_s}{z_v - z_s}, \quad v = 1, \ldots, N_v \\ \widetilde{z}_p\left(t_0 + j\tau\right) = z_p\left(t_0 + j\tau\right) \end{cases} \tag{4.6}$$

for $j = 0, 1, \ldots, n-2$, $t \in P_j$, and

$$\begin{cases} \underset{\substack{z_v\left(t_0+(n-1)\tau\right)\in\mathbb{C} \\ 1\le v\le N_v}}{\text{Minimize}} \quad \displaystyle\sum_{k=j\tau/h}^{\left(j+1\right)\tau/h} \sum_{p=1}^{N_p} ||\widetilde{z}_p\left(t_k\right) - z_p\left(t_k\right)||^2 \\ \text{subject to} \\ \dot{\widetilde{z}}_p^* = \dfrac{1}{2\pi i}\displaystyle\sum_{v=1}^{N_v} \dfrac{\widetilde{\Gamma}_v}{\widetilde{z}_p - z_v}, \quad p = 1,\dots,N_p \\ \dot{z}_v^* = \dfrac{1}{2\pi i}\displaystyle\sum_{\substack{s=1 \\ s\neq v}}^{N_v} \dfrac{\widetilde{\Gamma}_s}{z_v - z_s}, \quad v = 1,\dots,N_v \\ \widetilde{z}_p\left(t_0 + (n-1)\,\tau\right) = z_p\left(t_0 + (n-1)\,\tau\right) \end{cases} \tag{4.7}$$

for $t \in P_{n-1}$.

These n problems can thus be solved sequentially by a nonlinear solver, using $z_v\left(t_0 + \left(j+1\right)\tau\right)$ obtained in the problem associated to the interval P_j as an initial guess for the problem associated with the interval P_{j+1}. Algorithm 2 summarizes this full process.

Algorithm 2 Finding the vortex trajectories

```
Set α
p ← 1
while p ≤ N_p do
    Compute ρ_p(t), the autocorrelation function of z_p(t)
    Find τ_p : |ρ_p(t > τ_p)| ≤ α
    p ← p + 1
end while
τ ← min_{1≤p≤N_p} {τ_p}
n ← ⌈(t_f − t_0)/τ⌉
j ← 1
while j ≤ n do
    Use a nonlinear solver to solve problem (4.6) on the time interval P_j
    j ← j + 1
end while
Use a nonlinear solver to solve problem (4.7)
```

4.5 Results

We simulated a system comprised of $N_v = 4$ vortices with circulations $\Gamma_v = v, v = 1, 2, 3, 4$ and $N_p = 20$ passive particles. The vortices were initially placed in the position $z_1 (t = 0) = 2$, $z_2 (t = 0) = -1 - i$, $z_3 (t = 0) = \frac{1}{2} + \frac{i}{2}$, $z_4 (t = 0) = -2 + 3i$ and the passive particles were placed in random positions in the background between the vortices, and we let the system evolve for a time period of 10^5 units of time using a time step of 10^{-2}. The vortex circulations were all chosen to have the same sign in order to confine the movements of the particles and vortices to a certain area, which facilitates the simulation and analysis. If there are vortices with opposite signs in the system, pairs of vortices can be formed and travel long distances away from the remaining vortices. Even though we would only need 6 particles in order to obtain some estimators for the vortices' circulation and positions we chose $N_p = 20$ so that we have more information about the system. If we had only 6 particles, the estimation for the vortices' circulations and positions could be easily compromised if the data for one of the passive particles was too corrupted or was affected by some measurement errors. Having a higher number of particles helps to minimize these issues. The simulation ran for a long time in order to be possible for us to compute a good estimate of the maximum Lyapunov exponent of the vortex system, for which we found ~ 0.028. This was done in order to make a comparison with the time obtained from the autocorrelation function when applying the presented algorithms. However, since the problem of recovering the vortex trajectories is computationally heavy, we restrained to using a time interval of 10^3 units of time for this problem.

We then introduced Gaussian white noise $W \sim \mathcal{N}\left(\mu = 0, \sigma^2 = 0.01^2\right)$ in the particles' trajectory data, in order to simulate what actual real data could look like. After doing so, the data were too corrupted to be directly used, so we first smoothed them using a Gaussian filter. We then used the smoothed trajectories to compute particle velocities using a fourth-order finite-differences scheme and ran Algorithm 1 with $\epsilon = 0.1$. Integration was made using the Runge–Kutta–Fehlberg method with a step size of 10^{-2}, and the nonlinear equations were solved by MATLAB^{TM} routine *lsqcurvefit*.

We were able to recover the vortices' circulations with a relative error of $\sim 0.1\%$ (if we use the uncorrupted data, the relative error decreases to $\sim 10^{-5}\,\%$). The obtained values are summarized in Table 4.1, as well as the relative errors for each individual circulation.

Fig. 4.1 shows the boxplots for the values of $\widetilde{\Gamma}_{v_k}$ obtained by the algorithm. The values in the y axis were shifted down by $v - 1$ for easier visualization purposes.

TABLE 4.1: True values of the circulations and the values recovered by Algorithm 1. The circulations were recovered with a relative error of $\sim 0.1\,\%$.

Vortex v	1	2	3	4
$z_v(0)$	2	$-1-i$	$\frac{1}{2}+\frac{i}{2}$	$-2+3i$
Γ_v	1	2	3	4
$\widetilde{\Gamma}_v$	0.99625	2.00132	2.99746	4.00258
$\frac{\lvert\widetilde{\Gamma}_v-\Gamma_v\rvert}{\lvert\Gamma_v\rvert}$	$0.37\,\%$	$0.066\,\%$	$0.085\,\%$	$0.065\,\%$

Using the obtained values of $\widetilde{\Gamma}_v$, we then proceeded to recover the vortex trajectories using Algorithm 2. We set $\alpha = 0.2$, obtaining $\tau = 39.89$. This is in accordance with the value of the Lyapunov exponent we obtained in the initial simulation (~ 0.028), since $\tau^{-1} \approx 0.025$, which is of the same order of magnitude as the Lyapunov exponent. Once again, integration was made using the Runge–Kutta–Fehlberg method with a step size of 10^{-2} and the nonlinear problems were solved by MATLAB^{TM} using the routine *fmincon* with the *sqp* algorithm. We were able to recover the trajectories of the vortex system with a total relative error of $\sim 0.44\,\%$ (if we use the uncorrupted data, the relative error decreases to $\sim 0.08\,\%$).

Fig. 4.2 shows a portion of the recovered trajectories of the 4 vortices with different colored markers and the (smoothed) trajectory of a passive particle in a full black line. The color-filled dots mark the initial point of each trajectory.

Fig. 4.3 illustrates how the partitioning of the problem helps with controlling the error of the recovered trajectories. Due to the chaoticity of the system, errors can grow large and we can see that, in general, by integrating partitions of the trajectory with a time length similar to the inverse of the Lyapunov exponent of the vortex system will help to prevent exponential growth of the errors.

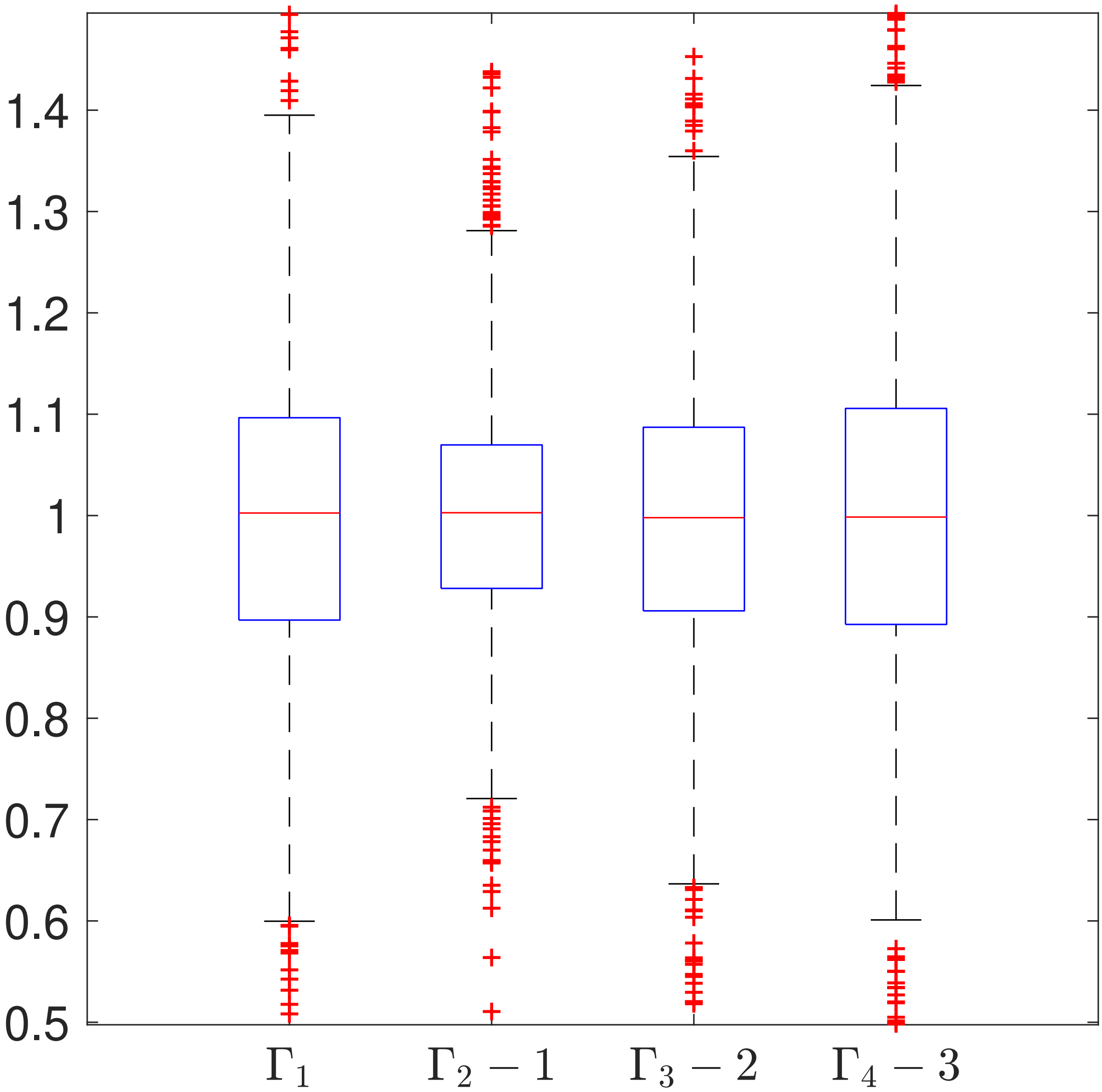

Figure 4.1: Boxplot for $\widetilde{\Gamma}_v - (v-1)$. The values are shifted down by $v-1$ for easier visualization purposes. We can see that the distribution of obtained values is centered around the true value of each circulation.

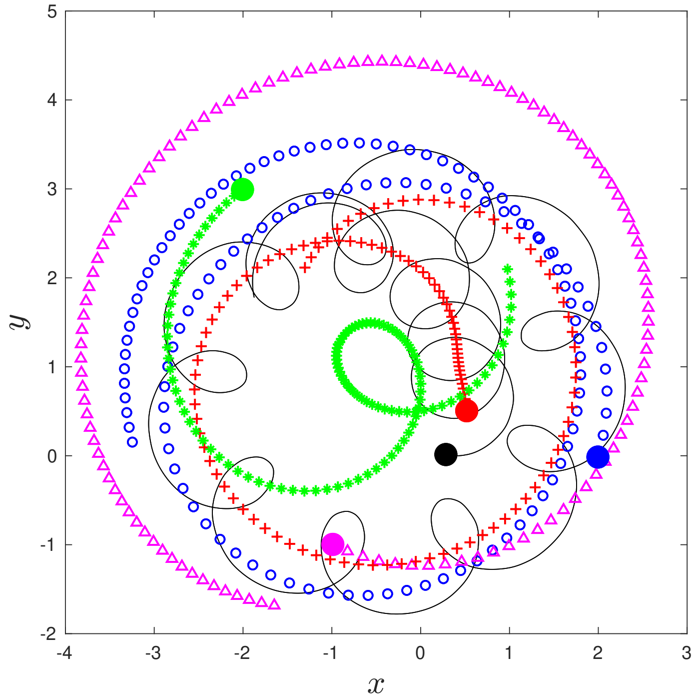

FIGURE 4.2: A portion of the recovered trajectories of the 4 vortices (blue dots, pink triangles, red crosses and green asterisks identify vortices 1, 2, 3 and 4, respectively) and an example of a smoothed trajectory for a passive particle in a full black line. The color-filled dots mark the initial point of each trajectory.

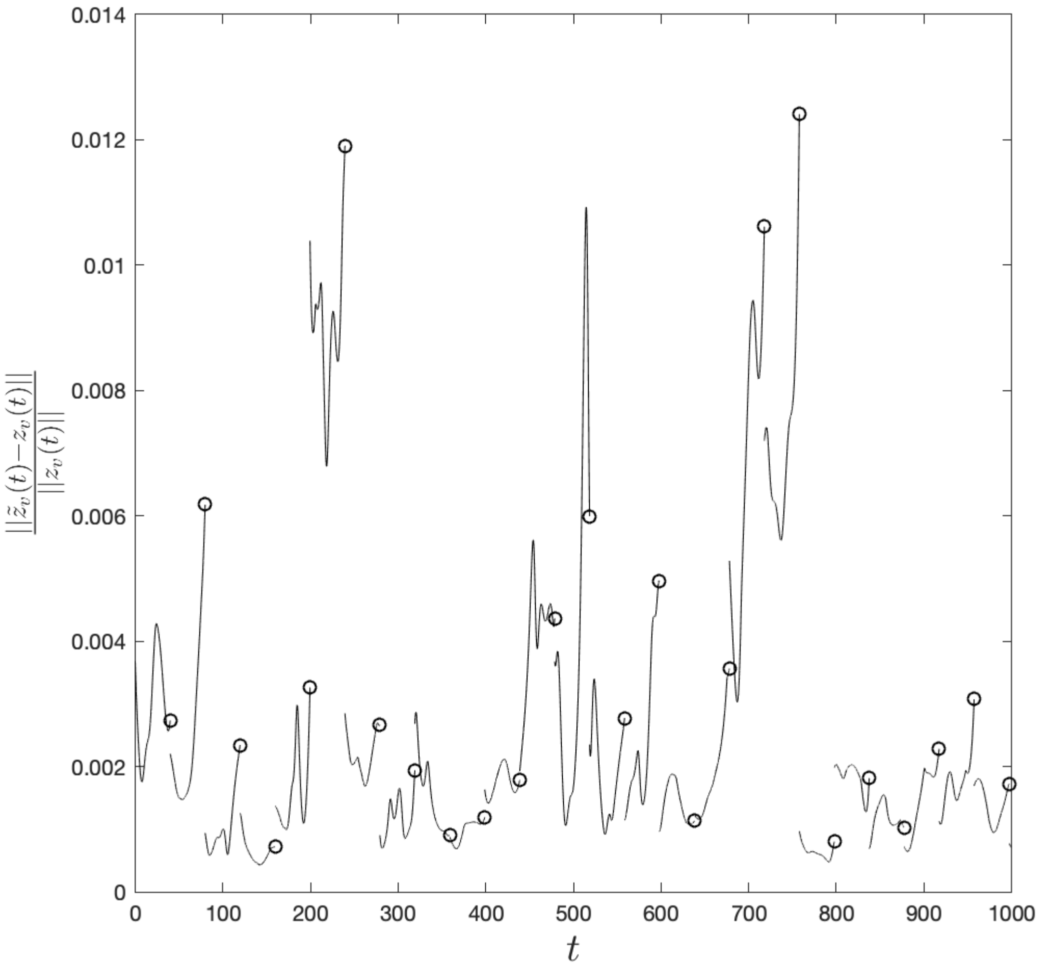

Figure 4.3: Relative error for the position of the vortex system at each time step. The circles identify the discontinuities that arise from the partition of the problem into various sub-problems. In general the relative error decreases every time we change from one partition to the following one.

4.6 Conclusion

We presented the basic ideas on how to try to recover vortex dynamics from data on the trajectories of advected passive particles. This is a problem that, as far as we are aware, has not been addressed before and can have relevant interest since it is easier to track the advected particles than tracking and measuring the strength of vortices themselves.

The method presented is a first study and we believe it can be improved largely. For example, using optimization techniques and algorithms specifically tailored for the problem and its equations, instead of using generic MATLAB^{TM} routines, will likely increase accuracy and speed up the computations. Moreover, in this work we assumed that the number of vortices N_v was known in advance. In situations where N_v in unknown, its estimation from the data of a set of passive particles is not an easy task and is left for a forthcoming paper.

Nevertheless, from the results of this study, we see that it is possible to effectively recover the full vortex dynamics with a good degree of accuracy, even in the presence of noisy data. This opens up the possibility of studying more complex problems, for instance, predicting positions of vortices and/or particles at future times, which enables the study of finding controls to move passive particles to a desired position in a given time.

Acknowledgements

This work was supported by (i) CMUP, member of LASI, which is financed by national funds through FCT −Fundação para a Ciência e a Tecnologia, I.P., under the project with reference UIDB/00144/2020, and (ii) project SNAP NORTE-01-0145-FEDER-000085, co-financed by the European Regional Development Fund (ERDF) through the North Portugal Regional Operational Programme (NORTE2020) under Portugal 2020 Partnership Agreement. GM thanks grant ref. PD/BD/150537/2019 through FCT.

References

[1] B. Protas, "Vortex dynamics models in flow control problems," *Nonlinearity*, vol. 21, no. 9, R203, Jul. 2008. DOI: 10.1088/0951-7715/21/9/R01.

[2] G. Boffetta, A. Celani, and P. Franzese, "Trapping of passive tracers in a point vortex system," *Journal of Physics A: Mathematical and General*, vol. 29, no. 14, p. 3749, Jul. 1996. DOI: 10.1088/0305-4470/29/14/004.

[3] Y. Huang and M. A. Green, "Detection and tracking of vortex phenomena using lagrangian coherent structures," *Experiments in Fluids*, vol. 56, no. 7, p. 147, 2015. DOI: 10.1007/s00348-015-2001-z.

[4] Z. Qian, Y. Qiu, and Y. Zhang, "Tracking the vortex motion by using brownian fluid particles," *Physics of Fluids*, vol. 33, no. 10, p. 105 113, Oct. 2021, ISSN: 1070-6631. DOI: 10.1063/5.0065073.

[5] V. V. Meleshko, M. Y. Konstantinov, A. A. Gurzhi, and T. P. Konovaljuk, "Advection of a vortex pair atmosphere in a velocity field of point vortices*," *Physics of Fluids A: Fluid Dynamics*, vol. 4, no. 12, pp. 2779–2797, Dec. 1992, ISSN: 0899-8213. DOI: 10.1063/1.858335.

[6] H. Aref and M. A. Stremler, "Point vortex models and the dynamics of strong vortices in the atmosphere and oceans," in *Fluid Mechanics and the Environment: Dynamical Approaches*, J. L. Lumley, Ed., Berlin, Heidelberg: Springer Berlin Heidelberg, 2001, pp. 1–17, ISBN: 978-3-540-44512-8. DOI: 10.1007/3-540-44512-9_1.

[7] I. I. Mokhov, S. G. Chefranov, and A. G. Chefranov, "Point vortices dynamics on a rotating sphere and modeling of global atmospheric vortices interaction," *Physics of Fluids*, vol. 32, no. 10, p. 106 605, Oct. 2020, ISSN: 1070-6631. DOI: 10.1063/5.0026014.

[8] P. Newton, *The N-Vortex Problem: Analytical Techniques* (Applied Mathematical Sciences). Springer New York, 2010, ISBN: 9781441929167. DOI: 10.1007/978-1-4684-9290-3.

[9] A. Chorin, *Vorticity and Turbulence* (Applied Mathematical Sciences). Springer, 1994, ISBN: 9780387941974. DOI: 10.1007/978-1-4419-8728-0.

[10] G. K. Batchelor, *An Introduction to Fluid Dynamics* (Cambridge Mathematical Library). Cambridge University Press, 2000. DOI: 10.1017/CBO9780511800955.

[11] P. G. Saffman, *Vortex Dynamics* (Cambridge Monographs on Mechanics). Cambridge University Press, 1993. DOI: 10.1017/CBO9780511624063.

[12] H. Helmholtz, "Über integrale der hydrodynamischen gleichungen, welche den wirbelbewegungen entsprechen.," ger, *Journal für die reine und angewandte Mathematik*, vol. 55, pp. 25–55, 1858.

[13] W. Thomson, "Vi.—on vortex motion," *Transactions of the Royal Society of Edinburgh*, vol. 25, no. 1, pp. 217–260, 1868. DOI: 10.1017/S0080456800028179.

[14] G. R. Kirchhoff, "Vorlesungenbër mathematische Physik.," ger, *Mechanik*, 1876.

[15] A. Babiano, G. Boffetta, A. Provenzale, and A. Vulpiani, "Chaotic advection in point vortex models and two-dimensional turbulence," *Physics of Fluids*, vol. 6, no. 7, pp. 2465–2474, Jul. 1994, ISSN: 1070-6631. DOI: 10.1063/1.868194.

[16] D. Ruelle, *Chaotic Evolution and Strange Attractors* (Lezioni Lincee). Cambridge University Press, 1989. DOI: 10.1017/CBO9780511608773.

[17] K. T. Alligood, T. D. Sauer, and J. A. Yorke, *Chaos An Introduction to Dynamical Systems*. Springer-Verlag, New York, 1997. DOI: 10.1007/b97589.

[18] G. Marques, M. J. Rodrigues, and S. Gama, "Passive particle dynamics in viscous vortex flow," in *CONTROLO 2020*, J. A. Gonçalves, M. Braz-César, and J. P. Coelho, Eds., Cham: Springer International Publishing, 2021, pp. 352–362, ISBN: 978-3-030-58653-9. DOI: 10.1007/978-3-030-58653-9_34.

Chapter 5

Energy optimal control in Lamb-Oseen vortex flow

Published in CONTROLO 2024, Lecture Notes in Electrical Engineering, Vol. 1325, 2025

Gil Marques and Sílvio Gama

Abstract: This work investigates how to optimally transport a passive particle between two prescribed points in the 2-D plane in the presence of a Lamb-Oseen (viscous) vortex. We study how to minimise the energy spent in moving the particle by applying a control that only acts on the radial component of the movement. Using Pontryagin's Maximum Principle, we find an explicit time-dependent extremal and convert the problem into a parameter search problem. Due to the geometry of the problem, we find that it is possible to have candidates to the optimal solution with different numbers of full turns around the vortex and that this number of turns limits the range of viscosities where solutions exist. We observe that there can be gaps in the viscosity range where solutions exist, and that solutions with lower turn count are preferred (in the sense of minimising the energy cost).

5.1 Introduction

In this article, we present a research work developed in the framework of optimal control of dynamical systems whose state is driven by ordinary differential equations [1], [2]. This work provides a solid foundation for the design and control of new advanced engineering systems operating in environments where the dynamics are governed by a fluid. For example, underwater gliders, i.e. winged autonomous underwater vehicles (AUVs) [3], [4] or robotic fish [5]. These robots can be used in order to perform a variety of tasks in real flows, such as transporting materials in a flow or measuring physical quantities of the flow itself. Controlling and automating these tasks is thus essential for system effectiveness.

One useful description of a flow is the vorticity description, which is based on entities called point vortices, which characterize the dynamics of the flow. A point vortex is a mathematical entity characterized by its location and circulation that generates a rotational flow field. Consider a non-viscous 2D flow specified in the complex plane by N point vortices, each located in z_i [6], [7]. In this context, the motion of any passive particle advected by this flow is given by the following dynamical equation

$$\dot{z}^*(t) = \frac{1}{2\pi i} \sum_{j=1}^{N} \frac{k_j}{z(t) - z_j(t)} , \tag{5.1}$$

where k_j is the circulation - or strength - of the j-th vortex, the initial conditions $z_j(0)$ are known, $i^2 = -1$, and the Cartesian coordinates are specified in a complex formulation as $z = x + yi$.

However, no real flow is completely free of viscosity, and it is important to consider this when modelling motion on real fluids. One of the simplest models of a point vortex in a viscous environment is the Lamb-Oseen formulation [8], [9]. The so-called Lamb-Oseen vortex is the solution of the Navier-Stokes equations for an initial condition in which the full vorticity of the flow is concentrated in a single point in the plane. This originates a vorticity field that decays and is diffused radially outwards with a Gaussian profile (see [6], [10]).

An important result about the Lamb-Oseen vortex is that it is an asymptotically stable attracting solution of the vorticity equation for any integrable initial vorticity configuration, as proved by Gallay & Wayne [11]. The superposition of N Lamb-Oseen vortices is one such configuration and it forms the basis of the idea of the multi-Gaussian model. This model assumes that the vorticity field is a superposition of Lamb-Oseen vortices at all times, modelling the behaviour of both the diffusive term and convective term of the vorticity equations through the interaction of the vortices with each other.

More recently, Gallay [12] has shown that under reasonable assumptions, the solution of the Navier-Stokes equations in the inviscid limit for δ-Dirac initial conditions converges to a superposition of Lamb-Oseen vortices. This further supports the applicability of the multi-Gaussian model in fluid description.

The motion of a passive particle in the multi-Gaussian model follows the velocity field generated by the system of N vortices and thus the dynamical equation [13]:

$$\dot{z}^* (t) = \frac{1}{2\pi i} \sum_{j=1}^{N} \frac{k_j}{z (t) - z_j (t)} \left[1 - \exp \left(- \frac{|z - z_j|^2}{4\nu t} \right) \right], \tag{5.2}$$

where ν is the kinematic viscosity of the flow. This is consistent with the inviscid model as we recover Eq. (5.1) by taking the limit $\nu \to 0^+$.

In this work, we consider an underlying flow which is characterised by a single Lamb-Oseen vortex. Our focus is the problem where we want to transport one passive particle between two points in the 2-D plane while only acting on the radial component of its movement and minimising the energy spent to perform that action. This paper is a follow-up to the two previous studies of Marques *et al.* [14], [15]: the first one treated the inviscid case ($\nu = 0$) and the second tackled the viscous scenario, while leaving some questions unanswered. In these papers, the problem was solved by applying necessary optimality conditions in the form of a maximum principle [16] and it is shown that the optimal radial control is explicitly time-dependent and that it can be determined exclusively by analytical methods only in the inviscid case. The viscous terms in the equations of motion (5.2) make it impossible to find an analytical solution to the viscous problem and it is thus needed to tackle the problem numerically. In Marques *et al.* [15] we gave a qualitative description of the solutions and presented a way to compute some of them. The present work expands on the computation of all the possible solutions and provides more insight on the behaviour of said solutions.

Sections 5.2 and 5.3 are devoted to the mathematical formulation of the problem. In Section 5.4, we pose the minimum energy problem and investigate the regimes of motion allowed for the passive particle, as well as the relations between viscosity, number of full turns around the vortex and energy for candidates to optimal solutions that arise from Pontryagin's maximum principle. The conclusions and future work constitute the last section.

5.2 Velocity field driven by a Lamb-Oseen vortex

Consider a viscous flow with some kinematic viscosity ν and a Lamb-Oseen vortex of vorticity k located at the origin $(0,0)$. Let $z(t) = x(t) + y(t)\,i$ be the position of a passive particle placed in this flow, at time t. The particle is advected only by the velocity field generated by the vortex, and thus its movement must follow the dynamics given by

$$\dot{z}^*(t) = \frac{1}{2\pi i}\frac{k}{z(t)}\left[1 - \exp\left(-\frac{|z(t)|^2}{4\nu t}\right)\right] . \tag{5.3}$$

In polar coordinates, the position of the particle is given by

$$z(t) = \rho(t)\, e^{i\theta(t)} , \tag{5.4}$$

and the derivative with respect to t is

$$\dot{z}(t) = \dot{\rho}(t)e^{i\theta(t)} + i\rho(t)\,\dot{\theta}(t)\,e^{i\theta(t)} . \tag{5.5}$$

Therefore, the complex conjugate of the derivative is

$$\dot{z}^*(t) = \dot{\rho}(t)\,e^{-i\theta(t)} - i\rho(t)\,\dot{\theta}(t)\,e^{-i\theta(t)} \tag{5.6}$$

and, from (5.3) and (5.6), we obtain

$$\dot{\rho}(t) - i\rho(t)\,\dot{\theta}(t) = -i\frac{k}{2\pi}\frac{1}{\rho(t)}\left[1 - \exp\left(-\frac{\rho^2(t)}{4\nu t}\right)\right] . \tag{5.7}$$

By identifying the real and imaginary factors in both sides of the equation, we find the following dynamic equations for the particle in polar form

$$\begin{cases} \dot{\rho}(t) = 0 \\ \dot{\theta}(t) = \frac{k}{2\pi}\frac{1}{\rho^2(t)}\left[1 - \exp\left(-\frac{\rho^2(t)}{4\nu t}\right)\right] \end{cases} , \tag{5.8}$$

which are not solvable analytically. Nevertheless, the equations of motion offer an insight on the qualitative behaviour of solutions: a circular motion with constant radius, centered on the Lamb-Oseen vortex, and a variable angular velocity, decreasing to 0, as $t \to +\infty$.

5.3 Control problem

Consider a flow like the one presented in Section 5.2 and a passive particle placed in it with initial position (x_0, y_0). The goal is to determine the control function $u(\cdot)$ that needs to be applied to the particle in order to move it from the initial position to the endpoint (x_f, y_f) in the time T and subject to the flow field, while minimising the cost function $g(X(T))$. Let $X(t) = (x(t), y(t))$ be the position of the particle at time t. The control problem can be formulated as follows:

$$\begin{cases} \text{Minimise} \quad g(X(T)) \\ \text{subject to} \\ \dot{X}(t) = F(X(t), u(t)) \\ X(0) = (x_0, y_0) \\ X(T) = (x_f, y_f) \\ \|u(t)\|_\infty \leq 1 \end{cases} , \quad \forall t \in [0, T]. \tag{5.9}$$

The maximum principle [16], allows us to determine the set of optimal control candidates u^* by using the maximisation of the Pontryagin-Hamiltonian function $H(X, P, u)$ almost everywhere with respect to the Lebesgue measure (from here on, functions are specified in this sense), together with the satisfaction of the appropriate boundary conditions. Here, P is the adjoint variable satisfying

$$-\dot{P}^T = \nabla_X H(X^*, P, u^*)$$

along the optimal reference control process, where ∇_X is the gradient of H with respect to X.

5.4 Minimum energy problem

As mentioned before, our control function will only act on the radial component of the particle motion. The cost function that we consider for this problem is the total control power consumption, i.e., the energy used to transport the particle,

$$\int_0^T u^2 \, dt \ .$$

We want to minimise the power spent on moving the particle between some specified initial (ρ_0, θ_0) and final points so that the particle is at (ρ_T, θ_T) at the final time T.

To obtain the Mayer's problem, we consider a new variable $w(t)$ satisfying the condition $\dot{w} = u^2$. Our control problem can thus be formulated as follows:

$$\begin{cases} \text{Minimize} \quad w(T) \\ \text{subject to} \\ \dot{\rho} = u \\ \dot{\theta} = \frac{k}{2\pi}\frac{1}{\rho^2}\left[1 - \exp\left(-\frac{\rho^2}{4\nu t}\right)\right] \\ \dot{w} = u^2 \\ \rho(0) = \rho_0 \\ \rho(T) = \rho_T \\ \theta(0) = \theta_0 \\ \theta(T) = \theta_T \\ w(0) = 0 \\ \|u(t)\|_\infty \leq 1 \end{cases}, \quad \forall t \in [0, T]. \tag{5.10}$$

Additionally, we impose the radial velocity $\dot{\rho}$ to go to zero at ρ_T, so that the control is smooth and differentiable during the arrival at the circular trajectory of radius ρ_T. For simplicity, we will only consider the case where $\rho_T < \rho_0$. The case $\rho_T > \rho_0$ follows analogously.

There is no straightforward or analytical solution to this problem due to the non-linearity of the dynamical equations. It is, however, possible to obtain the differential equations that must be satisfied by the optimal trajectories. The details are presented in Marques *et al.* [15]. From this study, it is possible to see that the optimal trajectory for the passive particle is composed of up to three regimes of motion with some *a priori* undetermined switching points ξ and $\tilde{t}$. Due to the nature of the problem, for Pontryagin's maximum principle to hold, these three regimes of motion have to appear in a predetermined order:

i) In the first regime of motion, the particle is pulled radially inwards with the maximum value of the control $u^* = -1$ in the time interval $[0, \xi]$, while its angular velocity changes due to two different factors: the decreasing distance between the particle and the vortex contributes to the acceleration of the movement, while the dissipation of energy due to viscosity decelerates the motion:

$$\begin{cases} \dot{\rho}^* = -1 \\ \dot{\theta}^* = \dfrac{k}{2\pi} \dfrac{1}{(\rho^*)^2} \left[1 - \exp\left(-\dfrac{(\rho^*)^2}{4\nu t} \right) \right] & , \quad t \in [0, \xi] \\ \rho^*(0) = \rho_0, \quad \theta^*(0) = \theta_0, \quad \rho^*(\xi) = \rho_\xi, \quad \theta^*(\xi) = \theta_\xi \end{cases} \tag{5.11}$$

ii) In the second regime, which happens on the time interval $]\xi, \tilde{t}]$, the control switches to a variable control. The particle continues to be pulled inwards, nevertheless at a lower rate, until it arrives at a trajectory with the same radial coordinate as the desired endpoint. The angular motion continues as in the first regime. The parameter C_θ appears from the equations for the adjoint variable, and is related to the strength of the applied control:

$$\begin{cases} \ddot{\rho}^* = \dfrac{C_\theta k}{2\pi (\rho^*)^3} \left[1 - \dfrac{(\rho^*)^2 + 4\nu t}{4\nu t} \exp\left(-\dfrac{(\rho^*)^2}{4\nu t} \right) \right] \\ \dot{\theta}^* = \dfrac{k}{2\pi} \dfrac{1}{(\rho^*)^2} \left[1 - \exp\left(-\dfrac{(\rho^*)^2}{4\nu t} \right) \right] & , \quad t \in]\xi, \tilde{t}] \\ \rho^*(\xi) = \rho_\xi, \quad \theta^*(\xi) = \theta_\xi, \quad \rho^*(\tilde{t}) = \rho_T, \quad \theta^*(\tilde{t}) = \theta_{\tilde{t}} \\ \dot{\rho}^*(\tilde{t}) = 0 \end{cases} \tag{5.12}$$

iii) Finally, in the third regime, the control is switched off completely, and the particle describes a circular motion with radius ρ_T until it arrives at the desired endpoint at the desired time T. The angular velocity decreases due to the dissipation of energy in the viscous fluid:

$$\begin{cases} \dot{\rho}^* = 0 \\ \dot{\theta}^* = \dfrac{k}{2\pi} \dfrac{1}{(\rho^*)^2} \left[1 - \exp\left(-\dfrac{(\rho^*)^2}{4\nu t} \right) \right] & , \quad t \in]\tilde{t}, T] \\ \rho^*(\tilde{t}) = \rho_T, \quad \theta^*(\tilde{t}) = \theta_{\tilde{t}}, \quad \rho^*(T) = \rho_T, \quad \theta^*(T) = \theta_T \end{cases} \tag{5.13}$$

Solving the optimization problem is now reduced to finding the parameter C_θ and the switching points ξ and $\tilde{t}$ that give us a solution of the systems (5.11), (5.12) and (5.13) with minimal energy. To do so, we have to work backwards from the final point, since the equations for the third regime of motion have an actual (numerically) solvable system of differential equations. The strategy is to integrate the system backwards and simulate an initial point for the trajectory. We have shown in Marques *et al.* [15] how C_θ and $\tilde{t}$ affect this simulated initial point and proposed a simple algorithm to solve this problem when the first regime is not present in the optimal solution of the problem. To determine ξ, we modify slightly the algorithm to follow $\dot{\rho}^*(t)$ during the backwards integration of (5.12) and, if $\dot{\rho}^*(t) = -1$ at some time $t = \xi$, we switch the control to $u^* = -1$ during the process, i.e, switch to integrating system (5.11).

Having now an algorithm that is able to identify every possible candidate to the optimal solution of this problem, our aim is to answer a question that was left unanswered in Marques *et al.* [15]: is it possible to find a solution for any value of kinematic viscosity for a given problem? Before proceeding, there are two important aspects to take into consideration:

a) Candidates to optimal solutions, including the optimal solution itself, may not necessarily involve trajectories encompassing all three presented motion regimes. For example, scenarios may occur where $\xi = 0$ or $\tilde{t} = T$, resulting in the absence of one motion regime in the passive particle's trajectory.

b) Due to the problem's geometry, we can have two (or more) possible solutions to the problem, where the passive particle takes a different number of full turns around the vortex before it arrives at the specified endpoint at time $t = T$. We expect these solutions to have different energy costs and thus the optimal trajectory would be the one that arises from a control that is less energy-intensive. This is illustrated in Figure 5.1.

We investigate what happens when we set a specific number of full turns for a solution. There are two limit cases: **a)** for a solution to have the highest energy cost possible, it must be composed of only the regimes of motion *i)* and *iii)* (thus $\tilde{t} = \xi = \rho_0 - \rho_T$) - the passive particle descends to the lower orbit as fast as possible and then arrives at the endpoint after the set number of turns; **b)** for a solution to have the lowest energy cost possible it must be composed of only the regime of motion *ii)* (thus $\xi = 0$ and $\tilde{t} = T$) - the passive particle descends as slowly as possible to the lower orbit, in fact, the descent time is the full time interval $[0, T]$.

We considered the problem where we want to transport a particle from $(2, 2)$ to $(1, 1)$ in $T = 250\,s$, advected by a Lamb-Oseen vortex with $k = 1\,m^2 s^{-1}$ and located at the origin of the 2-D plane. This corresponds to the parameters $\rho_0 = 2\sqrt{2}\,m$, $\rho_T = \sqrt{2}\,m$,

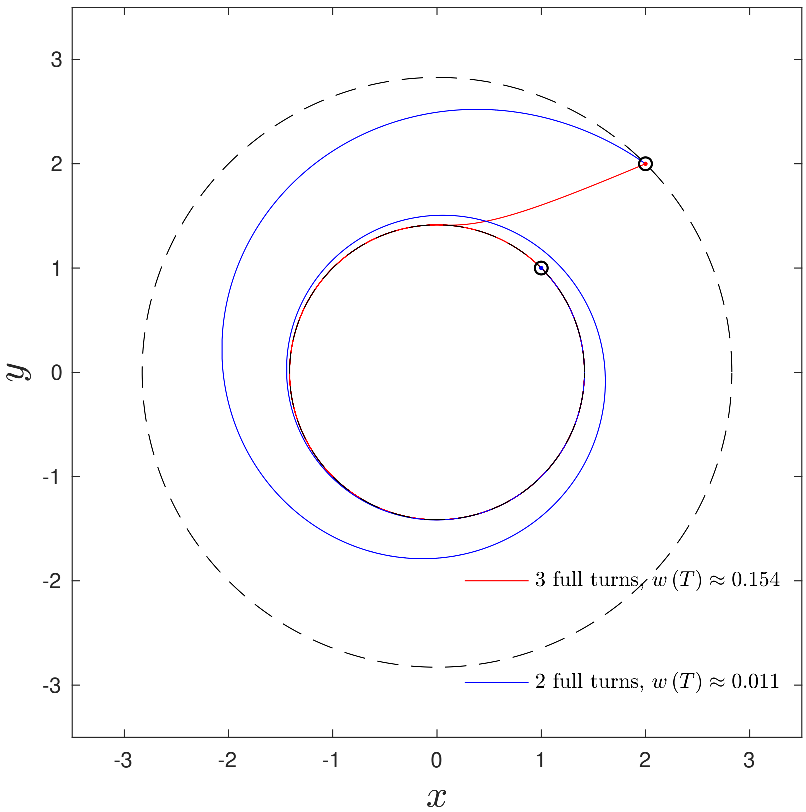

Figure 5.1: Two possible solutions for the problem with parameters $\nu = 9 \times 10^{-4}\, m^2 s^{-1}$, $\rho_0 = 2\sqrt{2}\, m$, $\rho_T = \sqrt{2}\, m$, $\theta_0 = \theta_T = \pi/4\, rad$, $k = 1\, m^2 s^{-1}$ and $T = 250\, s$. We found $\tilde{t} \approx 15.4\, s$, $C_\theta \approx 0.3181\, m^2$ for the trajectory depicted in red and $\tilde{t} \approx 224.7\, s$, $C_\theta \approx 0.0017\, m^2$ for the one in blue. The blue trajectory (optimal) has fewer turns around the vortex, as well as a lower energy ($w(T) \approx 0.011$) than the red one ($w(T) \approx 0.154$). Both of these candidates arose from applying the maximum principle to the problem.

$\theta_0 = \theta_T = \pi/4\, rad$ in the polar formulation presented in (5.10). The approximate solutions of the differential equations were obtained through a Runge-Kutta-Fehlberg method [17] with a step size of $\Delta t = 10^{-4} s$. All results presented below use SI units. In the real world, viscosity values depend on the physical conditions of the fluid such as temperature and are typically in the range of $10^{-2} - 10^{-7}\, m^2 s^{-1}$. For example, typical seawater at $20°C$ has a low kinematic viscosity of about $1.15 \times 10^{-6}\, m^2 s^{-1}$, while typical printer inks at about $38°C$ can have viscosities of up to $2.2 \times 10^{-3}\, m^2 s^{-1}$.

We found that this problem only has potential solutions with 1, 2 or 3 turns around the vortex. In fact, solutions with

i) 1 turn exist for $9.0 \times 10^{-3} \lesssim \nu \lesssim 1.6 \times 10^{-2}\, m^2 s^{-1}$;

ii) 2 turns exist for $0 \leq \nu \lesssim 4.6 \times 10^{-3}\, m^2 s^{-1}$;

iii) 3 turns exist for $0 \leq \nu \lesssim 1.1 \times 10^{-3}\, m^2 s^{-1}$;

There is a clear gap in potential solutions for kinematic viscosities in the range $4.6 \times 10^{-3} \lesssim \nu \lesssim 9.0 \times 10^{-3}\, m^2 s^{-1}$. This happens because the viscosity is high enough that the passive particle cannot complete two turns in the prescribed time $T = 250\, s$ and it is low enough for it not to go past the endpoint in only one full turn. Solutions with $\nu \geq 1.6 \times 10^{-2}\, m^2 s^{-1}$ do not exist since the viscosity is too high for the particle to even complete one full turn around the vortex. Since solutions with two full turns are allowed in the limit $\nu \to 0^+$, there is a region where solutions with both two and three full tuns are allowed. Solutions with four or more turns are not allowed even in the inviscid limit because the prescribed time $T = 250\, s$ is not enough for the particle to take four full turns around the vortex. Figure 5.2 shows the energy needed to move the particle from $(2, 2)$ to $(1, 1)$ in $T = 250\, s$ in various potential solutions corresponding to a set viscosity and number of full turns. The gap between solutions with one and two turns around the vortex is clearly identifiable here. We can also see that every solution with three or more full turns needs more energy than a trajectory with only two turns. This is expected, since solutions with more turns imply a faster orbit descent (the angular velocity increases on lower orbits) in order to give the particle time to complete more turns around the vortex.

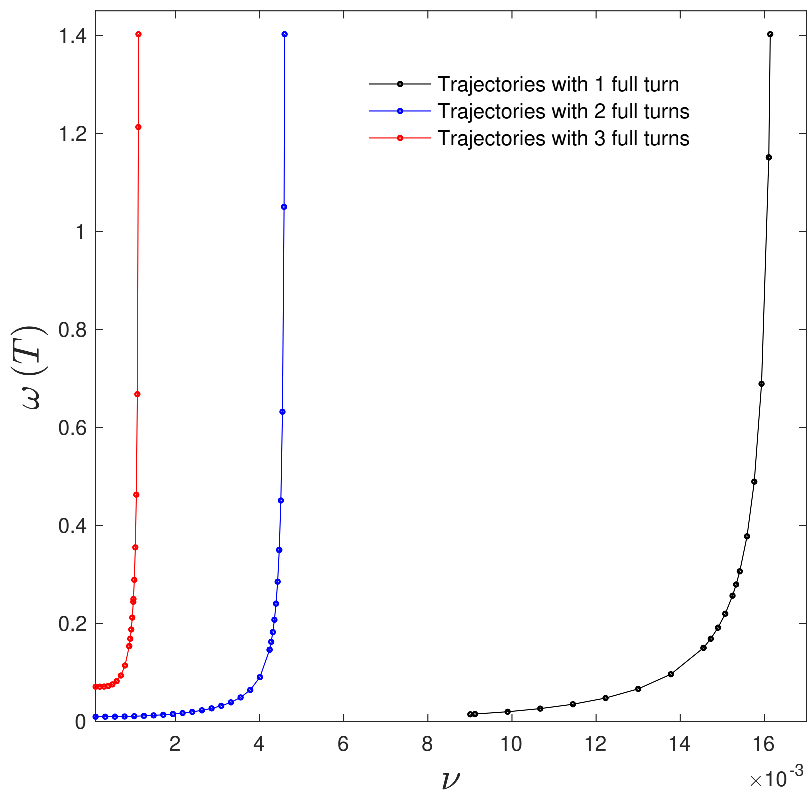

FIGURE 5.2: Energy required to move a passive particle particle from $(2, 2)$ to $(1, 1)$ in $T = 250\, s$ in the presence of a Lamb-Oseen vortex with $k = 1\, m^2 s^{-1}$ located at the origin. A distinct gap is evident between solutions with one and two turns around the vortex.

5.5 Conclusions and Future Work

The difficulties in integrating the full Navier-Stokes equations make the study of fluids a complex task, particularly if we intend to combine this with other areas, like optimal control. Using a simplified description for the flow - as long as it preserves the most important nonlinear features of flows - can allow us to tackle more complex problems, such as the optimal control of flows. The point vortex description is an example of a low-dimensional description that can be used for this purpose.

We study the optimal way to transport a passive particle between two points in space in a viscous flow and given a set time to perform this movement. The flow dynamics are represented by a Lamb-Oseen vortex model. Due to the nonlinearity of the dynamical equations, the problem cannot be solved explicitly; however, it is possible to understand qualitatively what the optimal trajectory should be and transform the problem in a parameter-search problem.

Due to the geometry of the problem, solutions with various numbers of full turns around the vortex may arise. We show that viscosity affects the allowed number of turns for (potential) solutions, i.e., for each number of turns a solution may have, there is a set range of viscosities that is allowed and that solutions with lower full turns are preferred to minimise the energy spent. In fact, if there is a turn count that allows for $\nu = 0$ viscosity, all solutions of the dynamical system with a higher turn count will have a higher energy cost. We also show that there may exist ranges in the viscosity domain where no potential solution can be found: in these gaps, the viscosity is too high for the particle to complete some number of turns, but also too low for the particle to not go past the endpoint in one less full turn than that.

We plan to further research in this area, eventually tackling an environment with multiple vortices or using different types of admissible controls.

Acknowledgments

This work was supported by CMUP, a member of LASI, which is financed by national funds through FCT –Fundação para a Ciência e a Tecnologia, I.P., under the project with reference UIDB/00144/2020. GM thanks the grant with reference PD/BD/150537/2019 through FCT.

References

[1] F. Clarke, Y. Ledyaev, R. Stern, and P. Wolenski, *Nonsmooth Analysis and Control Theory* (Graduate Texts in Mathematics). Springer New York, 2008, ISBN: 9780387226255. DOI: 10.1007/b97650.

[2] S. Mitter and J. Lions, *Optimal Control of Systems Governed by Partial Differential Equations* (Grundlehren der mathematischen Wissenschaften). Springer Berlin Heidelberg, 1971, ISBN: 9783540051152.

[3] N. Mahmoudian, J. Geisbert, and C. Woolsey, "Dynamics and control of underwater gliders i: Steady motions," Virginia Center for Autonomous Systems, Technical Report VaCAS-2007-01, 2009.

[4] N. Mahmoudian and C. Woolsey, "Dynamics and control of underwater gliders ii: Motion planning and control," Virginia Center for Autonomous Systems, Technical Report VaCAS-2010-02, 2010.

[5] J. Liu and H. Hu, "Biological inspiration: From carangiform fish to multi-joint robotic fish," *Journal of Bionic Engineering*, vol. 7, no. 1, pp. 35–48, 2010, ISSN: 1672-6529. DOI: 10.1016/S1672-6529(09)60184-0.

[6] G. K. Batchelor, *An Introduction to Fluid Dynamics* (Cambridge Mathematical Library). Cambridge University Press, 2000. DOI: 10.1017/CBO9780511800955.

[7] P. Newton, *The N-Vortex Problem: Analytical Techniques* (Applied Mathematical Sciences). Springer New York, 2010, ISBN: 9781441929167. DOI: 10.1007/978-1-4684-9290-3.

[8] C. Oseen, *Über Wirbelbewegung in einer reibenden Flüssigkeit* (Arkiv för matematik, astronomi och fysik). Almqvist & Wiksell, 1911.

[9] P. G. Saffman, *Vortex Dynamics* (Cambridge Monographs on Mechanics). Cambridge University Press, 1993. DOI: 10.1017/CBO9780511624063.

[10] S. B. Pope, *Turbulent Flows*. Cambridge University Press, 2000. DOI: 10.1017/CBO9781316179475.

[11] T. Gallay and C. E. Wayne, "Global stability of vortex solutions of the two-dimensional navier-stokes equation," *Communications in Mathematical Physics*, vol. 255, no. 1, pp. 97–129, 2005. DOI: 10.1007/s00220-004-1254-9.

[12] T. Gallay, "Interaction of vortices in weakly viscous planar flows," *Archive for Rational Mechanics and Analysis*, vol. 200, no. 2, pp. 445–490, 2011. DOI: 10.1007/s00205-010-0362-2.

[13] S.-C. Kim and S.-I. Sohn, "Interactions of three viscous point vortices," *Journal of Physics A: Mathematical and Theoretical*, vol. 45, no. 45, p. 455 501, Oct. 2012. DOI: 10.1088/1751-8113/45/45/455501.

[14] G. Marques, T. Grilo, S. Gama, and F. L. Pereira, "Optimal control of a passive particle advected by a point vortex," in *Advanced Research in Technologies, Information, Innovation and Sustainability*, T. Guarda, F. Portela, and M. F. Santos, Eds., Cham: Springer International Publishing, 2021, pp. 512–523, ISBN: 978-3-030-90241-4. DOI: 10.1007/978-3-030-90241-4_39.

[15] G. Marques, S. Gama, and F. L. Pereira, "Optimal control of a passive particle advected by a lamb–oseen (viscous) vortex," *Computation*, vol. 10, no. 6, 2022, ISSN: 2079-3197. DOI: 10.3390/computation10060087.

[16] L. S. Pontryagin, V. G. Boltyanskii, R. V. Gamkrelidze, and E. F. Mishchenko, *The Mathematical Theory of Optimal Processes*. New York, NY: Interscience Publishers, 1961, translated by K. N. Triruguf, edited by T. W. Neustadt.

[17] E. Fehlberg, *Low-order Classical Runge-Kutta Formulas with Stepsize Control and Their Application to Some Heat Transfer Problems* (NASA technical report). National Aeronautics and Space Administration, 1969.

Chapter 6

Geometric Characterization of Atmospheric Islands Formed by Two Point Vortices

Published in Axioms, 2025

Gil Marques and Sílvio Gama

Abstract: Generically, in a system with more than three point vortices, there exist regions of stability around each vortex, even if the system is chaotic. These regions are usually called stability islands, and they have a morphology that is hard to characterize. In a system of two or three point vortices, these stability islands are better named vortex atmospheres or atmospheric islands, since the whole system is regular. In this work, we present an analytical study to characterize these atmospheres in two point vortex systems for arbitrary values of the circulations Γ_1 and Γ_2 in the infinite two-dimensional plane $(x, y) \in \mathbb{R}^2$—the simplest scenario—by studying the dynamics of passive particles in these environments. We use the trajectories of passive particles to find the stagnation points of these systems, the special trajectories that partition $\mathbb{R}^2$ in different regions and the analytical expressions that define the boundary of the atmospheric islands. In order to characterize the geometry of these atmospheres, we compute their perimeter and area as a function of $\gamma = \frac{\Gamma_1}{\Gamma_1+\Gamma_2}$, if $\Gamma_1 + \Gamma_2 \neq 0$. The case $\Gamma_1 + \Gamma_2 = 0$ is treated separately, as the perimeter and area of the atmospheres do not depend on the circulations. Furthermore,

in this latter case, we observe that the atmospheric island has a very similar morphology to an ellipse, only differing from the ellipse that best approximates the atmosphere by a relative error of ≈3.76‰ in area.

6.1 Introduction

Point vortices are singular solutions of the two-dimensional (2D) incompressible Euler equations, which were first studied by Helmholtz [1], and, some years later, received the attention of Lord Kelvin [2] and Kirchhoff [3]. Since then, and until the present day, point vortices have become the subject of research in domains as varied as torus [4], [5], spheres [6], [7], [8], hyperbolic surfaces [9], [10], etc. They correspond to a scenario where the vorticity of a flow is concentrated in some well-defined points in space and enable a simpler description of the dynamics of such a system. Knowing the position and strength (or circulation) of each vortex in the system suffices to obtain the full velocity field at that instant, and thus knowing the dynamics of the vortices themselves in some time interval is enough to characterize the velocity field during that same time interval. The dynamics of these vortices follow ordinary differential equations that are akin to the ones in the gravitational n-body problem, and their trajectories can be found analytically for some specific spacial configurations, such as relative equilibria [11]. Consider a 2D inviscid flow in the complex plane that is described by n point vortices located in the positions $z_\alpha = x_\alpha + iy_\alpha \, (\alpha = 1, \ldots, n)$. The motion of the vortices is defined by the initial value problem determined by

$$\dot{z}_\alpha^* = \frac{1}{2\pi i} \sum_{\substack{\beta=1 \\ \beta \neq \alpha}}^{n} \frac{\Gamma_\beta}{z_\alpha - z_\beta}, \quad \alpha = 1, \ldots, n, \tag{6.1}$$

and the initial positions of the vortices. Here, Γ_α is the circulation of the α^{th} vortex. Moreover, since the flow is incompressible, we know that the information of the velocity field can also be represented in a stream function formulation, with

$$\psi(z,t) = -\frac{1}{4\pi} \sum_{\alpha=1}^{n} \Gamma_\alpha \log |z - z_\alpha(t)| \,. \tag{6.2}$$

To retrieve the velocity field, it suffices to consider the partial derivatives of the following stream function: $\dot{x} = \frac{\partial \psi}{\partial y}$, $\dot{y} = -\frac{\partial \psi}{\partial x}$, or, in complex notation, $\dot{z}^* = 2i \frac{\partial \psi}{\partial z}$.

Studying the velocity field that arises from a system of point vortices can be thought of as studying the trajectories of passive particles that move in the velocity field. A passive particle is a particle that does not change the flow itself but is transported by it; it can be thought of as a point vortex with zero strength, and, thus, its motion follows the same differential equations as the vortices. This is analogous to the restricted $n+1$ body problem in celestial mechanics, where one of the bodies of the system is assumed to have zero mass. More explicitly, the equation of motion for a passive particle is

$$\dot{z}^* = \frac{1}{2\pi i} \sum_{\alpha=1}^{n} \frac{\Gamma_\alpha}{z - z_\alpha} \,. \tag{6.3}$$

It is known that around each vortex there exists what is usually called an island of stability, where the motion of passive particles is always regular and is mostly ruled by the associated vortex, while suffering little influence from the other $n-1$ vortices [12]. Outside of these islands, one expects the movement of passive particles to be chaotic for $n \geq 4$ [13]. The boundaries of these islands constitute barriers to particle motion and, thus, to fluid transportation: particles inside of these regularity islands cannot be ejected from them, and particles moving in the background between the vortices cannot enter the stability regions associated with each vortex.

In this work, we will cover the simplest case $n = 2$. Even though in this scenario every particle trajectory is regular (thus, chaotic dynamics are not contemplated here), the presence of the vortices is enough to create rigid boundaries in the 2D plane from where particles are not able to escape. These boundaries partition $\mathbb{R}^2$ in different regions, and particles inside one of them present similar trajectories to one another, but these are generally different from particle trajectories in another one of these regions. The regions in which the vortices are contained are simpler versions of the stability islands that arise in the chaotic $n \geq 4$ scenario and are usually called vortex atmospheres or atmospheric islands. To characterize them geometrically, we present computations of their perimeter and area, as well as analytical expressions that define their boundary.

This paper is organized as follows. In Section 6.2, we report the dynamics of passive particles in two-point-vortex systems in two subsections, corresponding to the cases $\Gamma_1 + \Gamma_2 = 0$ and $\Gamma_1 + \Gamma_2 \neq 0$. In the former, we find analytical expressions for the boundary, perimeter and area of the vortex atmospheres, which give the geometric characterization of the regions. We find that the islands form approximately an ellipse, and we compare their area to that of the best approximating ellipse. In the latter, we present an implicit expression for the boundary of the atmospheric islands. Due to the nature of this expression, we had to resort to numerical methods to compute the perimeter and area. The concluding remarks are presented in Section 6.3.

6.2 Dynamics of Passive Particles on Two-Point-Vortex Systems

We now consider a system comprising only two vortices located, at time t, in $z_1(t)$ and $z_2(t)$, with non-zero circulations Γ_1 and Γ_2, respectively. There are two different regimes for the motion of the vortices depending on if the sum of their circulations is zero or non-zero. In the following two subsections, we will treat these two cases separately, describing the dynamics of passive particles in the plane and analyzing the boundaries that separate the plane in different regions from which particles cannot escape.

6.2.1 Case $\Gamma_1 + \Gamma_2 = 0$

We consider two vortices with circulations $\Gamma_1 = -\Gamma_2 = k \in \mathbb{R}^+$ (if $k \in \mathbb{R}^-$, the motion of the system will simply happen in the opposite direction). It is known that in such a system, both vortices will move in straight lines, parallel to one another with a constant velocity [14]. Without any loss of generality, it is possible to consider a system where the vortices are initially on the imaginary axis and separated by a distance $d \in \mathbb{R}^+$, i.e., $z_1(0) = \frac{d}{2}i$, $z_2(0) = -\frac{d}{2}i$.

The solutions of Equation (6.1) for this case are thus

$$\begin{cases} z_1(t) = \dfrac{d}{2}i + \dfrac{k}{2\pi d}t\ , \\ z_2(t) = -\dfrac{d}{2}i + \dfrac{k}{2\pi d}t\ . \end{cases} \tag{6.4}$$

The equation of motion for a passive particle in this system is non-autonomous and given by

$$\begin{aligned} \dot{z}^* &= \frac{k}{2\pi i}\left[\frac{1}{z - z_1(t)} - \frac{1}{z - z_2(t)}\right] \\ &= \frac{k}{2\pi i}\left[\frac{1}{z - \frac{k}{2\pi d}t - \frac{d}{2}i} - \frac{1}{z - \frac{k}{2\pi d}t + \frac{d}{2}i}\right]. \end{aligned} \tag{6.5}$$

Now, consider the change of coordinates $w = \dfrac{z}{d} - \dfrac{k}{2\pi d^2}t$. This corresponds to changing the frame that is co-moving with the pair of vortices at a constant velocity.

Thus, in this frame, the vortices are stationary, and their positions are $w_1(t) = i/2$ and $w_2(t) = -i/2$. The equation of motion of a passive particle is now governed by the autonomous differential equation

$$\dot{w}^* = \frac{k}{2\pi d^2 i}\left[\frac{1}{w - i/2} - \frac{1}{w + i/2} - i\right]. \tag{6.6}$$

Our aim is to describe the trajectories of passive particles. In this co-moving frame, stagnation points are the simplest possible trajectories and correspond to particles that move with the same velocity as the vortices in the original frame. These correspond to zeros of $\dot{w}$, and it is easy to see that the system has only two of them: $w = \pm\sqrt{3}/2$. These correspond to the Lagrangian points of the system and are real solutions of Equation (6.6), but they are not the only real solutions for this equation.

We can also see that, if there is a solution of Equation (6.6), with $Im\left(w(t)\right) = 0$ ($Im(w)$ denoting the imaginary part of w) at some time t, such a solution will have $Im\left(\dot{w}(t)\right) = 0\,\forall t$. As such, solutions of the form $w(t) = x(t) \in \mathbb{R}$ for Equation (6.6) must satisfy the equation

$$\dot{x} = \frac{k}{2\pi d^2}\left[\frac{4}{4x^2+1} - 1\right]. \tag{6.7}$$

It is possible to integrate Equation (6.7) and find an implicit expression for its non-stationary solutions:

$$\frac{1}{\sqrt{3}}\left[\log\left(\frac{2x(t)+\sqrt{3}}{2x(0)+\sqrt{3}}\right) - \log\left(\frac{2x(t)-\sqrt{3}}{2x(0)-\sqrt{3}}\right)\right] = x(t) - x(0) + \frac{k}{2\pi d^2}t,$$
$$x(0) \in \mathbb{R}\setminus\left\{\sqrt{3}/2, -\sqrt{3}/2\right\}. \tag{6.8}$$

Note that this equation defines three different solutions of Equation (6.7), depending on the initial value $x(0)$, and that these three solutions and the stagnation points make up the full real axis. This means that the real axis is a physical barrier to the motion of passive particles, as, by the existence and uniqueness of solutions theorem for ordinary differential equations, there can not exist a passive particle trajectory that crosses it. Furthermore, we can see that as $t \to +\infty$, the following hold:

- If $x(0) < -\sqrt{3}/2$, then $x(t) \to -\infty$;
- If $x(0) > \sqrt{3}/2$, then $x(t) \to \frac{\sqrt{3}}{2}^{+}$;
- If $|x(0)| < \sqrt{3}/2$, then $x(t) \to \frac{\sqrt{3}}{2}^{-}$.

Thus, solutions in the real axis are attracted to $\sqrt{3}/2$ and repelled from $-\sqrt{3}/2$.

To understand the motion of passive particles in the rest of the 2D plane, we rewrite Equation (6.6) as a system of two real ODEs, $(\dot{x}, \dot{y}) = F(x,y)$,

$$\begin{cases} \dot{x} = - \dfrac{y-\frac{1}{2}}{x^2+\left(y-\frac{1}{2}\right)^2} + \dfrac{y+\frac{1}{2}}{x^2+\left(y+\frac{1}{2}\right)^2} - 1\,, \\ \dot{y} = \dfrac{x}{x^2+\left(y-\frac{1}{2}\right)^2} - \dfrac{x}{x^2+\left(y+\frac{1}{2}\right)^2}\,, \end{cases} \tag{6.9}$$

where we have rescaled time $t \to k\,t/\left(2\pi d^2\right)$ for simplicity.

We first analyze the stability of the Lagrangian points by checking the eigenvalues and eigenvectors of the linearization of $F(x,y)$ on those points.

Defining the quantities $\ell_+(x,y) = x^2 + \left(y+\frac{1}{2}\right)^2$ and $\ell_-(x,y) = x^2 + \left(y-\frac{1}{2}\right)^2$, we have

$$DF(x,y) = \begin{pmatrix} -\frac{2x\left(y+\frac{1}{2}\right)}{\ell_+^2} + \frac{2x\left(y-\frac{1}{2}\right)}{\ell_-^2} & \frac{1}{\ell_+} - \frac{1}{\ell_-} - \frac{2\left(y+\frac{1}{2}\right)^2}{\ell_+^2} + \frac{2\left(y-\frac{1}{2}\right)^2}{\ell_-^2} \\ -\frac{1}{\ell_+} + \frac{1}{\ell_-} - \frac{2x^2}{\ell_+^2} - \frac{2x^2}{\ell_-^2} & \frac{2x\left(y+\frac{1}{2}\right)}{\ell_+^2} - \frac{2x\left(y-\frac{1}{2}\right)}{\ell_-^2} \end{pmatrix}, \tag{6.10}$$

$$DF\left(\pm\tfrac{\sqrt{3}}{2}, 0\right) = \begin{pmatrix} \mp\sqrt{3} & 0 \\ 0 & \pm\sqrt{3} \end{pmatrix}.$$

Thus, the stagnation points are both saddle points. Locally, $\left(-\frac{\sqrt{3}}{2}, 0\right)$ attracts solutions on the $(0,1)$ direction and repels them on the $(1,0)$ direction, while we observe the exact opposite behavior in a neighborhood of $\left(\frac{\sqrt{3}}{2}, 0\right)$.

Using a stream function formulation, the system (6.9) can be further rewritten as $\dot{x} = \dfrac{\partial\psi}{\partial y}$, $\dot{y} = -\dfrac{\partial\psi}{\partial x}$. The stream function for this system is time-independent and can be written as

$$\psi(x,y) = -\frac{1}{2}\left[\log\left(x^2+\left(y-\frac{1}{2}\right)^2\right) - \log\left(x^2+\left(y+\frac{1}{2}\right)^2\right) + 2y\right]. \tag{6.11}$$

Thus, the trajectories of passive particles can be identified as the level sets of $\psi(x,y)$ (this is only true if the stream function is time-independent [15]). Equivalently, this can be rewritten in a clearer manner as a modified stream function

$$\widetilde{\psi}(x,y) = e^{-2\psi(x,y)} = \left[x^2+\left(y-\frac{1}{2}\right)^2\right]\left[x^2+\left(y+\frac{1}{2}\right)^2\right]^{-1} e^{2y}. \tag{6.12}$$

Notice that for $\forall y : |y| > 1/2, \;\; \dot{x} < 1$. This, together with the fact that $\widetilde{\psi}\left(-\frac{\sqrt{3}}{2}, 0\right) = \widetilde{\psi}\left(\frac{\sqrt{3}}{2}, 0\right)$, means that there should be a trajectory of a passive particle linking the stagnation points other than the one on the real axis. These trajectories thus separate the infinite plane in four regions. A particle that starts its trajectory in one region cannot cross into any of the other three regions. We can further assess that two of these regions are closed and each of them contains one of the vortices. In fact, it is possible to easily draw the phase diagram of the system with this information. The phase diagram is drawn in Figure 6.1. This figure and its interpretation is already depicted in Lamb's textbook [16].

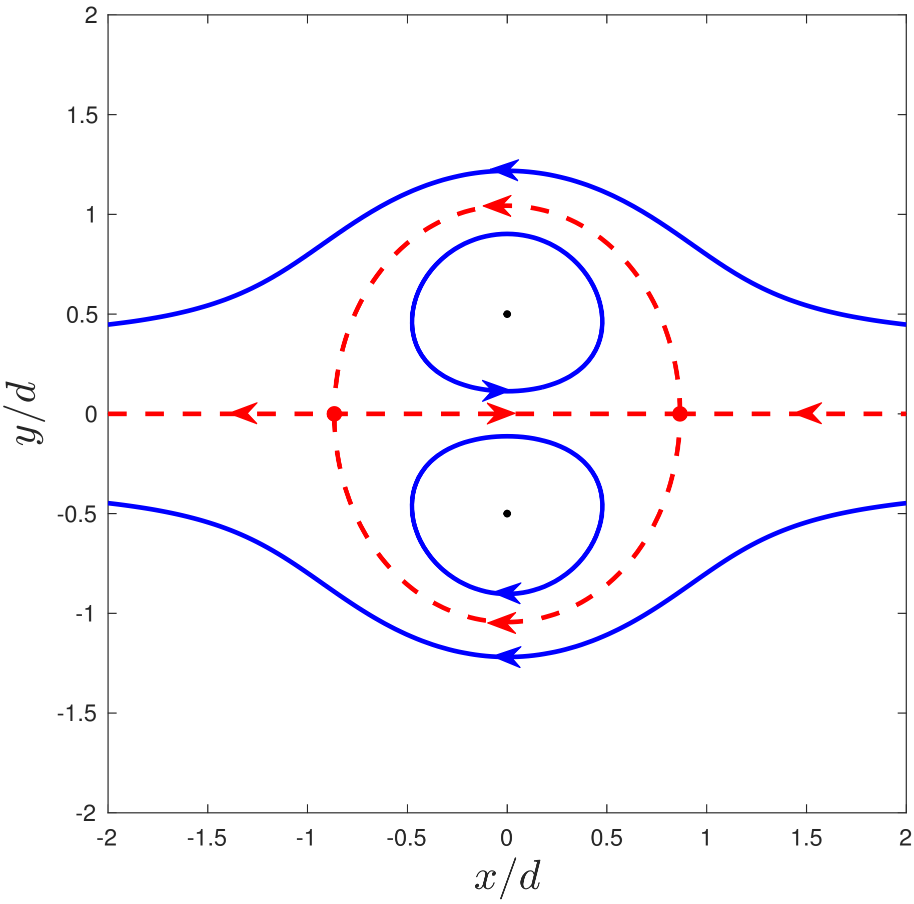

Figure 6.1: Phase diagram for a system of two point vortices in the co-moving frame. The vortices (black dots) are located in $w_1 = i/2$ and $w_1 = -i/2$, and the circulations are such that $\Gamma_1 + \Gamma_2 = 0$. The red dots identify the stagnation points of the system. The red dashed lines correspond to special particle trajectories that constitute a boundary between regions of the infinite plane where particles present different types of trajectories (exemplified in blue lines).

The boundary between the different regions can be defined implicitly using the modified stream function as $\widetilde{\psi}\left(x,y\right) = \widetilde{\psi}\left(0,0\right) = 1$, or, more explicitly,

$$\left[x^2 + \left(y - \frac{1}{2}\right)^2\right] e^{2y} = x^2 + \left(y + \frac{1}{2}\right)^2. \tag{6.13}$$

The two closed regions defined by Equation (6.13) are called the atmospheres of the vortices, and their existence has been shown in simulations in numerous works [12], [17] for systems of any number of vortices.

It is also possible to obtain an expression for the area of each of these closed regions. Notice that the x- and y-axis are also symmetry axes for the solutions of the system. Thus, we only need to calculate the area enclosed in the region of interest that lies on the first quadrant, i.e., the area below the curve,

$$\xi = \left\{ \left(x,y\right) \in \mathbb{R}^+ \times \mathbb{R}^+ : \left[x^2 + \left(y - \frac{1}{2}\right)^2\right] e^{2y} = \left[x^2 + \left(y + \frac{1}{2}\right)^2\right] \right\}. \tag{6.14}$$

It is possible to rewrite Equation (6.13) as

$$x^2\left(y\right) = -y^2 + y\,\coth\left(y\right) - \frac{1}{4}, \tag{6.15}$$

and by finding (numerically) some $\widetilde{y} > 0$ such that $x^2\left(\widetilde{y}\right) = 0$, the area of each atmosphere can be calculated as

$$A = 2\int_0^{\widetilde{y}} \sqrt{-y^2 + y\,\coth\left(y\right) - \frac{1}{4}}\,dy = 1.42505829613753 \pm 5 \times 10^{-14}, \tag{6.16}$$

and thus, for a system where the vortices are separated by a distance d, the area of each atmosphere is $A\,d^2 \approx 1.425\,d^2$.

It is also possible to compute the perimeter of each atmosphere. The length of the curve ξ can be found as

$$L = \int_0^{\widetilde{y}} \sqrt{1 + \frac{\left(\coth\left(y\right) - y\left(1 + \coth^2\left(y\right)\right)\right)^2}{4y\left(\coth\left(y\right) - y\right) - 1}}\,dy = 1.50587929704238 \pm 5 \times 10^{-14}. \tag{6.17}$$

Thus, the perimeter of each atmospheric island is $\left(2L + \sqrt{3}\right) d \approx 4.744\,d$. Notice that in this case, the shape of the islands does not depend on the circulation k. The results are summarized in Table 6.1.

Table 6.1: Summary of stagnation points and geometric characterization of the atmospheric islands for the case $\Gamma_1 + \Gamma_2 = 0$.

$\Gamma_1 + \Gamma_2 = 0$		
Stagnation points	$\left(\pm\frac{\sqrt{3}}{2}, 0\right)$	unstable saddle
Perimeter of each atmospheric island	$\approx 4.744\, d$	
Area of each atmospheric island	$\approx 1.425\, d^2$	

Lamb [16] and Meleshko et al. [18] have described the region comprising these two islands as approximately an ellipse; however, it is clear that Equation (6.15) is not the equation for an ellipse. We can find numerically the points $\tilde{x} > 0$ such that $y = 0$ and $\tilde{y} > 0$ such that $x = 0$ on the curve. These points can then be identified as the semi-axes of the ellipse that approximates the vortex atmospheres.

We find $\tilde{x} = 0.86602540378444 \pm 5 \times 10^{-14}$ and $\tilde{y} = 1.04362689559154 \pm 5 \times 10^{-14}$, which makes the elliptical approximation for each island have an area of $\approx 1.41969734979125\ d^2$. This corresponds to a relative error of $\approx 3.76‰$ for the area (so, the actual atmospheres have an area slightly bigger than the approximating ellipse). The values we found for $\tilde{x}$, $\tilde{y}$ and the area of the approximating ellipse are in line with the findings of [16], [18] after adjusting for the difference in the initial distance of the vortices in each study.

6.2.2 Case $\Gamma_1 + \Gamma_2 \neq 0$

We now consider the scenario where the sum of the non-zero circulations of the two vortices is not equal to zero. It is known that in such a system, the vortices will rotate around their center of vorticity, which can be defined by

$$C_{\text{vort}} = \frac{\Gamma_1 z_1(0) + \Gamma_2 z_2(0)}{\Gamma_1 + \Gamma_2}, \tag{6.18}$$

with a velocity

$$\theta = \frac{\Gamma_1 + \Gamma_2}{2\pi |d|^2}, \tag{6.19}$$

where $d = z_1(0) - z_2(0)$ [7], [14], [19].

Defining the parameter $\gamma = \dfrac{\Gamma_1}{\Gamma_1 + \Gamma_2}$ (note that $\gamma \neq \{0, 1\}$), the equations of motion of the two vortices can be written as

$$\begin{cases} z_1\left(t\right) = C_{\text{vort}} + \left(1 - \gamma\right) d\, e^{i\theta t} \,, \\ z_2\left(t\right) = C_{\text{vort}} - \gamma\, d\, e^{i\theta t} \,. \end{cases} \tag{6.20}$$

Notice that having $\gamma = 0$ corresponds to $\Gamma_1 = 0$, which means that one of the point vortices would have zero circulation, and thus the system would actually be composed of a single point vortex: the vortex would stay in its initial position and give rise to a velocity field that is proportional to the inverse of the distance to the vortex. The case $\gamma = 1$ is equivalent, as it corresponds to having $\Gamma_2 = 0$ instead. The equation of motion for a passive particle in this system is thus

$$\dot{z}^* = \frac{\Gamma_1 + \Gamma_2}{2\pi i} \left[\frac{\gamma}{z - z_1\left(t\right)} + \frac{1 - \gamma}{z - z_2\left(t\right)} \right]. \tag{6.21}$$

Note that the parameter γ determines the nature of the system. If $\gamma \in \left]0, 1\right[$, both vortices will have circulations with the same sign. However, if $\gamma \in \mathbb{R} \setminus [0, 1]$, the vortices will have circulations of opposite signs (though not symmetrically).

Consider the change of coordinates $w = \left(\dfrac{z - C_{\text{vort}}}{d}\right) e^{i\theta t}$. This corresponds to changing a frame that is rigidly rotating with the vortices around the center of vorticity of the system—located in the origin—at the constant velocity θ. Thus, in this rotating frame, the vortices have stationary trajectories $w_1\left(t\right) = 1 - \gamma$ and $w_2\left(t\right) = -\gamma$. Furthermore, since $\dot{w}^* = \dfrac{\dot{z}^*}{d^*} e^{i\theta t} + i\,\theta\, w^*$, we obtain an autonomous equation of motion for a passive particle in this frame:

$$\dot{w}^* = \frac{\Gamma_1 + \Gamma_2}{2\pi |d|^2 i} \left[\frac{\gamma}{w - \left(1 - \gamma\right)} + \frac{1 - \gamma}{w + \gamma} - w^* \right]. \tag{6.22}$$

While not as trivial as in the previous case, finding analytical expressions for the stagnation points of this system is still possible. These points should satisfy

$$\dot{w}^* = 0 \quad \Longleftrightarrow \quad \left(1 - |w|^2\right) w + \gamma\left(1 - \gamma\right) w^* = \left(1 - 2\gamma\right)\left(1 - |w|^2\right). \tag{6.23}$$

Using $z = x + iy$ and writing a system of equations that both the real and imaginary parts of z must satisfy, we obtain

$$\begin{cases} \left[1 - \left(x^2 + y^2\right)\right] x + \gamma\left(1-\gamma\right) x = \left(1 - 2\gamma\right)\left[1 - \left(x^2 + y^2\right)\right] , \\ \left[1 - \left(x^2 + y^2\right)\right] y - \gamma\left(1-\gamma\right) y = 0 . \end{cases} \tag{6.24}$$

From the second equation, if $y \neq 0$, we obtain $1 - \left(x^2 + y^2\right) = \gamma\left(1-\gamma\right)$ and, using this in the first equation, we can conclude that

$$y \neq 0 \Longrightarrow x = \frac{1-2\gamma}{2} \Longrightarrow y = \pm\frac{\sqrt{3}}{2}. \tag{6.25}$$

Therefore, there are two stagnation points here, defined by the following:

$$p_3 = \left(\frac{1-2\gamma}{2}, \frac{\sqrt{3}}{2}\right) , \qquad \text{and} \qquad p_4 = \left(\frac{1-2\gamma}{2}, -\frac{\sqrt{3}}{2}\right) . \tag{6.26}$$

In the case where y is equal to zero, we obtain a third-order equation for x:

$$x^3 + \left(2\gamma - 1\right) x^2 + \left[\gamma\left(\gamma - 1\right) - 1\right] x + \left(1 - 2\gamma\right) = 0, \tag{6.27}$$

which has either one or three real roots [20], depending on if the sign of the discriminant is negative or positive:

$$\Delta = -\gamma\left(\gamma - 1\right)\left(3\gamma^2 - 3\gamma + 32\right). \tag{6.28}$$

Since $3\gamma^2 - 3\gamma + 32 > 0$, $\forall\gamma$, we cannot have $\Delta = 0$—which would mean that (6.27) has a repeated root—since that would only happen if γ is 0 or 1. We thus conclude that

$$\operatorname{sgn}\left(\Delta\right) = \begin{cases} +1, & \text{if} \quad \gamma \in \left]0,1\right[, \\ -1, & \text{if} \quad \gamma \in \mathbb{R} \setminus \left[0,1\right] . \end{cases} \tag{6.29}$$

Thus, if $\gamma \in \left]0,1\right[$, there are three stagnation points along the real axis, which can be expressed in trigonometric form as

$$\begin{aligned} x_k = &- \frac{2\gamma - 1}{3} + \\ &+ \frac{2}{3}\sqrt{\gamma^2 - \gamma + 4}\, \cos\left[\frac{1}{3}\cos^{-1}\left(\frac{\left(2\gamma-1\right)\left(\gamma^2 - \gamma + 16\right)}{2\left(\gamma^2 - \gamma + 4\right)^{3/2}}\right) - \frac{2k\pi}{3}\right], \end{aligned} \tag{6.30}$$

for $k \in \{0, 1, 2\}$.

If $\gamma \in \mathbb{R} \setminus [0,1]$, the sole stagnation point along the real axis can be written as

$$\begin{aligned}\overline{x}_0 = &-\frac{2\gamma-1}{3}+\frac{2}{3}\operatorname{sgn}(\gamma)\sqrt{\gamma^2-\gamma+4}\times \\ &\times \cosh\left[\frac{1}{3}\cosh^{-1}\left(\operatorname{sgn}(\gamma)\frac{(2\gamma-1)\left(\gamma^2-\gamma+16\right)}{2\left(\gamma^2-\gamma+4\right)^{3/2}}\right)\right].\end{aligned} \tag{6.31}$$

As such, in addition to the previously defined p_3 and p_4, if $\gamma \in \,]0,1[\,$, we have the stagnation points

$$p_0 = (x_0, 0), \quad p_1 = (x_1, 0) \quad \text{and} \quad p_2 = (x_2, 0),$$

and, if $\gamma \in \mathbb{R} \setminus [0,1]$, we only have

$$\overline{p}_0 = (\overline{x}_0, 0),$$

as an additional stagnation point.

In order to obtain more information about the stability of each of the stagnation points and the non-stationary orbits of the system, we need to analyze the equations of motion. Writing them as a system of two real ODEs, we obtain

$$\begin{cases} \dot{x} = -\dfrac{\gamma y}{\left(x-(1-\gamma)\right)^2+y^2} - \dfrac{(1-\gamma)\,y}{(x+\gamma)^2+y^2} + y\,, \\ \dot{y} = \dfrac{\left(x-(1-\gamma)\right)\gamma}{\left(x-(1-\gamma)\right)^2+y^2} + \dfrac{(1-\gamma)\,(x+\gamma)}{(x+\gamma)^2+y^2} - x\,, \end{cases} \tag{6.32}$$

where we have rescaled time as $t \to \dfrac{\Gamma_1+\Gamma_2}{2\pi|d|^2}t$ for simplicity.

The linearization of the flow F defined by the previous equations is thus

$$DF(x,y) = \begin{pmatrix} \dfrac{2(1-\gamma)(x+\gamma)y}{\ell_+^2} + \dfrac{2\gamma\Big(x-(1-\gamma)\Big)y}{\ell_-^2} & \begin{array}{c} -\dfrac{1-\gamma}{\ell_+} - \dfrac{\gamma}{\ell_-} + \dfrac{2(1-\gamma)y^2}{\ell_+^2} \\ + \dfrac{2\gamma y^2}{\ell_-^2} + 1 \end{array} \\ \begin{array}{c} \dfrac{1-\gamma}{\ell_+} + \dfrac{\gamma}{\ell_-} - \dfrac{2(1-\gamma)(x+\gamma)^2}{\ell_+^2} \\ - \dfrac{2\gamma\Big(x-(1-\gamma)\Big)^2}{\ell_-^2} - 1 \end{array} & -\dfrac{2(1-\gamma)(x+\gamma)y}{\ell_+^2} - \dfrac{2\gamma\Big(x-(1-\gamma)\Big)y}{\ell_-^2} \end{pmatrix}. \tag{6.33}$$

where, from now on, $\ell_+\left(x,y\right) = (x+\gamma)^2+y^2$ and $\ell_-\left(x,y\right) = \left(x-(1-\gamma)\right)^2+y^2$.

For the points p_3 and p_4, we have

$$DF\left(\frac{1-2\gamma}{2}, \pm\frac{\sqrt{3}}{2}\right) = \begin{pmatrix} \pm\frac{\sqrt{3}}{2}(1-2\gamma) & \frac{3}{2} \\ -\frac{1}{2} & \mp\frac{\sqrt{3}}{2}(1-2\gamma) \end{pmatrix}. \tag{6.34}$$

So the eigenvalues λ_1, λ_2 of DF in these stagnation points must satisfy

$$\begin{cases} \lambda_1\lambda_2 = -\frac{3}{4}(1-2\gamma)^2 + \frac{3}{4}, \\ \lambda_1 + \lambda_2 = 0, \end{cases} \tag{6.35}$$

and, thus, $\lambda_1 = -\lambda_2 = \sqrt{3\gamma(\gamma-1)}$. Therefore, if $\gamma \in]0,1[$, then $\gamma(\gamma-1) < 0$ and the stagnation points are both centers; if $\gamma \in \mathbb{R} \setminus [0,1]$, then $\gamma(\gamma-1) > 0$, which means that the stagnation points are both unstable saddle points.

For the points p_0, p_1 and p_2, which are of the form $(\tilde{x}, 0)$, we have

$$DF(\tilde{x}, 0) = \begin{pmatrix} 0 & 1-\varphi \\ -1-\varphi & 0 \end{pmatrix}, \tag{6.36}$$

where $\varphi = \frac{1-\gamma}{(\tilde{x}+\gamma)^2} + \frac{\gamma}{(\tilde{x}-(1-\gamma))^2}$. So, the eigenvalues λ_1, λ_2 of $DF(\tilde{x}, 0)$ in these stagnation points must satisfy

$$\begin{cases} \lambda_1\lambda_2 = (1+\varphi)(1-\varphi), \\ \lambda_1 + \lambda_2 = 0, \end{cases} \tag{6.37}$$

and, thus, $\lambda_1 = -\lambda_2 = \sqrt{-(1+\varphi)(1-\varphi)}$.

Theorem 6.1. $(1+\varphi)(1-\varphi)$ *is negative if* $\gamma \in]0,1[$ *and positive if* $\gamma \in \mathbb{R} \setminus [0,1]$.

Proof. Using the the fact that $\dot{y} = 0$ on the stagnation points and their analytical expressions, it is possible to infer the signs of $(1+\varphi)$ and $(1-\varphi)$ for every γ. We can write

$$\begin{aligned} 1+\varphi &= 1 + \frac{1-\gamma}{(\tilde{x}+\gamma)^2} + \frac{\gamma}{(\tilde{x}-(1-\gamma))^2} \\ &= 1 + \frac{1}{(\tilde{x}+\gamma)^2} + \gamma\left[\frac{1}{(\tilde{x}-(1-\gamma))^2} - \frac{1}{(\tilde{x}+\gamma)^2}\right] \\ &= 1 + \frac{1}{(\tilde{x}+\gamma)^2} + \frac{[2(\tilde{x}+\gamma)-1]\gamma}{(\tilde{x}-(1-\gamma))^2(\tilde{x}+\gamma)^2}. \end{aligned} \tag{6.38}$$

Since $\dot{y} = 0$ on the stagnation points, we have

$$\frac{\gamma}{\tilde{x} - (1-\gamma)} + \frac{1-\gamma}{\tilde{x}+\gamma} - \tilde{x} = 0 \Longleftrightarrow \frac{1-\gamma}{(\tilde{x}+\gamma)^2} = 1 - \frac{\gamma}{\tilde{x}+\gamma} - \frac{\gamma}{(\tilde{x}+\gamma)\left(\tilde{x}-(1-\gamma)\right)}. \tag{6.39}$$

Using this on the expression for $1-\varphi$, we can write

$$\begin{aligned} 1-\varphi &= 1 - \frac{1-\gamma}{(\tilde{x}+\gamma)^2} - \frac{\gamma}{\left(\tilde{x}-(1-\gamma)\right)^2} \\ &= \frac{\gamma}{\tilde{x}+\gamma} + \frac{\gamma}{(\tilde{x}+\gamma)\left(\tilde{x}-(1-\gamma)\right)} - \frac{\gamma}{\left(\tilde{x}-(1-\gamma)\right)^2} \\ &= \frac{\gamma}{\left(\tilde{x}-(1-\gamma)\right)^2}\left[\frac{\left(\tilde{x}-(1-\gamma)\right)^2}{\tilde{x}+\gamma} + \frac{\tilde{x}-(1-\gamma)}{\tilde{x}+\gamma} - 1\right] \\ &= \frac{\gamma}{\left(\tilde{x}-(1-\gamma)\right)^2}\left[\tilde{x}+\gamma-2\right]. \end{aligned} \tag{6.40}$$

Case $\gamma \in \,]0,1[$:

Since γ and $1-\gamma$ are both positive, from Equation (6.38) we see that $1+\varphi$ is a sum of three positive quantities, and thus it is positive. From Equation (6.40), we see that the sign of $1-\varphi$ is the same as the sign of $\tilde{x}+\gamma-2$. Using Equation (6.30), we can write

$$\tilde{x}+\gamma-2 \leq -\frac{2\gamma-1}{3} + \frac{2}{3}\sqrt{\gamma^2-\gamma+4} + \gamma - 2 = \frac{\gamma-5}{3} + \frac{2}{3}\sqrt{\gamma^2-\gamma+4} < 0. \tag{6.41}$$

Thus, $\left(1+\varphi\right)\left(1-\varphi\right) < 0$.

Case $\gamma \in \mathbb{R} \setminus [0,1]$:

We start by checking the sign of $\left[2\left(\tilde{x}+\gamma\right)-1\right]\gamma$. If $\gamma > 1$, from Equation (6.31) we can write

$$2\left(\tilde{x}+\gamma\right) - 1 \geq -\frac{4\gamma-2}{3} + \frac{4}{3}\sqrt{\gamma^2-\gamma+4} + 2\gamma - 1 = \frac{2\gamma-1}{3} + \frac{4}{3}\sqrt{\gamma^2-\gamma+4} > 3 > 0. \tag{6.42}$$

And, if $\gamma < 0$, we have

$$2\left(\tilde{x}+\gamma\right) - 1 \leq \frac{2\gamma-1}{3} - \frac{4}{3}\sqrt{\gamma^2-\gamma+4} < -3 < 0. \tag{6.43}$$

Thus, for $\gamma \in \mathbb{R} \setminus [0,1]$, we have $\left[2\left(\tilde{x}+\gamma\right)-1\right]\gamma > 0$, and $1+\varphi$ is a sum of three positive quantities (Equation (6.38)) and thus positive.

We now check the sign of $\left(\tilde{x}+\gamma-2\right)\gamma$. If $\gamma > 1$, from Equation (6.30), we have

$$\tilde{x}+\gamma-2 \geq -\frac{2\gamma-1}{3} + \frac{2}{3}\sqrt{\gamma^2-\gamma+4} + \gamma - 2 = \frac{\gamma-5}{3} + \frac{2}{3}\sqrt{\gamma^2-\gamma+4} > 0. \tag{6.44}$$

And, if $\gamma < 0$,

$$\widetilde{x} + \gamma - 2 \leq -\frac{2\gamma - 1}{3} - \frac{2}{3}\sqrt{\gamma^2 - \gamma + 4} + \gamma - 2 = \frac{\gamma - 5}{3} - \frac{2}{3}\sqrt{\gamma^2 - \gamma + 4} < -3 < 0\,. \tag{6.45}$$

Hence, for $\gamma \in \mathbb{R} \setminus [0,1]$, we have $(\widetilde{x} + \gamma - 2)\,\gamma > 0$, and $1 - \varphi$ is positive (Equation (6.40)) and $\left(1 + \varphi\right)\left(1 - \varphi\right) > 0\,.$ □

Thus, if $\gamma \in \,]0,1[$, the three stagnation points in the real axis are unstable saddle points, and, if $\gamma \in \mathbb{R} \setminus [0,1]$, the single stagnation point in the real axis is a center. The information about the stagnation points in both scenarios is summarized in Table 6.2.

Table 6.2: Stagnation points for the system depending on the parameter γ.

$\gamma \in \,]0,1[$		$\gamma \in \mathbb{R} \setminus [0,1]$	
$(x_0, 0)$, see (6.30)	unstable saddle	$(\overline{x}_0, 0)$, see (6.31)	center
$(x_1, 0)$, see (6.30)	unstable saddle	$--$	
$(x_2, 0)$, see (6.30)	unstable saddle	$--$	
$\left(\frac{1-2\gamma}{2}, \frac{\sqrt{3}}{2}\right)$	center	$\left(\frac{1-2\gamma}{2}, \frac{\sqrt{3}}{2}\right)$	unstable saddle
$\left(\frac{1-2\gamma}{2}, -\frac{\sqrt{3}}{2}\right)$	center	$\left(\frac{1-2\gamma}{2}, -\frac{\sqrt{3}}{2}\right)$	unstable saddle

Once again, it is possible to write a time-independent stream function for this system:

$$\psi\left(x,y\right) = -\frac{1}{2}\left[\gamma \log\left(\left(x - (1-\gamma)\right)^2 + y^2\right) + (1-\gamma)\log\left((x+\gamma)^2 + y^2\right) - \left(x^2 + y^2\right)\right]. \tag{6.46}$$

The trajectories of passive particles are thus the level sets of this stream function, or, equivalently, the level sets of

$$\widetilde{\psi}\left(x,y\right) = e^{-2\psi(x,y)} = \left[\left(x - (1-\gamma)\right)^2 + y^2\right]^{\gamma}\left[(x+\gamma)^2 + y^2\right]^{1-\gamma} e^{-\left(x^2+y^2\right)}, \tag{6.47}$$

which, for the symmetric case $\gamma = \frac{1}{2}$, can be thought of as Cassini ovals [21] that have been deformed by the rotational movement of the system: the curves are compressed along the y-axis and elongated along the x-axis due to the presence of the exponential term $e^{-\left(x^2+y^2\right)}$ in $\widetilde{\psi}\left(x,y\right)$.

Using the stream function and the information on the stagnation points, it is possible to draw the phase diagram of this system for any γ. We see once again that there exists an atmosphere around each vortex. The boundary of these regions can be characterized as a part of the curve that is implicitly defined by $\widetilde{\psi}\left(x,y\right) = \widetilde{\psi}\left(x_1,0\right)$ in the $\gamma \in \,]0,1[$

case, or $\widetilde{\psi}(x,y) = \widetilde{\psi}(p_3)$ in the $\gamma \in \mathbb{R} \setminus [0,1]$ case. In fact, the curves resulting from these equations separate the 2D plane in various regions. Typically, two passive particles inside of the same region will have similar trajectories, while two particles that are located in two different regions will have distinct trajectories. For instance, particles inside the atmosphere of one vortex will rotate around that region's vortex; particles that are far away from the vortices will have trajectories similar to the trajectory of a particle rotating around a single vortex in the vorticity center of the system, while other passive particles can have more complex trajectories where they orbit both vortices or none of them. As examples, we plot the phase diagrams for $\gamma = \frac{1}{2}$ in Figure 6.2, $\gamma = \frac{3}{4}$ in Figure 6.3 and $\gamma = \frac{4}{3}$ in Figure 6.4. Notice that there exists a significant distinction in the dynamics of the system depending on the value of γ and that the case $\gamma \in \mathbb{R} \setminus [0,1]$ shows some dynamical similarities to the case $\Gamma_1 + \Gamma_2 = 0$. In fact, the case $\Gamma_1 + \Gamma_2 = 0$ is obtained when $\gamma \to \pm\infty$. The transitions at $\gamma = 0$ and $\gamma = 1$ are bifurcations where two stagnation points on the x-axis collide with one another and the system goes from five to three (or vice versa) stagnation points. Notice that in these bifurcations, the stability of the stagnation points also changes (see Table 6.2).

Due to the complexity of the expression for the stream function and its dependence on the parameter γ, it is not possible to obtain an explicit expression for the area or perimeter of the vortex atmospheres in this case. However, using (6.47) it is possible to compute them numerically, and the results are shown in Figure 6.5, where we plot these quantities for each of the atmospheres as well as their sum for different values of γ.

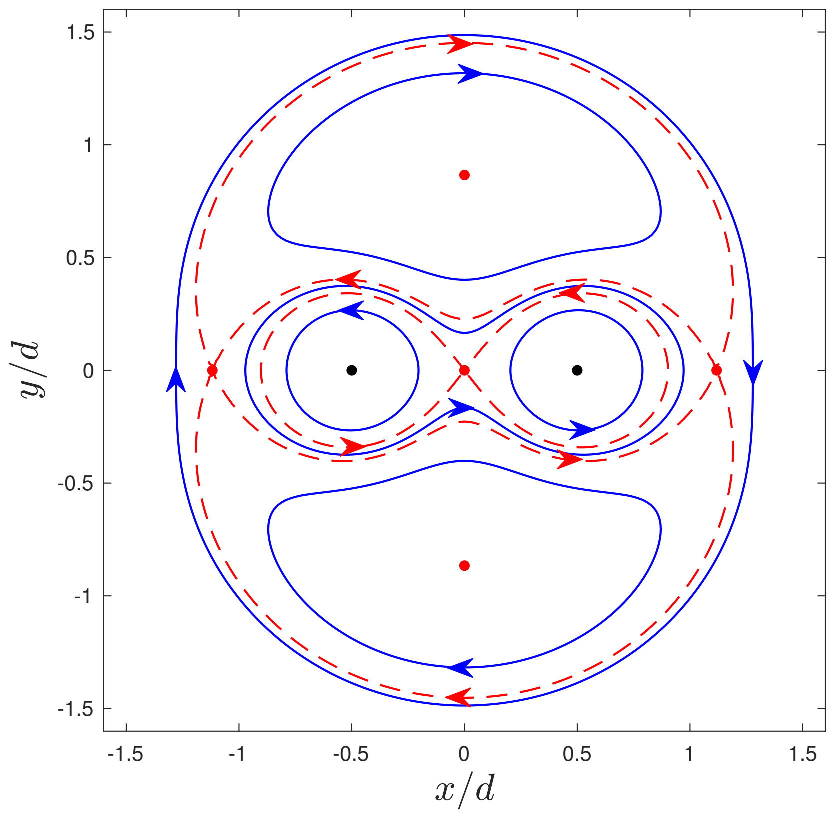

Figure 6.2: Phase diagram for a system of two point vortices in the co-moving frame. The vortices (black dots) are located at $w_1 = 1/2$ and $w_1 = -1/2$, and the circulations are such that $\Gamma_1 + \Gamma_2 \neq 0$ and $\gamma = 1/2$. The red dots identify the stagnation points of the system. The red dashed lines correspond to special particle trajectories that constitute a boundary between regions of the infinite plane where particles present different types of trajectories (exemplified in blue lines).

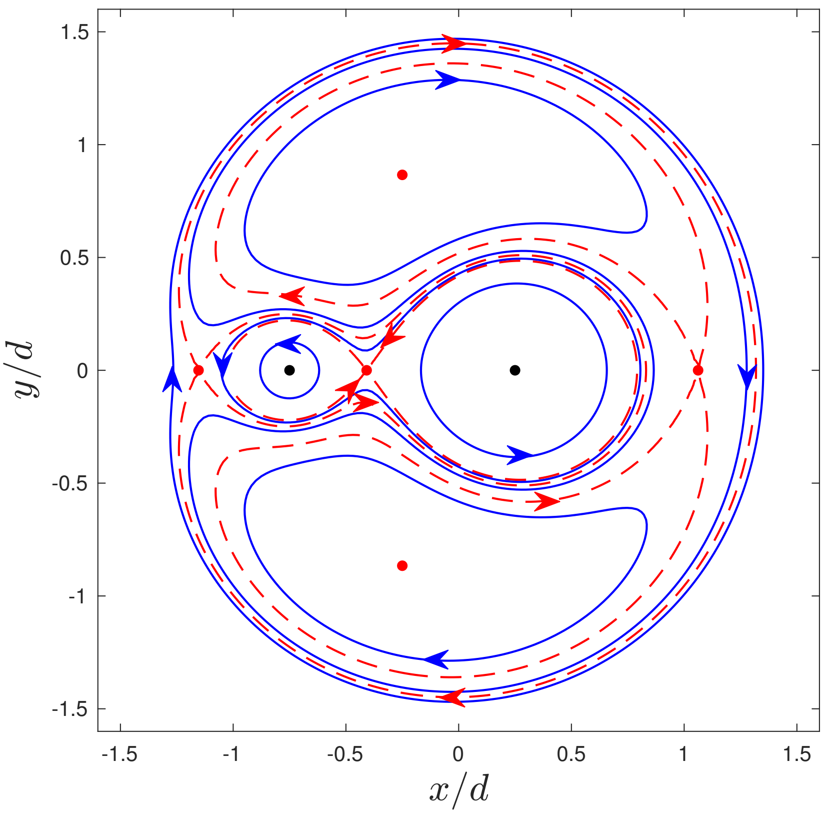

Figure 6.3: Phase diagram for a system of two point vortices in the co-moving frame. The vortices (black dots) are located at $w_1 = 1/4$ and $w_1 = -3/4$, and the circulations are such that $\Gamma_1 + \Gamma_2 \neq 0$ and $\gamma = 3/4$. The red dashed lines correspond to special particle trajectories that constitute a boundary between regions of the infinite plane where particles present different types of trajectories (exemplified in blue lines). The red dots identify the stagnation points.

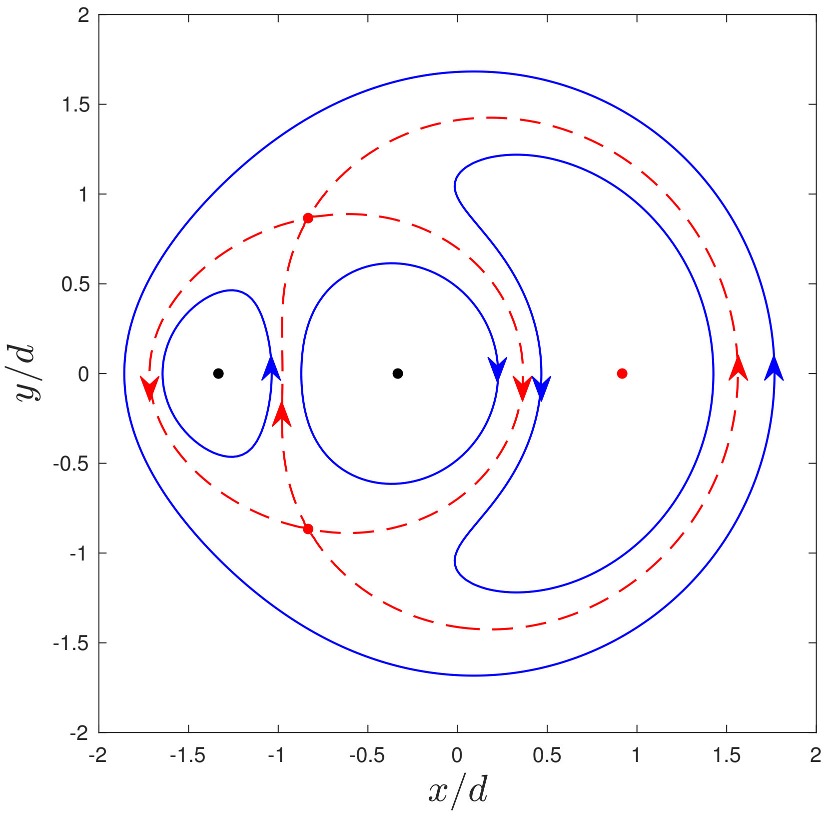

Figure 6.4: Phase diagram for a system of two point vortices in the co-moving frame. The vortices (black dots) are located at $w_1 = -1/2$ and $w_1 = -3/2$, and the circulations are such that $\Gamma_1 + \Gamma_2 \neq 0$ and $\gamma = 4/3$. The red dashed lines correspond to special particle trajectories that constitute a boundary between regions of the infinite plane where particles present different types of trajectories (exemplified in blue lines). The red dots identify the stagnation points.

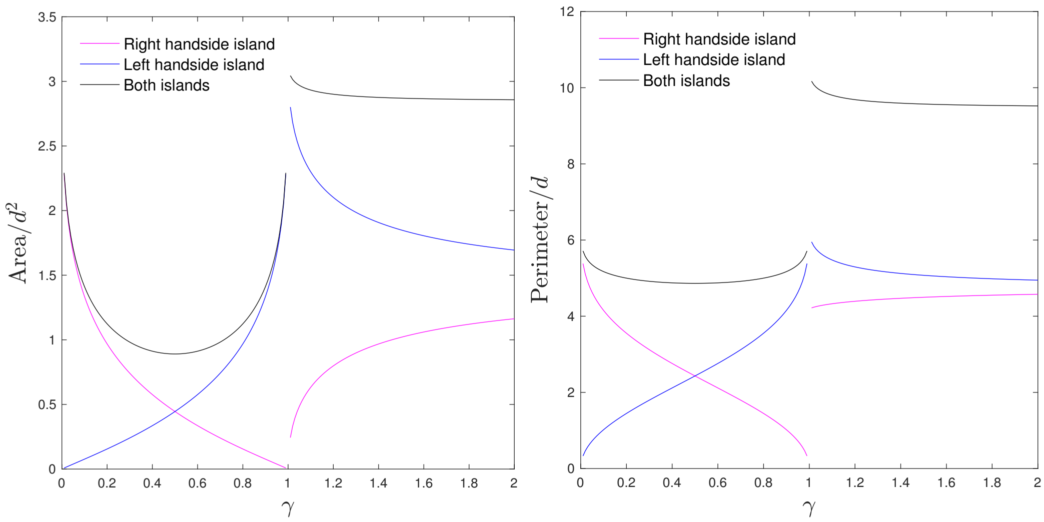

Figure 6.5: Area and perimeter of the atmospheric islands around the vortices for $0 < \gamma < 2$.

6.3 Conclusions and Future Work

Inspired by studies that have shown the existence of stability islands around point vortices in 2D flows, we study and characterize the geometry of the analogous regions for systems of two point vortices (vortex atmospheres). Passive particles in a flow cannot cross the boundary of these regions, and on the inside of the atmosphere, particles are mainly advected by the vortex on the inside of that atmosphere, having a regular trajectory.

In the scenario where the total circulation of the system is zero ($\Gamma_1 + \Gamma_2 = 0$), the dynamics can be completely characterized without any parameter dependence. In the frame that is co-moving with the vortices, passive particles on the outside of the atmosphere will eventually move away from the vortices and never approach them again. Passive particles on the inside of the atmosphere of each vortex will describe closed trajectories around them indefinitely. Due to the symmetries in the system, the corresponding regions for each vortex have the same perimeter and area, which can be calculated with arbitrary precision. We found that each atmospheric island has a perimeter $\approx 4.744\, d$ and an area $\approx 1.425\, d^2$ (d is the distance between the vortices). The set of both atmospheric islands in this scenario differ from an ellipse by ≈3.76‰ in area.

If the total circulation is not zero, however, the dynamics are completely characterized by a parameter $\gamma = \dfrac{\Gamma_1}{\Gamma_1 + \Gamma_2}$. If $\gamma \in \,]0, 1[$, in the frame that is co-moving with the vortices, passive particles can have a multitude of trajectories: if they are on the inside of an atmosphere, they will describe closed trajectories inside the region formed by the associated vortex; in a certain vicinity of the vortices, particles may orbit both vortices in closed loops or describe closed trajectories without orbiting any of the vortices; and if a particle is sufficiently far away from the vortices, it will describe a closed trajectory around both of the vortices. The area and perimeter of the vortex atmospheres cannot be computed analytically due to the complexity of the mathematical expressions involved, but numerical computations clearly show that these quantities scale with the strength of the vortex located on the inside of the region.

If $\gamma \in \mathbb{R} \setminus [0, 1]$, in the frame that is co-moving with the vortices, particles describe closed, regular trajectories on the inside of the vortex atmospheres once again. There is a third closed region in the 2D plane where particles describe closed trajectories without orbiting any of the vortices, while on the rest of the 2D plane, every particle will orbit both vortices in a closed trajectory. Analytical computation of the area and perimeter of these regions is once again impossible due to the complexity of the mathematical expressions, but numerical computations show that as $\gamma \to \infty$ (equivalently $\Gamma_1 \to -\Gamma_2$), the values for these quantities approach the values obtained in the $\Gamma_1 + \Gamma_2 = 0$ analysis, as one would expect.

We plan to further research in this area, tackling the problem for a configuration of three point vortices. This problem is more challenging due to the fact that we are now dealing with three different circulations.

Author Contributions: Conceptualization, G.M. and S.G.; methodology, G.M. and S.G.; software, G.M.; validation, G.M.; formal analysis, G.M.; writing—original draft preparation, G.M.; writing—review and editing, G.M. and S.G.; visualization, G.M.; supervision, S.G.; project administration, S.G.; funding acquisition, G.M. and S.G. All authors have read and agreed to the published version of the manuscript.

Funding: This research was funded by the CMUP project UIDB/00144/2020. GM gratefully acknowledges support from the FCT grant PD/BD/150537/2019.

Data Availability Statement: No new data were created or analyzed in this study. Data sharing is not applicable to this article.

Acknowledgments: This work honors the memory of Fernando Lobo Pereira, a world-renowned Portuguese expert in Optimal Control, who left us in June 2022.

Conflicts of Interest: The authors declare no conflicts of interest.

References

[1] H. Helmholtz, "Über integrale der hydrodynamischen gleichungen, welche den wirbelbewegungen entsprechen.," ger, *Journal für die reine und angewandte Mathematik*, vol. 55, pp. 25–55, 1858.

[2] W. Thomson, "Vi.—on vortex motion," *Transactions of the Royal Society of Edinburgh*, vol. 25, no. 1, pp. 217–260, 1868. DOI: 10.1017/S0080456800028179.

[3] G. R. Kirchhoff, "Vorlesungenbër mathematische Physik.," ger, *Mechanik*, 1876.

[4] M. Umeki, "Clustering analysis of periodic point vortices with the l function," *Journal of the Physical Society of Japan*, vol. 76, no. 4, p. 043 401, 2007. DOI: 10.1143/JPSJ.76.043401.

[5] M. A. Stremler, "On relative equilibria and integrable dynamics of point vortices in periodic domains," *Theoretical and Computational Fluid Dynamics*, vol. 24, no. 1, pp. 25–37, 2010. DOI: 10.1007/s00162-009-0156-z.

[6] D. Crowdy, "Point vortex motion on the surface of a sphere with impenetrable boundaries," *Physics of Fluids*, vol. 18, no. 3, p. 036 602, Mar. 2006, ISSN: 1070-6631. DOI: 10.1063/1.2183627.

[7] P. Newton, *The N-Vortex Problem: Analytical Techniques* (Applied Mathematical Sciences). Springer New York, 2010, ISBN: 9781441929167. DOI: 10.1007/978-1-4684-9290-3.

[8] I. I. Mokhov, S. G. Chefranov, and A. G. Chefranov, "Point vortices dynamics on a rotating sphere and modeling of global atmospheric vortices interaction," *Physics of Fluids*, vol. 32, no. 10, p. 106 605, Oct. 2020, ISSN: 1070-6631. DOI: 10.1063/5.0026014.

[9] J. Montaldi and C. Nava-Gaxiola, "Point vortices on the hyperbolic plane," *Journal of Mathematical Physics*, vol. 55, no. 10, p. 102 702, Oct. 2014, ISSN: 0022-2488. DOI: 10.1063/1.4897210.

[10] C. G. Ragazzo, "The motion of a vortex on a closed surface of constant negative curvature," *Proceedings of the Royal Society A: Mathematical, Physical and Engineering Sciences*, vol. 473, no. 2206, p. 20 170 447, Oct. 2017, ISSN: 1364-5021. DOI: 10.1098/rspa.2017.0447.

[11] H. Aref, "Point vortex dynamics: A classical mathematics playground," *Journal of Mathematical Physics*, vol. 48, no. 6, p. 065 401, Jun. 2007, ISSN: 0022-2488. DOI: 10.1063/1.2425103.

[12] A. Babiano, G. Boffetta, A. Provenzale, and A. Vulpiani, "Chaotic advection in point vortex models and two-dimensional turbulence," *Physics of Fluids*, vol. 6, no. 7, pp. 2465–2474, Jul. 1994, ISSN: 1070-6631. DOI: 10.1063/1.868194.

[13] Z. Neufeld and T. Tél, "The vortex dynamics analogue of the restricted three-body problem: Advection in the field of three identical point vortices," *Journal of Physics A: Mathematical and General*, vol. 30, no. 6, p. 2263, Mar. 1997. DOI: 10.1088/0305-4470/30/6/043.

[14] G. K. Batchelor, *An Introduction to Fluid Dynamics* (Cambridge Mathematical Library). Cambridge University Press, 2000. DOI: 10.1017/CBO9780511800955.

[15] S. B. Pope, *Turbulent Flows*. Cambridge University Press, 2000. DOI: 10.1017/CBO9781316179475.

[16] H. Lamb, *Hydrodynamics* (Dover Books on Physics). Dover publications, 1945, ISBN: 9780486602561.

[17] S. Boatto and R. T. Pierrehumbert, "Dynamics of a passive tracer in a velocity field of four identical point vortices," *Journal of Fluid Mechanics*, vol. 394, no. 1, pp. 137–174, Sep. 1999. DOI: 10.1017/S0022112099005492.

[18] V. V. Meleshko, M. Y. Konstantinov, A. A. Gurzhi, and T. P. Konovaljuk, "Advection of a vortex pair atmosphere in a velocity field of point vortices*," *Physics of Fluids A: Fluid Dynamics*, vol. 4, no. 12, pp. 2779–2797, Dec. 1992, ISSN: 0899-8213. DOI: 10.1063/1.858335.

[19] A. Chorin, *Vorticity and Turbulence* (Applied Mathematical Sciences). Springer, 1994, ISBN: 9780387941974. DOI: 10.1007/978-1-4419-8728-0.

[20] R. W. D. Nickalls and R. H. Dye, "The geometry of the discriminant of a polynomial," *The Mathematical Gazette*, vol. 80, no. 488, pp. 279–285, 1996. DOI: 10.2307/3619560.

[21] A. Basset, *An Elementary Treatise on Cubic and Quartic Curves*. Deighton, Bell, 1901.

Chapter 7

Discussion

This thesis focused on the dynamics of two-dimensional vortex flows, covering both inviscid and viscous environments. Passive-particle trajectories play a central role in this context, serving both as diagnostic and control tools: on one hand, they can be used as an instrument to characterise the velocity field and identify the coherent structures that partition the phase space of the flow; on the other hand, they carry information about the underlying flow dynamics and can be exploited to track and reconstruct the trajectories of the point vortices that shape the dynamics of a system.

Knowledge of the vortices present in a system (i.e., their positions and circulations) allows for the dynamical and geometrical description of the flow, as exemplified in Chapter 6: vortices give rise to physical transport barriers that partition the flow into regions from which passive objects cannot escape. These constraints can strongly limit material transport in a flow and lead to highly complex dynamics and phase space structures, especially in systems with a large number of vortices. Real flows are not as idealised as the ones treated in this thesis, as the dynamics are often altered due to external influences that can happen over time. As such, the ability to track and eventually predict the dynamics of vortices in real time can be a valuable tool for the analysis of real systems.

Following the trajectories of tracers, or passive particles, is considerably easier to do with current technology than directly observing the movement of vortices. As shown in Chapter 4, in a vortex flow, passive-particle trajectories can be used to recover both the circulations and trajectories of point vortices. This makes it possible to predict a system's dynamics over a finite time interval with some degree of confidence. Being able to retrieve this kind of information in real time has a significant impact on the understanding of flows and can help achieve better results in control-oriented questions, such as the optimal transport of objects between prescribed locations, as explored in Chapters 2, 3 and 5.

7.1 Thesis outcomes

The work developed during this thesis contributed to deepening the understanding of two-dimensional vortex flows. Although the results are presented independently, in the form of multiple published articles, they constitute a coherent framework that aims to use the dynamics of passive particles to both obtain more information about a vortex-dominated flow and to design strategies to move objects between prescribed locations in such a flow.

This thesis provided a first geometric characterisation of the atmospheric islands in systems of two point vortices, as presented in Chapter 6. In these systems, the number of point vortices is not high enough to produce chaotic regions. However, these atmospheric islands are the analogue of the stability islands found in systems with a higher number of point vortices and highlight the key features that are observed in more complex systems. The physical barriers created by the vortices separate the phase space into regions with qualitatively distinct dynamics. These coherent structures impose strong constraints on the motion of passive particles and suggest that it should be possible to take advantage of the different dynamical regions for different tasks.

The usefulness of the chaotic regions of a flow is illustrated by the work done in Chapter 4. By observing the trajectories of passive particles influenced by multiple vortices (i.e., particles outside of the stability island of a vortex), it is possible to probe the vortex dynamics and retrieve key parameters of vortex flows: the circulations and positions of the point vortices over finite time intervals. This establishes these tracers as a possible measurement tool of the characteristics of a flow, since direct observation of vortices can be difficult, or even impossible. It also provides a foundation for real-time estimation of vortex dynamics.

On the other hand, the stability islands can be exploited for control purposes, as it is firstly illustrated in Chapter 2 by deriving the optimal control to move a particle between two prescribed locations in a flow dominated by a single point vortex. In this simplified scenario, it was possible to understand the interplay between the time interval available for the movement and the energy cost from applying a control on a particle. In particular, it was shown that the energy-optimal control will always move the particle as slowly as possible. While the analytical expressions for this type of control were possible to derive in an inviscid scenario, for a viscous flow the problem needs to be solved numerically, as discussed in Chapter 3. Due to the rotational behaviour of these systems, the number of full turns a passive particle takes around a vortex is also an important parameter when considering optimal-control problems. This was further explored and discussed in Chapter 5, where it is seen that energy-optimal controls prioritise lower full-turn counts and that there may exist gaps in the viscosity range for which an optimal solution does not exist due to the interplay between viscosity and time availability.

7.2 Future Work

The work presented in this thesis is based on fairly simple systems and motivates further research on more complex systems of vortices, different models of viscous vortices and potentially different forms of admissible controls.

Vortex flows are typically not characterised by a singular vortex and, as such, moving a passive particle in a velocity field generated by a singular vortex is not completely realistic. However, due to the existence of stability islands around each vortex, the movement of a particle located inside one of these regions is locally dictated by the corresponding vortex alone. In a system composed by multiple point vortices, it is expected that one can take advantage of these stability islands to design control strategies to move objects in a flow.

An interesting problem would be to put together all these pieces and analyse how one can optimally move a passive particle between two locations in a flow ruled by multiple vortices. Even if it is possible to take advantage of the stability islands to perform the displacement of a passive particle, the fact that the geometry of the stability islands seems to change due to vortex-vortex interactions poses an additional degree of complexity to this problem, even in an inviscid scenario.

In addition, the geometry and dynamics of the atmospheric islands in systems of viscous vortices are still not fully comprehended. It would be interesting to explore how viscous forces alter the geometry of these islands over time and to compare different approaches to the modelling of viscosity.

7.3 Final Remarks

The full Navier–Stokes equations are hard to solve for generic initial and boundary conditions. As such, the study of alternative, simpler models plays a significant role in trying to understand the dynamics of fluids. Two-dimensional vortex flow models, in particular, are good approximations to many real systems, where the full three-dimensional dynamics seem to be captured by a set of quasi-two-dimensional systems. These two-dimensional approximations are nevertheless both geometrically and dynamically rich, exhibiting coherent structures that partition the phase space into regions of stability and chaoticity. Generically speaking, the stability regions appear close to each vortex, while the chaotic regions emerge away from the vortex centres. By understanding the behaviour of these systems, it is possible to further exploit the underlying dynamics for one's advantage, for instance, to design optimal control strategies for a variety of tasks, such as moving objects in a flow while minimising the associated energy costs or building a strategy to perform a certain task in the shortest time interval possible.

These features were explored in this thesis through passive-particle dynamics, which provided a unified way to analyse transport, retrieve vortex dynamics, and design control strategies for vortex-dominated flows.

General Bibliography

K. T. Alligood, T. D. Sauer, and J. A. Yorke, *Chaos An Introduction to Dynamical Systems*. Springer-Verlag, New York, 1997. DOI: 10.1007/b97589.

H. Aref, "Integrable, chaotic, and turbulent vortex motion in two-dimensional flows," *Annual Review of Fluid Mechanics*, vol. 15, no. Volume 15, 1983, pp. 345–389, 1983, ISSN: 1545-4479. DOI: 10.1146/annurev.fl.15.010183.002021.

H. Aref, "Point vortex dynamics: A classical mathematics playground," *Journal of Mathematical Physics*, vol. 48, no. 6, p. 065 401, Jun. 2007, ISSN: 0022-2488. DOI: 10.1063/1.2425103.

H. Aref and M. A. Stremler, "Point vortex models and the dynamics of strong vortices in the atmosphere and oceans," in *Fluid Mechanics and the Environment: Dynamical Approaches*, J. L. Lumley, Ed., Berlin, Heidelberg: Springer Berlin Heidelberg, 2001, pp. 1–17, ISBN: 978-3-540-44512-8. DOI: 10.1007/3-540-44512-9_1.

A. V. Arutyunov, D. Y. Karamzin, and F. L. Pereira, "The maximum principle for optimal control problems with state constraints by r.v. gamkrelidze: Revisited," *Journal of Optimization Theory and Applications*, vol. 149, no. 3, pp. 474–493, 2011. DOI: 10.1007/s10957-011-9807-5.

A. Babiano, G. Boffetta, A. Provenzale, and A. Vulpiani, "Chaotic advection in point vortex models and two-dimensional turbulence," *Physics of Fluids*, vol. 6, no. 7, pp. 2465–2474, Jul. 1994, ISSN: 1070-6631. DOI: 10.1063/1.868194.

A. Basset, *An Elementary Treatise on Cubic and Quartic Curves*. Deighton, Bell, 1901.

G. K. Batchelor, *An Introduction to Fluid Dynamics* (Cambridge Mathematical Library). Cambridge University Press, 2000. DOI: 10.1017/CBO9780511800955.

H. Bhatia, G. Norgard, V. Pascucci, and P.-T. Bremer, "The helmholtz-hodge decomposition—a survey," *IEEE Transactions on Visualization and Computer Graphics*, vol. 19, no. 8, pp. 1386–1404, 2013. DOI: 10.1109/TVCG.2012.316.

S. Boatto and R. T. Pierrehumbert, "Dynamics of a passive tracer in a velocity field of four identical point vortices," *Journal of Fluid Mechanics*, vol. 394, no. 1, pp. 137–174, Sep. 1999. DOI: 10.1017/S0022112099005492.

G. Boffetta, A. Celani, and P. Franzese, "Trapping of passive tracers in a point vortex system," *Journal of Physics A: Mathematical and General*, vol. 29, no. 14, p. 3749, Jul. 1996. DOI: 10.1088/0305-4470/29/14/004.

J. Buzhardt and P. Tallapragada, "Controlled transport of fluid particles by microrotors in a stokes flow using linear transfer operators," *Physics of Fluids*, vol. 36, no. 3, p. 032 021, Mar. 2024, ISSN: 1070-6631. DOI: 10.1063/5.0195528.

C. Calascibetta, L. Biferale, F. Borra, A. Celani, and M. Cencini, "Optimal tracking strategies in a turbulent flow," *Communications Physics*, vol. 6, no. 1, p. 256, 2023. DOI: 10.1038/s42005-023-01366-y.

D. Chang, C. R. Edwards, F. Zhang, and J. Sun, "A data assimilation framework for data-driven flow models enabled by motion tomography," *International Journal of Intelligent Robotics and Applications*, vol. 3, no. 2, pp. 158–177, 2019. DOI: 10.1007/s41315-019-00092-5.

A. Chorin, *Vorticity and Turbulence* (Applied Mathematical Sciences). Springer, 1994, ISBN: 9780387941974. DOI: 10.1007/978-1-4419-8728-0.

I. Chueshov, J. Duan, and B. Schmalfuss, *Probabilistic dynamics of two-layer geophysical flows*, 2001. arXiv: math/0104143 .

C. J. Clarke and R. F. Carswell, *Principles of Astrophysical Fluid Dynamics*. 2003. DOI: 10.2277/0521853311.

F. Clarke, Y. Ledyaev, R. Stern, and P. Wolenski, *Nonsmooth Analysis and Control Theory* (Graduate Texts in Mathematics). Springer New York, 2008, ISBN: 9780387226255. DOI: 10.1007/b97650.

D. Crowdy, "Point vortex motion on the surface of a sphere with impenetrable boundaries," *Physics of Fluids*, vol. 18, no. 3, p. 036 602, Mar. 2006, ISSN: 1070-6631. DOI: 10.1063/1.2183627.

M. C. Denes, G. Froyland, and S. R. Keating, "Persistence and material coherence of a mesoscale ocean eddy," *Phys. Rev. Fluids*, vol. 7, p. 034 501, 3 Mar. 2022. DOI: 10.1103/PhysRevFluids.7.034501.

E. Fehlberg, *Low-order Classical Runge-Kutta Formulas with Stepsize Control and Their Application to Some Heat Transfer Problems* (NASA technical report). National Aeronautics and Space Administration, 1969.

M. Ferreira, V. Carvalho, J. Ribeiro, R. A. Lima, S. Teixeira, and D. Pinho, "Advances in microfluidic systems and numerical modeling in biomedical applications: A review," *Micromachines*, vol. 15, no. 7, 2024, ISSN: 2072-666X. DOI: 10.3390/mi15070873.

T. Gallay, "Interaction of vortices in weakly viscous planar flows," *Archive for Rational Mechanics and Analysis*, vol. 200, no. 2, pp. 445–490, 2011. DOI: 10.1007/s00205-010-0362-2.

T. Gallay and C. E. Wayne, "Global stability of vortex solutions of the two-dimensional navier-stokes equation," *Communications in Mathematical Physics*, vol. 255, no. 1, pp. 97–129, 2005. DOI: 10.1007/s00220-004-1254-9.

S. Gama and P. Milheiro-Oliveira, "Statistical properties of passive tracers in a positive four-point vortex model," *Phys. Rev. E*, vol. 62, pp. 1424–1426, 1 Jul. 2000. DOI: 10.1103/PhysRevE.62.1424.

H. Helmholtz, "Über integrale der hydrodynamischen gleichungen, welche den wirbelbewegungen entsprechen.," ger, *Journal für die reine und angewandte Mathematik*, vol. 55, pp. 25–55, 1858.

Y. Huang and M. A. Green, "Detection and tracking of vortex phenomena using lagrangian coherent structures," *Experiments in Fluids*, vol. 56, no. 7, p. 147, 2015. DOI: 10.1007/s00348-015-2001-z.

S.-C. Kim and S.-I. Sohn, "Interactions of three viscous point vortices," *Journal of Physics A: Mathematical and Theoretical*, vol. 45, no. 45, p. 455 501, Oct. 2012. DOI: 10.1088/1751-8113/45/45/455501.

G. R. Kirchhoff, "Vorlesungenbër mathematische Physik.," ger, *Mechanik*, 1876.

H. Lamb, *Hydrodynamics* (Dover Books on Physics). Dover publications, 1945, ISBN: 9780486602561.

M. Levi, *Classical Mechanics with Calculus of Variations and Optimal Control: An Intuitive Introduction* (Student Mathematical Library). American Mathematical Society, 2014, ISBN: 9780821891384.

J. Liu and H. Hu, "Biological inspiration: From carangiform fish to multi-joint robotic fish," *Journal of Bionic Engineering*, vol. 7, no. 1, pp. 35–48, 2010, ISSN: 1672-6529. DOI: 10.1016/S1672-6529(09)60184-0.

N. Mahmoudian, J. Geisbert, and C. Woolsey, "Dynamics and control of underwater gliders i: Steady motions," Virginia Center for Autonomous Systems, Technical Report VaCAS-2007-01, 2009.

N. Mahmoudian and C. Woolsey, "Dynamics and control of underwater gliders ii: Motion planning and control," Virginia Center for Autonomous Systems, Technical Report VaCAS-2010-02, 2010.

G. Marques, T. Grilo, S. Gama, and F. L. Pereira, "Optimal control of a passive particle advected by a point vortex," in *Advanced Research in Technologies, Information, Innovation and Sustainability*, T. Guarda, F. Portela, and M. F. Santos, Eds., Cham: Springer International Publishing, 2021, pp. 512–523, ISBN: 978-3-030-90241-4. DOI: 10.1007/978-3-030-90241-4_39.

G. Marques, S. Gama, and F. L. Pereira, "Optimal control of a passive particle advected by a lamb–oseen (viscous) vortex," *Computation*, vol. 10, no. 6, 2022, ISSN: 2079-3197. DOI: 10.3390/computation10060087.

G. Marques, M. J. Rodrigues, and S. Gama, "Passive particle dynamics in viscous vortex flow," in *CONTROLO 2020*, J. A. Gonçalves, M. Braz-César, and J. P. Coelho, Eds., Cham: Springer International Publishing, 2021, pp. 352–362, ISBN: 978-3-030-58653-9. DOI: 10.1007/978-3-030-58653-9_34.

V. V. Meleshko, M. Y. Konstantinov, A. A. Gurzhi, and T. P. Konovaljuk, "Advection of a vortex pair atmosphere in a velocity field of point vortices*," *Physics of Fluids A: Fluid Dynamics*, vol. 4, no. 12, pp. 2779–2797, Dec. 1992, ISSN: 0899-8213. DOI: 10.1063/1.858335.

S. Mitter and J. Lions, *Optimal Control of Systems Governed by Partial Differential Equations* (Grundlehren der mathematischen Wissenschaften). Springer Berlin Heidelberg, 1971, ISBN: 9783540051152.

H. K. Moffatt, “The degree of knottedness of tangled vortex lines,” *Journal of Fluid Mechanics*, vol. 35, pp. 117–129, Jan. 1969. DOI: 10.1017/S0022112069000991.

I. I. Mokhov, S. G. Chefranov, and A. G. Chefranov, “Point vortices dynamics on a rotating sphere and modeling of global atmospheric vortices interaction,” *Physics of Fluids*, vol. 32, no. 10, p. 106 605, Oct. 2020, ISSN: 1070-6631. DOI: 10.1063/5.0026014.

J. Montaldi and C. Nava-Gaxiola, “Point vortices on the hyperbolic plane,” *Journal of Mathematical Physics*, vol. 55, no. 10, p. 102 702, Oct. 2014, ISSN: 0022-2488. DOI: 10.1063/1.4897210.

Z. Neufeld and T. Tél, “The vortex dynamics analogue of the restricted three-body problem: Advection in the field of three identical point vortices,” *Journal of Physics A: Mathematical and General*, vol. 30, no. 6, p. 2263, Mar. 1997. DOI: 10.1088/0305-4470/30/6/043.

P. Newton, *The N-Vortex Problem: Analytical Techniques* (Applied Mathematical Sciences). Springer New York, 2010, ISBN: 9781441929167. DOI: 10.1007/978-1-4684-9290-3.

R. W. D. Nickalls and R. H. Dye, “The geometry of the discriminant of a polynomial,” *The Mathematical Gazette*, vol. 80, no. 488, pp. 279–285, 1996. DOI: 10.2307/3619560.

C. Oseen, *Über Wirbelbewegung in einer reibenden Flüssigkeit* (Arkiv för matematik, astronomi och fysik). Almqvist & Wiksell, 1911.

F. L. Pereira, T. Grilo, and S. Gama, “Optimal multi-process control of a two vortex driven particle in the plane,” *IFAC-PapersOnLine*, vol. 50, no. 1, pp. 2193–2198, 2017, 20th IFAC World Congress, ISSN: 2405-8963. DOI: 10.1016/j.ifacol.2017.08.280.

F. L. Pereira, T. Grilo, and S. Gama, “Optimal power consumption motion control of a fish-like vehicle in a vortices vector fiele,” in *OCEANS 2017 - Aberdeen*, 2017, pp. 1–4. DOI: 10.1109/OCEANSE.2017.8085026.

L. S. Pontryagin, V. G. Boltyanskii, R. V. Gamkrelidze, and E. F. Mishchenko, *The Mathematical Theory of Optimal Processes*. New York, NY: Interscience Publishers, 1961, translated by K. N. Triruguf, edited by T. W. Neustadt.

S. B. Pope, *Turbulent Flows*. Cambridge University Press, 2000. DOI: 10.1017/CBO9781316179475.

B. Protas, "Vortex dynamics models in flow control problems," *Nonlinearity*, vol. 21, no. 9, R203, Jul. 2008. DOI: 10.1088/0951-7715/21/9/R01.

Z. Qian, Y. Qiu, and Y. Zhang, "Tracking the vortex motion by using brownian fluid particles," *Physics of Fluids*, vol. 33, no. 10, p. 105 113, Oct. 2021, ISSN: 1070-6631. DOI: 10.1063/5.0065073.

C. G. Ragazzo, "The motion of a vortex on a closed surface of constant negative curvature," *Proceedings of the Royal Society A: Mathematical, Physical and Engineering Sciences*, vol. 473, no. 2206, p. 20 170 447, Oct. 2017, ISSN: 1364-5021. DOI: 10.1098/rspa.2017.0447.

D. Ruelle, *Chaotic Evolution and Strange Attractors* (Lezioni Lincee). Cambridge University Press, 1989. DOI: 10.1017/CBO9780511608773.

P. G. Saffman, *Vortex Dynamics* (Cambridge Monographs on Mechanics). Cambridge University Press, 1993. DOI: 10.1017/CBO9780511624063.

M. A. Stremler, "On relative equilibria and integrable dynamics of point vortices in periodic domains," *Theoretical and Computational Fluid Dynamics*, vol. 24, no. 1, pp. 25–37, 2010. DOI: 10.1007/s00162-009-0156-z.

H. Tennekes and J. L. Lumley, *A First Course in Turbulence*. Cambridge, Massachusetts: MIT Press, 1972.

W. Thomson, "Vi.—on vortex motion," *Transactions of the Royal Society of Edinburgh*, vol. 25, no. 1, pp. 217–260, 1868. DOI: 10.1017/S0080456800028179.

C. Truesdell, *The Kinematics of Vorticity* (Indiana University Publications Science Series 19). Bloomington, Indiana: Indiana University Press, 1954.

M. Umeki, "Clustering analysis of periodic point vortices with the l function," *Journal of the Physical Society of Japan*, vol. 76, no. 4, p. 043 401, 2007. DOI: 10.1143/JPSJ.76.043401.

G. K. Vallis, *Atmospheric and Oceanic Fluid Dynamics*. Cambridge, U.K.: Cambridge University Press, 2006, p. 745. DOI: 10.1017/9781107588417.

J. Weiss and A. Provenzale, *Transport and Mixing in Geophysical Flows* (Lecture Notes in Physics). Springer Berlin Heidelberg, 2008, ISBN: 9783540752141. DOI: 10.1007/978-3-540-75215-8.

K. Zhou and S. J. Grauer, *On the joint observability of flow fields and particle properties from lagrangian trajectories: Evidence from neural data assimilation*, 2025. DOI: 10.48550/arXiv.2510.00479.